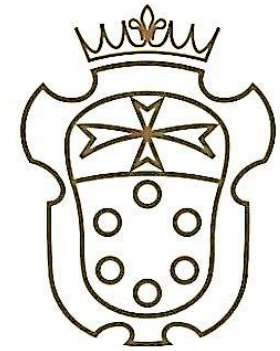

SCUOLA
NORMALE
SUPERIORE
PISA

MicroRNA miR-29 controls a compensatory response to limit neuronal iron accumulation during adult life and aging.

Years: **2011-2015**

CANDIDATE: **TUTOR:**

Roberto Ripa **Alessandro Cellerino**

CONTENTS

Abstract

Iron is an essential metal cofactor for enzymes involved in many cellular functions, such as energy generation and cell proliferation. However, excessive iron concentration leads to increased oxidative stress and toxicity. As such, iron homeostasis is strictly controlled by two RNA binding proteins known as Iron Regulatory Proteins (IRPs) that regulate the expression of iron management genes at post-transcriptional level. Despite this fine regulation, an impairment of iron homeostasis occurs during aging: iron progressively accumulates in several organs and, in turn, it exacerbates cellular vulnerability and tissue damage. Moreover, excessive iron accumulation within the CNS is observed in many neurodegenerative diseases. I investigated the age-dependent changes of iron homeostasis using the short lived fish *Nothobranchius furzeri*. Here, I show that: i) both iron content and expression of microRNA family miR-29 increase during adult life and aging in the *N. furzeri* brain; ii) iron up-regulates miR-29 expression in fish brain and murine neurons, while, in turn, miR-29 targets the 3'-UTR of *IREB2* mRNA, reducing iron intake; iii) Transgenic fish with knock-down of miR-29 show significant adult-onset up-regulation of IRP2 and its target TFR1 in neurons and display enhanced age-dependent accumulation of brain iron; iv) miR-29 triggers a global gene expression response that partially overlaps with that induced by aging. My studies indicate that miR-29 modulates intracellular iron homeostasis and is up-regulated as an adaptive response to limit excessive iron accumulation and to contrast aging-induced processes.

1.0 INTRODUCTION

1.1 Systemic iron homeostasis

Iron is an indispensable element for all living organisms. Healthy adults contain 4–5 g of iron, about 65% of which is contained in hemoglobin where it participates in oxygen transport, 30–35% is stored in liver, primarily in the storage protein, ferritin, and 1–2% is found in the form of iron–sulfur clusters or heme in the catalytic centers of numerous essential enzymes and multi-protein complexes such as the mitochondrial respiratory chain complexes, which contain twelve iron–sulfur clusters and seven hemes (Rouault, 2013). Due to the essential role of iron *in vivo,* tissues have developed sophisticated mechanisms to maintain appropriate iron concentrations through the entire organism (**Figure 1.1**). Inorganic iron is absorbed at duodenal tract by enterocytes via the divalent metal transporter 1 (DMT1/SLC11A2, solute carrier family 11, member 2) (Gunshin et al., 1997). Given that iron is largely in the oxidized state, it must first be reduced by the membrane-associated ferrireductase DcytB (Cybrd1). Cytosolic iron can then be exported into the circulation by the basolateral iron exporter ferroportin (McKie et al., 2000; Donovan et al., 2000). Enterocytic iron export through ferroportin requires hephaestin, a multi-copper oxidase homologous to ceruloplasmin, which oxidases Fe(II) to Fe(III) for loading onto transferrin (TF-Fe_2). Since iron cannot be excreted from the organism in an active way, iron absorption is the only critically controlled process. Iron absorption can be enhanced when the demand increases (for example, because of increased erythropoiesis or during pregnancy) and suppressed in conditions of iron overload. Hepcidin (encoded by the *HAMP* gene) has emerged as the central regulatory molecule of systemic iron homeostasis, its function is to regulate iron entry into the circulation. Hepcidin is mainly produced and secreted from hepatocytes and circulates in plasma bound to α2-macroglobulin (Peslova et al., 2009). Hepcidin is a negative regulator of ferroportin

activity, indeed, it binds to ferroportin and induces its internalization, ubiquitination, and subsequent lysosomal degradation (Nemeth et al., 2004). By inhibiting ferroportin serum iron falls due to iron trapping within macrophages and liver cells and decreased gut iron absorption. In this way, iron overload (when the iron amount is higher that serum transferrin binding capacity) is prevented. Hepcidin is regulated at transcriptional level and it is positively regulated when bloodstream iron concentration increases. Two different factors regulate *HAMP* expression: the human hemochromatosis protein (HFE) and the BMP signaling pathway. HFE has been suggested to act as a bimodal switch between two sensors of the concentration of Tf-Fe_2, TfR1, and TfR2, on the plasma membrane of hepatocytes (Goswamiand Andrews, 2006). This model is supported by the following findings: HFE binds the ubiquitously expressed TfR1 on the same site of transferrin binding domain, and Tf-Fe_2 thus competes with HFE binding to TfR1. By contrast, TfR2 can bind both HFE and Tf-Fe_2 simultaneously (Gao et al., 2009). Engineered mouse mutants carrying tfR1 with increased HFE binding show low hepcidin expression suggesting that TfR1 sequesters HFE to prevent its participation in hepcidin activation. Conversely, mutations that abolish the HFE-TfR1 interaction or mice with increased HFE levels display elevated hepcidin expression and succumb to iron deficiency (Schmidt et al., 2008). Although HFE system contributes to regulate hepcidin expression, BMP signaling pathway is the most critical regulator. BMP6 mRNA expression is activated by increased iron levels and repressed by iron deficiency. *Bmp6* knockout mice show hepcidin deficiency and tissue iron overload (Andriopouloset al., 2009; Meynard et al., 2009). BMP6 is thought to act in an autocrine manner and binds the co-factor HJV that adapts BMP receptors for iron regulation (Babitt et al., 2006). The BMP/HJV complex joins the type I (Alk2 and Alk3) and the type II (ACTRIIA) BMP receptors to induce phosphorylation of receptor activated SMAD (R-SMAD) proteins and subsequent formation of active transcriptional complexes involving the co-SMAD factor, SMAD4 (Wang et al., 2005). Two sequence motifs (the proximal BMP-RE1 and the distal BMP-RE2) of the hepcidin promoter are critical for transcription via HJV, BMP6, and SMAD4 (Casanovas et al., 2009). Different evidence highlight the importance of HJV/BMP/SMAD

signaling for hepcidin activation: (1) mice lacking HJV show attenuated R-SMAD phosphorylation in the liver (Babitt et al., 2006), (2) administration of BMP2 and BMP6 to mice induces hepcidin mRNA and decreases serum iron levels, (3) BMP antagonists (such as dorsomorphin) inhibit hepcidin mRNA expression and increase serum iron levels (Yu et al., 2008), (4) liver-specific disruption of the co-SMAD4 causes severe iron overload with diminished hepcidin transcription (Wang et al., 2005), and (5) the inhibitory iSMAD7 potently suppresses hepcidin transcription in cellular models (Mleczko-Sanecka et al., 2010).

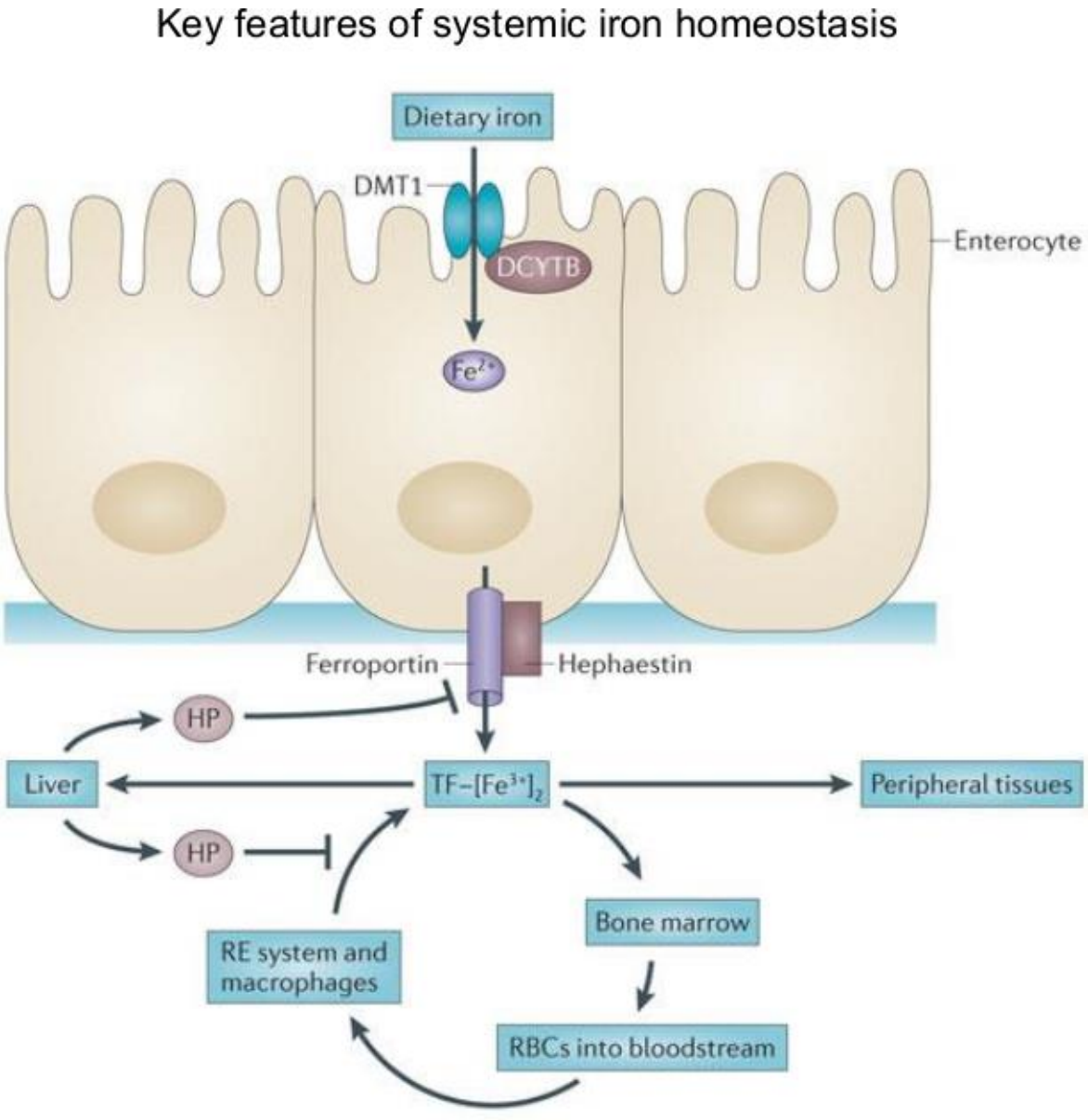

From Suzy et al., 2013

Figure 1.1: Systemic iron homeostasis. Dietary iron (predominantly in the form of ferric iron (Fe3+)) is absorbed in the duodenum through the concerted action of a reductase, such as duodenal cytochrome b (DCYTB), which produces ferrous iron (Fe2+), and divalent metal transporter 1 (DMT1). Iron exits the basolateral surface of the enterocyte through the iron efflux pump ferroportin, which functions together with the oxidase hephaestin to oxidize ferrous iron to form ferric iron, which is loaded onto transferrin (TF). The diferric iron transferrin complex (TF–[Fe3+]2) circulates through the bloodstream to deliver iron to sites of utilization. Principal among these sites is the bone marrow, where iron is used in the synthesis of haemoglobin and red blood cells (RBCs). RBCs circulate for approximately 90 days before they are catabolized by macrophages of the reticuloendothelial (RE) system. Iron is released from catabolized haem and effluxed out of the macrophage through the action of ferroportin, where it is loaded onto TF in the bloodstream, in a process termed iron recycling. TF–[Fe3+]2 is also delivered to peripheral tissues and the liver, which is the primary organ for the storage of excess iron. Since there is no excretory pathway for iron, so levels of iron in the body are primarily regulated at the absorption step. Excess iron induces the synthesis of the peptide hormone hepcidin (HP), which serves as a master regulator of systemic iron homeostasis. HP binds to ferroportin and triggers its degradation, inhibiting both delivery of dietary iron through the enterocyte and iron recycling through the macrophage.

1.3 Intracellular iron homeostasis

The maintenance of iron homeostasis by cells requires processes that are very similar to those observed at the systemic level: coordination of iron uptake, utilization, and storage to assure the availability of appropriate supplies and to prevent toxicity (**Figure 1.2**). However the machinery and the mechanisms are entirely different. In contrast to systemic iron metabolism, cellular iron traffic also involves regulated iron excretion. The Tf-Fe_2/TfR1 complex is internalized by clathrin-dependent endocytosis. Subsequent acidification of early endosomes triggers conformational changes in both transferrin and its receptor that promote the release of iron as Fe(III) (Dautry-Varsat et al., 1983). Iron is then reduced to Fe(II) by members of the STEAP familly of metalloreductases (Ohgami et al., 2005, 2006) for transport into the cytosol via DMT1. Transferrin and TfR1 are then largely recycled to the cell surface. Once into the cyctosol, iron forms the labile iron pool (LIP), a loosely bound and redox-active iron. High levels of LIP trigger oxydative stress, damage and cell death, for this reason, iron is rapidly bound by different protein factors in the cytosol in order to neutralize its toxicity and use it for metallation reactions. “Not-

utilized" iron is stored in ferritin heteropolymers made of 24 subunits of heavy (FtH1) and light (FtL) chains. Ferritin provides cells with a mechanism to sequester excess iron in a redox inactive form to prevent iron-mediated cell and tissue damage; it also constitutes an iron store and its mobilization involves both proteasomal and lysosomal ferritin degradation. Ferritin is essential, as shown by the early embryonic lethality of FTH1 knockout mice (Ferreira et al., 2000). Homopolymers of a nuclearly-encoded H-type ferritin are present also in mitochondria (Arosio and Levi, 2010). Iron export occurs from many cells, including neuronal and erythroid cells, but it is particularly important in cells that maintain plasma iron levels. Such cells include macrophages and duodenal enterocytes. These cells express relatively high levels of ferroportin (SLC40A1) and the effects of targeted disruption of the *Slc40a1*locus in the mouse reflects the unique, non-redundant functions of ferroportin in iron release from these cell types (Donovan et al., 2005). As mentioned above, ferroportin transports Fe(II) and acts along with the ferroxidases hephaestin (HEPH, enterocytes) or ceruloplasmin (CP, other cell types) that facilitate iron extraction from the ferroportin channel and subsequent loading onto plasma transferrin (De Domenico et al., 2007).

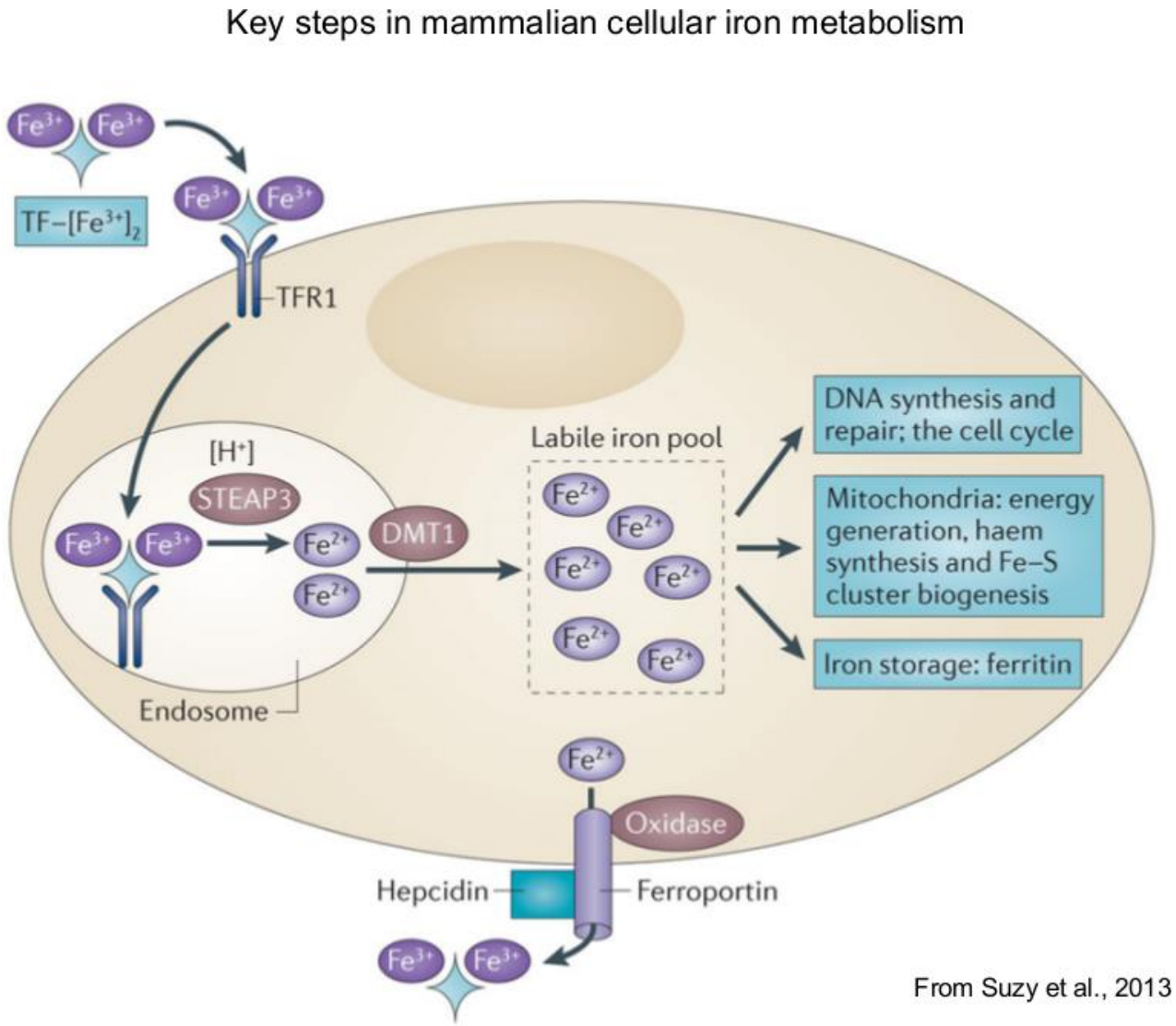

Figure 1.2: Intracellular iron metabolism. Iron circulates in the bloodstream bound to transferrin (TF), which binds two ferric iron atoms (Fe^{3+}). TF-bound iron binds to transferrin receptor 1 (TFR1) exposed on cell surface. All the complex is endocytosed and in the acidic environment of the endosome ferric iron is released from TF and reduced to ferrous iron (Fe^{2+}) by the activity of ferrireductase STEAP3. The TF-TFR1 complex then recycles back to the cell surface. Fe^{2+} is transported out of the endosome into the cytosol by the carrier DMT1 and enters the metabolically active pool of iron (labile iron pool). Here iron can undergoes toward multiple destinations: a) transported into the mitochondria for haem and iron-sulfur clusters synthesis, b) stored in ferritin, c) leaves cells through the activity of the ferroportin, an iron efflux pump and be oxidized to ferric iron by ceruloplasmin or hephaestrin to enable the loading onto TF.

While key aspects of systemic iron metabolism are regulated transcriptionally (hepcidin expression) and posttranslationally (ferroportin function by hepcidin), cellular iron homeostasis is coordinately regulated post-transcriptionally by two iron regulatory proteins (IRP1 and IRP2), encoded by the genes *ACO1* and *IREB2*, respectively. The two RNA-binding proteins interact with conserved cis-regulatory hairpin structures known as IREs, which are present in the 5′ or 3′ untranslated regions (UTRs) of target mRNAs. Either of the two IRPs inhibits translation initiation when bound to the single 5′ UTR IREs of ferritin H- or L-chain (iron storage), ferroportin (export) or hypoxia-inducible factor 2α (HIF2α/EPAS1) mRNAs, whereas their binding to the multiple IRE motifs within the 3′ UTR of *TFR1* (uptake) mRNA prevents its endonucleolytic cleavage and subsequent degradation (Muckenthaler et al., 2008; Recalcatti et al., 2010). The IRPs also appear to positively regulate *DMT1* (uptake) mRNA expression via a single 3′ UTR IRE motif, but the molecular mechanism is not known. Single IRE like structures with restricted phylogenetic conservation have been identified in the 3′ UTR of the CDC14A (cell division cycle 14 homolog A), HAO1 (hydroxyacid oxidase 1), and CDC42BPA (CDC42 binding protein kinase α), NDUFS1, and in the 5′UTR of SCNA and APP mRNAs, but their functional roles are not yet clear (Lin, Graziano, & Freyer, 2001; Recalcati, Tacchini, Alberghini, Conte, & Cairo, 2003; Sanchez et al., 2006; Duce et al., 2010; Febbraro et al., 2012; Friedlich et al., 2012). IRP-binding to IREs responds to cellular iron levels. In iron-replete cells, IRP2 interacts with the FBXL5 (F-box and leucine-rich repeat protein 5) adaptor protein that recruits a SCF (SKP1-CUL1-F-box) E3 ligase complex, promoting IRP ubiquitination and subsequent degradation by the proteasome (**Figure 1.3A**). In iron-repleted conditions, FBLX5 is stabilized by iron and starts to accumulate and interacts with IRP2 mediating its ubiquitination and degradation (Salahudeen et al., 2009, Vashisht et al., 2009). Instead, in iron-deficient conditions, the FBXL5-dependent degradation of IRPs decreases. IRP1, unlikely IRP2 degraded in iron-replete conditions, ligates a cubane 4Fe-4S cluster that precludes IRE binding (Walden et al., 2006; Muckenthaler et al., 2008). Once IRP1 binds 4Fe-4S cluster functions as a cytosolic aconitase. On the contrary, in iron-deficient conditions, IRP1 loses its Fe/S cluster and aconitase activity and adopts its IRE-binding

conformation (**Figure 1.3B**). The molecular details of this iron-regulated Fe/S cluster assembly/disassembly are not yet known, but disruption of critical components of Fe/S cluster biogenesis stimulate the IRE-binding activity of IRP1 (Sheftel & Lill, 2009). It is thus possible that the ratio between the two conformation of IRP1 depends primarily on mitochondrial iron availability and Fe/S cluster synthesis, whereas cytosolic iron sensing may primarily involve IRP2. Genetic ablation of both IRPs in the mouse causes embryonic lethality (Smith et al., 2006, Galy et al., 2008). By contrast, animals lacking either protein are viable and fertile. IRP2 knockout mice show a mild microcytic anemia, a tendency toward increased neurodegeneration, and abnormal body iron distribution (Cooperman et al., 2005, Galy et al., 2005). IRP1 knockout mice are asymptomatic under laboratory conditions, demonstrating that the cytosolic aconitase activity is not essential (Meyron-Holtz et al., 2004a). Taken together, IRP expression is essential, but the two proteins are largely redundant. Experiments with animals and cultured cells show that the two IRPs respond differentially to non-iron signals. For example, hypoxic conditions inactivate IRP1 by favoring its aconitase activity (Meyron-Holtz et al., 2004b) while stabilizing IRP2 as a result of the oxygen requirement for iron-mediated FBXL5 degradation. Furthermore, reactive oxygen species selectively activate IRP1 by causing disassembly of Fe/S clusters (Pantopoulos and Hentze, 1998). Phosphorylation of IRP1 and IRP2 by specific kinases can also regulate their activity although the exact physiology remains to be determined, it could in principle allow cells to finely control iron metabolism over a wide range of conditions and to alter the set points of the two regulatory proteins independently from iron control.

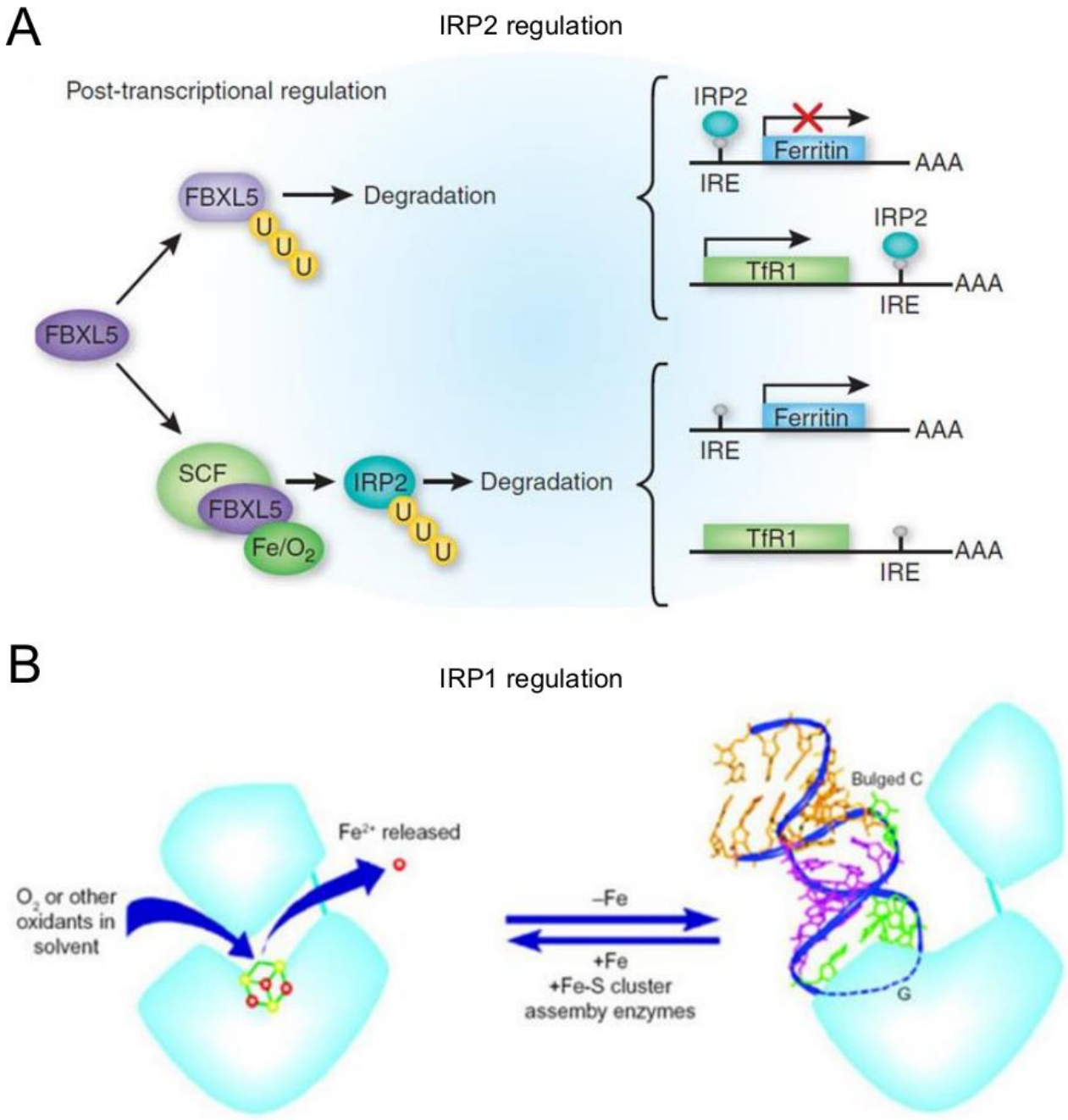

Figure 1.3: IRPs proteins regulation. **A**) IRP2 is ubiquitinated by the SKP1-CUL1-FBXL5 E3 ubiquitin ligase complex in an iron-dependent manner and degraded. Under low iron conditions, IRP2 binds to specific sequences in the untranslated regions of mRNA that encode proteins involved in iron acquisition and storage. Binding of IRP to a 5′-IRE inhibits mRNA translation, and binding to a 3′-IRE increases mRNA stability. In the presence of iron, there is an increase in the stability and thus concentration of the FBXL5-containing E3 SCF ubiquitin ligase. This E3 ligase ubiquitinates IRP2, leading to its degradation by the proteasome. The loss of IRP2 allows translation of 5′-IRE–containing mRNA and degradation of 3′-IRE–

containing mRNA. **B**) IRP1 is a bifunctional protein that can exist as a functional cytosolic aconitase when it binds an iron-sulfur cluster, interconverting citrate and isocitrate, or can bind IRE to regulate the expression of iron genes. The active site cleft that is responsible for aconitase activity overlaps with the region that binds to IRE, and binding of the iron-sulfur cluster prevents the binding with IRE. In iron-replete conditions, IRP1 will have an iron-sulfur cluster and will not bind IRE.

Although the model described above holds true also for the CNS, it should be noted that iron metabolism probably differs between neurons, astrocytes, oligodendrocytes and microglia, as each of these cell types has distinct metabolic requirements and morphological features. In fact, it has been shown that the amount of each iron-management protein varies greatly depending on the cell type and its iron status. In the brain, oligodendrocytes stain strongly for transferrin (TF), whereas microglia and astrocytes stain most strongly for ferritin (FTH, FTL), and neurons stain strongly for transferrin receptor (TFRC). CP is mostly expressed by astrocytes and exposed on the membrane surface or released in the cerebrospinal fluid (CSF) (Rouault T, 2013). Although both IRP proteins are expressed in all cells types, IRP2 result much more expressed in the CNS (Meyron-Holtz et al., 2004). Thus, it appears likely that each resident CNS cell type regulates its own iron homeostasis, distributing and storing iron according to the particular needs and functions of each cell type. Nevertheless, there is some specialization of iron metabolism within the brain: astrocytes express CP, instead transferrin is synthesized and secreted into CSF mainly by oligodendrocytes. The secreted transferrin binds iron that has been imported into the CNS and newly constituted holo-transferrin redistributes iron to cells exposed to CSF and interstitial fluid (Rouault T, 2013).

1.4 Age-dependent iron deposition

Age-dependent iron accumulation has been described so far in different model organisms such us: *C. elegans (Klang et al., 2014), D melanogaster (Massie et al., 1984)*, *M. musculus (Massie et al., 1983)* and *H. sapiens* (Acosta-Cabronero et al., 2016) (**figure 1.4**). In the human brain, iron accumulates especially in areas primarily associated with motor activity, including the globus pallidus, red nucleus, dentate nucleus and substantia nigra, but the factors that induce regional iron accumulation remain unknown. In the 1950, Hallgren and Sourander (1958) reported non-heme iron accumulation in several regions of the aged human brain such as putamen, motor cortex, prefrontal cortex, sensory cortex and thalamus (Hallgren and Sourander 1958). In 1983, Massie HR reported age-dependent iron accumulation in different rodent organs (brain, liver, kidney, heart) (Massie HR et al., 1983). In addition to these observations, studies in post-mortem brains showed an age-dependent accumulation of ferritin, indicative of increased storage iron in different brain regions (Thomas et al. 1993; Connor et al. 1995; Zecca et al. 2001). Recent studies using high-field magnetic resonance imaging and quantitative susceptibility mapping (QSM) (a new post-processed MRI contrast mechanism) confirmed increased iron levels in several deep brain nuclei and across motor, premotor, posterior insular, superior prefrontal, and cerebellar cortices, suggesting that iron accumulation with age predominantly affects brain regions involved in motor/output functions (Pfefferbaum et al. 2009; Aquino et al. 2009; Peran et al. 2009; Cherubini et al. 2009; Acosta-Cabronero et al., 2016). Age-dependent enhanced iron deposition was described also in microglia, in older individuals (60–90 years of age) compared with younger subjects (28–49 years), intense iron staining is observed in the microglia and astrocytes of the cortex, cerebellum, hippocampus, basal ganglia and amygdala, and ferritin immunoreactivity is also stronger in these cells (Zecca et al., 2004). Oligodendrocytes contain the largest amount of iron, ferritin and Tf, but this content remains constant during ageing suggesting the presence of a tight control and buffering mechanisms (Connors JR et al., 1990). Moreover, it has been showed that iron deposition occurs also in extracellular spaces as direct

consequence of micro-hemorrhages. Brain micro-bleeds and superficial siderosis are two conditions commonly observed in older patiens. Brain micro-bleeds, tiny deposits of blood degradation products contained within macrophages, are in close spatial relationship with structurally abnormal vessels (Martinez- Ramirez et al. 2014). Superficial siderosis manifests in the sub-pial layers of the brain as hemosiderin accumulation, due to recurrent and persistent bleeding into the subarachnoid space (Kumar 2009). Even if it is still matter of debate, the prevailing opinion is that iron imbalance, in particular the age-dependent iron deposition, may play a central role in the aging process due to its ability to produce oxygen reactive species, which over time causes extensive mitochondrial and cellular dysfunction. For instance, dietary iron supplementation has been shown to reduce lifespan both in nematodes (Klang et al., 2014), especially in *C. elegans,* iron addition accelerates the aging process and promotes protein aggregation especially of ribosome and mitochondria key proteins (Klang et al., 2014). Instead, increase in longevity can be induced by applying caloric intake restriction (Lee CK et al., 1999; Mair W et al., 2008; Piper DWM et al., 2011) as it appears to reduce both the production of ROS (Lee CK et al., 1999; Masoro EJ, 2000), as well as decrease iron deposition both in old mice and monkeys (Kastman EK et al., 2010; Wei S et al., 2014). Promoting antioxidants or using iron chelant therapy has been shown to increase longevity in animal models such as *Caenorhabditis elegans*, *Drosophila melongaster* and yeast (Massie HR et al, 1993; Melov S et al, 2000; Bonilla E et al., 2002; Gakh O et al., 2006). Strikingly, a recent work lead by Schiavi A and collegues argued that mitochondria iron starvation extends lifespan in *C. elegans* throught the activation of mitophagy (Schiavi A et al., 2015).

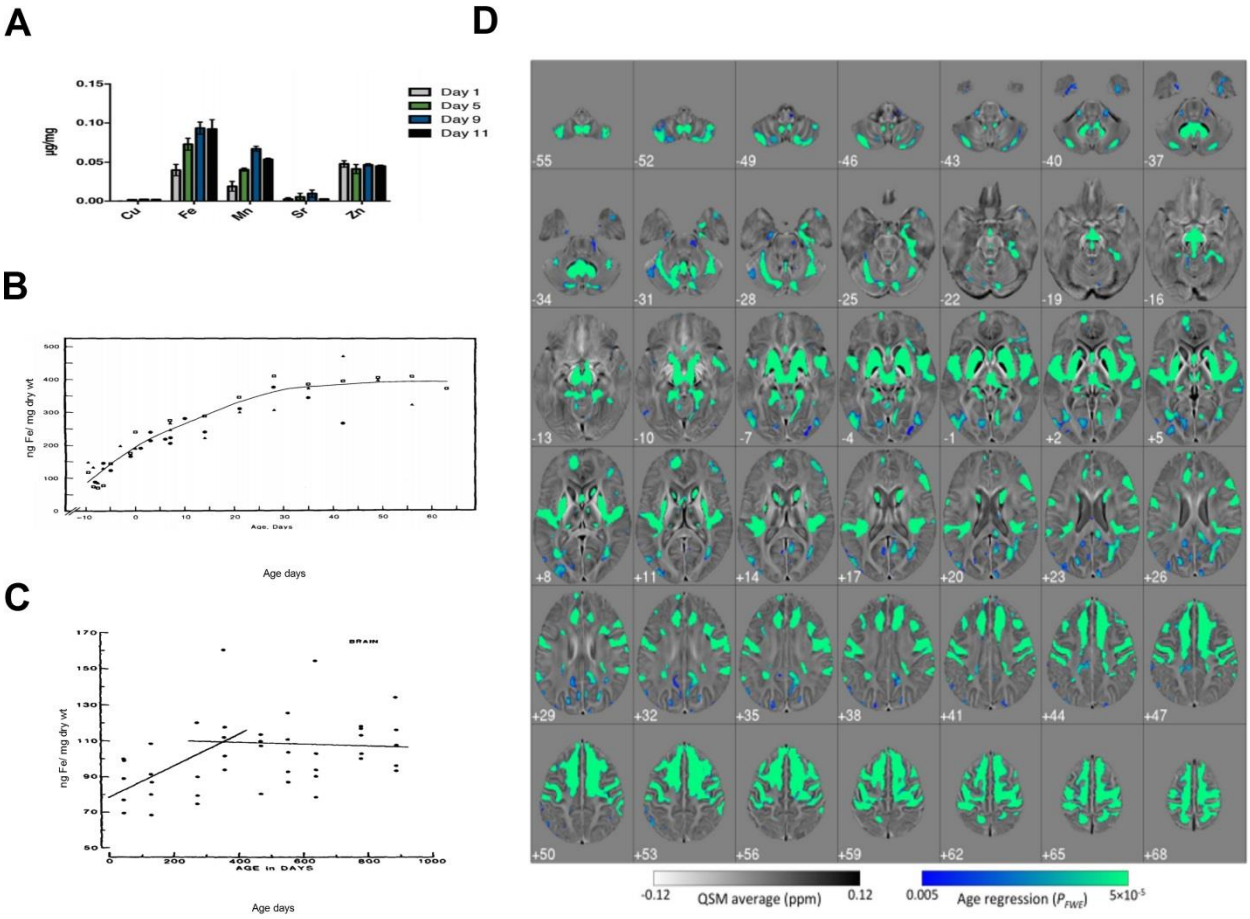

Figura 1.4. Age dependent iron accumulation. A) Alteration of the metal profile with age in *C. elegans* (Klang et al., 2014). B) Whole-body iron concentration versus age in days for male Oregon R Drosophila melanogaster for both developmental and adult stages at 25°C (Massie et al., 1984). C) Iron content versus age for brain from C57BL/6J male mice for ages 45-355 days (Massie et al., 1983). D) whole-brain imaging approach known as quantitative susceptibility mapping (QSM) provides insights into iron accumulation in the brain across the adult lifespan. Correlation between QSM and age in 116 healthy subjects (20 –79 years old). Iron deposition due to aging is spatially selective. Strong positive correlations, markedly bilateral and confluent, were identified in several cortical and subcortical regions. In deep gray matter, this included the striatum (putamen and caudate nucleus), mesencephalic structures (substantia nigra and red nucleus), diencephalic structures (subthalamic nucleus, mammillary bodies, parts of medial, and posterior thalamic subnuclei groups), and the cerebellar dentate nucleus. QSM co-varied with age in the sensory-motor cortex; this was extensive and confluent in superior premotor cortex, prefrontal, insular areas, and dorsomedial frontal cortices down to the cingulate sulcus and cerebellar cortex; and in supra-marginal and posterior para-hippocampal gray matter and was minor in the posterior cingulate and precuneus cortical regions. White matter QSM relationships, conversely, were overall weaker (Acosta-Cabronero et al., 2016).

1.5 Iron toxicity and neurodegenerative disease

Excessive brain iron accumulation results in a large increase in the chelatable free iron pool that exceeds the sequestering capability of ferritin within cells (Breuer, Greenberg, & Cabantchik, 1997). Studies in hepatocytes treated with $FeSO_4$ showed significant cellular damage with a large increase in cellular iron, but without a significant increase in the total amount of ferritin. These findings further suggest that iron-induced cellular damage is dependent on ferritin iron incorporation (Cable, Connor, & Isom, 1998). Moreover, it has been suggested that iron accumulation may induce neuronal damage even after it has become bound to ferritin because iron can be released in its ferrous form under acidic conditions (Bishop, & Robinson, 2001) and through interaction with components such as excess superoxide radicals (Siesjö, Agardh, & Bengtsson, 1989). Conditions such as intracerebral hemorrhage or hypoxia-ischemia further aggravate the potential for iron release from transferrin or ferritin due to a decrease in pH (Ying, Han, Miller, & Swanson, 1999). Iron toxicity is largely based on Fenton chemistry, iron reacts with reactive oxygen intermediates, including hydrogen peroxide (H_2O_2) and the superoxide anion ($O2^-$) both byproducts of aerobic metabolism and produces highly reactive free radical species such as the hydroxyl radical ($OH^\cdot$).

$Fe^{2+} + H_2O_2 \rightarrow Fe^{3+} + OH^\cdot + OH^-$

Reduction of the oxidized form of iron by ascorbate or other cellular reductants regenerates the Fenton active form of iron ($Fe^{3+} + O^-_2 \rightarrow Fe^{2+} + O_2$) which re-enters the oxidation-reduction cycle, a process called redox cycling. Thus, a continuous production of free radicals perpetuates under these conditions. Ferrous iron is a 5-fold greater pro-oxidant as compared to ferric iron (Rauhala & Chiueh, 2000) and if sufficient iron is present, free radical production will overcome the cellular antioxidant mechanisms and cause massive production of free radicals. As a consequence, ROS damage DNA and mtDNA, oxidise proteins and lipids. Peroxidation of polyunsaturated fatty acids in membrane lipids can generate highly reactive aldehydes, such as 4-hydroxynonenal,

which irreversibly modify proteins by carbonylation. ROS can induce the release of iron from mitochondrial iron–sulphur cluster proteins of the respiratory chain and other iron storage proteins, which will lead to further ROS production via Fenton's reaction (Dixon & Stockwell, 2014; Melis, van Steeg, & Luijten, 2013). Cathecolamines, such as dopamine, might be oxidized to highly reactive or toxic quinones either via the reduction of ferric iron or enzymatically (Paris et al., 2005). The aggregation of proteins involved in neurodegenerative disorders (APP, α-synuclein and hyper-phosphorylated tau protein) has been shown to be triggered *in vitro* by elevated ferric iron concentrations (Mantyh et al., 1993; Li, Jiang, Song, & Xie, 2010; Yamamoto et al., 2002). The proteolytic activation of the inactive forms of α secretase and β secretase is modulated by furin. Excessive amounts of total iron will decrease furin activity since transcription of furin is modulated by cellular concentrations of iron, leading to decreased furin protein concentrations which thereby favours β-secretase activity and enhances the amyloidogenic pathway. By contrast, iron deficiency will increase furin activity, thereby enhancing α secretase and stimulating the non-amyloidogenic pathway (Wichaiyo et al., 2015). Iron modulates APP processing through the interaction of IRPs with a putative IRE in the 5'-untranslated region of its mRNA. APP translation therefore is up-regulated in conditions of iron excess, increasing the amount of APP available to enter the amyloidgenic pathway, which is favoured by decreased furin activity (Rogers et al., 2002). Moreover, APP was suggested to have ferroxidase activity and to physically interact with the carrier protein ferroportin improving its ability to export iron across membrane (Duce et al., 2010). Microtubule-associated protein tau (MAPT) deficiency induces intracellular iron accumulation, which causes degeneration of dopaminergic neurons, leading to parkinsonism with dementia in mice (Lei et al., 2012). Tau deficiency impairs ferroportin iron export by retaining APP in the endoplasmic reticulum so that it can no longer be trafficked to the neuronal surface, where it can couple its ferroxidase activity to ferroportin. In Parkinson's disease spectroscopic methods measured total iron concentrations in specific brain regions, such as substantia nigra pars compacta and reticulate and revealed that iron concentrations in these regions increase with disease severity (Dexter et al., 1989). Ferric iron can, in vitro,

catalyse the conversion of α-synuclein from the α-helix to the β-sheet conformation that is present in Lewy bodies (Uversky, Li, & Fink, 2001). A contributing factor to the increased iron accumulation in Parkinson's disease might be increased DMT1 activity or decreased ferroxidase activity of ceruloplasmin, both of which would increase total intracellular iron, as reported in an animal model of Parkinson's disease (Salazar et al., 2008; Olivieri et al., 2011).

1.6 MicroRNA and aging

MicroRNAs (miRNAs) are abundant non-coding RNAs around 20–22 nucleotides in length, which are emerging as important key players in the regulation of gene expression. MiRNAs are transcribed by RNA Polymerase II (i.e., the same Polymerase which transcribes protein-coding RNAs) as long transcripts called primary transcripts (pri-microRNAs) and undergo a complex processing before being included in a ribonucleic complex. Pri-miRNAs contain one or more miRNAs within hairpins. These hairpins are cleaved from the pri-miRNA transcript in the nucleus by the Microprocessor complex, which consists of the RNA-binding protein (RBP) DGCR8 and the RNA endonuclease Drosha. The resulting pre-miRNA hairpins are transported to the cytoplasm where they are further processed into approximately 21‑nucleotide-long double stranded RNAs (dsRNAs) by the endonuclease Dicer. Several miRNAs can be grouped in a genomic cluster and co-transcribed, and may be hosted within an intron of a protein-coding gene. MiRNAs bind, due to sequence complementarity, to specific sites in the 3' untranslated region of their target mRNAs, thereby silencing expression of the gene product via translational repression and/or mRNA degradation. Indeed, they represent a new level of gene regulation acting at the post-transcriptional level. Up to now, several thousands of miRNAs have been predicted and identified in animals, plants and viruses (http://www.mirbase.org). A feature of miRNAs is their combinatorial regulation: a given miRNA can target a multitude of different mRNAs and a given target might similarly be

targeted by multiple miRNAs; for this reason, they frequently represent the central nodes of several regulatory networks and may act as rheostat to provide stability and fine-tuning to gene expression networks (Osella et al., 2011; Siciliano et al., 2013). Moreover, they are promising candidates for functional studies by genome-wide transcriptional analysis, thanks to some specific features: (i) miRNAs are highly conserved in vertebrates (cases of 100% identity between fish and mammals are not uncommon) and are thought to be an evolutionarily ancient component of genetic regulation; (ii) in a single tissue, relatively few miRNAs are expressed (hundreds vs. tenths of thousands mRNAs); (iii) they represent in their context the biologically active molecule, since they directly bind and control the target mRNAs: measurements of miRNA concentrations allow a more direct inference of a biological function. The ability to regulate multiple targets simultaneously makes miRNA a crucial regulator in many physiological conditions, including aging, which is a complex process involving multiple interconnected signaling pathways. An emerging concept is that microRNAs are crucial to restore homeostasis upon transient environmental changes, or, if these changes are prolonged, enforce a new gene expression program so cells can tolerate the new environment. This concept is based on the observation that cells or intact organisms with deficiency of a single microRNA very often are apparently unaffected, but exhibit a phenotypic crisis under stress condition (X. Li, Cassidy, Reinke, Fischboeck, & Carthew, 2009). If aging is considered as a long-term exposure to a broad type of stressors that tend to change tissue homeostasis, the buffering activity operated by microRNAs on the global gene expression could be of fundamental importance. The role of specific miRNAs in regulating the aging processes was established only recently. Only about ten years ago, it was observed for the first time that overexpression of a microRNA (lin-4) increases lifespan of *C. elegans* (Boehm & Slack, 2005). To date, numerous miRNAs were reported to be significantly up- or down-regulated with aging, both in invertebrate and vertebrate species (Somel et al., 2010; Ibáñez-Ventoso et al., 2006). In *C. elegans*, more than 50 of the ~200 known miRNAs are differentially expressed during aging (de Lencastre et al., 2010; Ibanez-Ventoso et al., 2006; Kato et al., 2011). Remarkably, although some key miRNAs, such as miR-34 and

miR-71, are upregulated during aging, the vast majority of *C. elegans* miRNAs that are differentially expressed during aging are downregulated (de Lencastre et al., 2010; Ibanez-Ventoso et al., 2006), while in mammals have been reported a general up-regulation of tissue specific microRNAs was reported (Maes et al., 2008; Li et al., 2009) This suggests the existence of possibly important differences between global and tissue-specific miRNA expression, or between the role of microRNAs in the biology of aging of worms and mice aging biology (Li et al., 2011a; Maes et al., 2008). MiR-34 and miR-71, are upregulated microRNAs during aging in *C. elegans* and were shown to affect aging phenotypes and modulate longevity. Loss of function of mir-34 results in extended lifespan and increased resistance to heat and oxidative stress (Yang et al., 2013). MiR-71 targets the PI3K AGE-1 and PDK-1 components of the IIS pathway, is upregulated during the starvation-induced diapause state known as the dauer and during the post-dauer recovery stage (Karp et al., 2011), suggesting that this miRNA functions in the cellular response to environmental stress. Indeed deletion of miR-71 impairs survival during dauer and shortens lifespan while overexpression of miR-71 extends lifespan (Boulias & Horvitz, 2012). Overexpression of miR‑246 or deletion of mir‑239 also have been reported to extended *C. elegans* lifespan (Boulias & Horvitz, 2012; De Lencastre et al., 2010; Yang et al., 2013). While miR-71, miR-246 and miR-239 are not evolutionary conserved, miR-34 is present in flies and vertebrates. In *D. melanogaster*, miR‑34 expression increases during ageing and deletion of mir‑34 accelerates brain degeneration and shortens lifespan. Elevated expression of miR‑34 increases median lifespan and mitigates neurodegeneration induced by human pathogenic polyglutamine disease protein (Liu et al., 2012). In mammals also, miR‑34 exhibits up-regulation during aging in different tissues (heart, brain). In contrast to the protective roles of *D. melanogaster* miR ‑34 but similarly to *C. elegans*, high level of miR‑34a in murine models contribute to the age-related decline of cardiac functions. Indeed, genetic deletion or antagomir-mediated silencing of mir‑34a improved the performance of aged heart, suggesting that mouse miR ‑34a could be a driving factor during heart ageing (R. a Boon et al., 2013). To date, the

demonstration that miRNAs regulate pathways that eventually lead to modulations of lifespan, as described above, exist only for invertebrates, whereas studies in vertebrate species (mainly mouse and human) focused to investigate miRNAs roles in regulating tissue- and cell-type-specific aging phenotypes. In fact, in vertebrates, although some microRNAs such as: mir-29, mir-34 or mir-17-92 are found commonly up- or downregulated among different tissues during aging, the available evidence indicates that each tissue/organ age in a different way exhibiting a specific age-dependent gene and microRNA expression profile. For instance mouse miR-22, miR-101a, miR-720 and miR-721 are specifically up-regulated in brain but not in other organs (Li et al., 2013), instead mir-93, mir-214, mir-669c and mir-700 are up-regulated specifically in liver and mir-7, mir-468, mir-542, mir-698 are up-regulated in muscle (Smith-Vikos & Slack, 2012). Due to this diversity in tissue -specific microRNA expression profile, the effects are also quite different among tissues. For instance, the age-dependent regulation of some microRNA seems to have a detrimental effect exacerbating age-associated dysfunctions in some organs and to protect from age-associated dysfunctions in other organs triggering an adaptive response to damage. In the liver, miR-93, miR-214 and miR-669c all target glutathione-S-transferases, which are crucial for oxidative defense, and cytochrome c complex (UQCRC1), important for mitochondrial function or maintenance, indicating that these microRNAs operates repressing factors that normally maintain an healty liver (Maes, An, Sarojini, & Wang, 2008) and might be considered pro-aging microRNAs. Another example of pro-aging microRNA, as described above, is the age-dependent mir-34 upregulation that is associated with decreased heart performance in mouse. Mir-34 inhibition reduces cell death and fibrosis following acute myocardial infarction and improves recovery of myocardial function through the upregulation of the protein PNUTS that reduces telomere shortening, DNA damage responses and cardiomyocyte apoptosis (R. a Boon et al., 2013). Brain upregulation of mir-101a, mir-22, mir-720 (and other microRNA) seems to play a crucial role repressing genes involved in the oxidative phosphorylation, decreasing the respiration rate in age-dependent manner (N. Li, Bates, An, Terry, & Wang, 2011). Since reduction in oxidative phosphorylation

correlates with longer lifespan (Dillin et al., 2002; Copeland et al., 2009; Baumgart et al., 2016), these microRNA might be considered to have an anti-aging effect. On the contrary, let-7b expression in the nervous system increases with age and contributes to the decline of the self-renewal capacity of neural stem cells by targeting the chromatin factor HMGA2 (Nishino, Kim, Chada, & Morrison, 2008). One of the most relevant aging-related phenotype is cellular replicative senescence, i.e. the irreversible exit from the cell cycle of mitotically-competent cells. In recent years, it was reported that cellular senescence occurs in vivo and significantly contributes to aging-related dysfunctions. Mice selectively depleted of senescent cells exhibit an attenuated progression of age-related disorders like cataract, sarcopenia and spinal cord curvature (Baker et al., 2011). To date, many senescence-associated microRNAs were identified. For instance, in endothelial progenitor cells P53 upregulates mir-34 that in turn repress SIRT1 and activates FOXO1-mediated senescence (Zhao et al., 2010). In mammals, miR-29 family miRNAs are upregulated in multiple tissues with increasing age, as well as in a mouse model of progeria syndrome. Induction of miR-29 is associated with DNA damage responses and depends on the activation of the tumor suppressor p53 (Ugalde et al., 2011). The miR-29 along with miR-30 families are upregulated during cellular senescence as well, and their upregulation requires activation of the Rb pathway (Martinez et al., 2011). The miR-17-92 cluster represent another microRNA family with strong implication in the aging phenotype, along with its paralogous clusters miR-106a-363 and miR-106b-25, it has been shown to sustains cell cycle progression and survival, repressing numerous target genes such us: p21, p27, p57, PTEN, RB1 (Grillari, Hackl, & Grillari-Voglauer, 2010). However miR-17-92 has been shown also to be oncogenic and to promote tumorigenesis (Olive et al., 2009). Expression of these clusters are downregulated during aging in multiple cells types (Hackl et al., 2010; Baumgart et al., 2012, Terzibasi Tozzini et al., 2015). Mir-17-92 age-dependent downregulation is associated with increased expression of PTEN, that acts as a negative regulator of the m-TOR pathway (Olive et al., 2009) and regulates via this pathway neurogenesis and neurite outgrowth (Zhang et al., 2013; Bian et al., 2013). In

conclusion, the age-dependent downregulation of mir-17-92 on one hand reduces the cell cycle progression reducing the cancerous event and on the other hands it has been suggested to reduce activity of the mTOR pathway, whose negative modulation is associated with a delay of the aging phenotype and extended lifespan. These studies suggest that microRNAs can have context-dependent functions during ageing and that they can regulate diverse aspects of ageing at the level of the organism as well as of individual organs.

1.7 MicroRNA and iron homeostasis

Iron appears to play a critical role in miRNA processing via its physiological role as the functional component in heme. This potential role for iron to participate in miRNA biogenesis was first demonstrated when DGCR8 was identified as a heme-binding protein (Faller, Matsunaga, Yin, Loo, & Guo, 2007). Heme binds to DGCR8 via its Fe (III) iron co-factor and greatly increases pri-miRNA processing, instead impaired ability to synthesize heme, as a result of inadequate iron, consistently decreases pri-miRNA processing (Faller et al., 2007). Heme excess also produces changes in miRNA profiles, suggesting that it strongly influences the modulation of targeted mRNA expressions (Bonkovsky et al., 2013). Recently, it has been reported that cytosolic iron, but not heme-bound iron, regulates the activity of the miRNA pathway through poly(C)-binding protein 2 (PCBP2). PCBP2 is associated with Dicer and promotes the processing of miRNA precursors (Höck et al., 2007). Given that iron affects microRNA processing, there are many example of how microRNAs influence iron homeostasis as well. Systemic iron homeostasis is likely influenced by miRNA expression via the liver-specific miR-122. Inhibition of miR-122 by locked nucleic acid (LNA) modified oligonucleotides is associated with an increased expression of hemochromatosis gene (HFE), hemojuvelin (HJV or HFE2), bone morphogenetic protein receptor type 1a (BMPR1A), and hepcidin (HAMP) mRNA, all contributing to a reduction in both plasma and liver iron compromising hematopoiesis

(Castoldi et al., 2011). Moreover, it has been suggested that microRNAs might integrate the IRE-IRPs system. In fact, many of the genes regulated by IRP proteins, also generate spicing variants that lack the 5' or 3' IRE sequence and were shown to be regulated exclusively by iron-responsive microRNAs. In duodenal and erythroid precursor cells, was reported that the most abundant splice variant of the Ferroportin (FPN) mRNA lacks the IRE sequence within the 5'UTR (Zhang, Hughes, Ollivierre-Wilson, Ghosh, & Rouault, 2009) and it is targeted by iron-responsive mir-485 which is induced during iron deficiency and represses FPN expression by directly targeting the FPN 3'UTR (Sangokoya, Doss, & Chi, 2013). In hematopoietic precursor cells, divalent metal transporter 1 (DMT1), exhibits alternative splicing at 3' UTR, differing by the inclusion of a specific sequence either containing or lacking an IRE element (+IRE and -IRE, respectively). DMT1-IRE expression is under the regulation of miR-Let-7d and it is necessary for the erythroid differentiation (Andolfo et al., 2010).

1.8 microRNA mir-29 family in the CNS

MiR-29 family members (miR-29a, miR-29b and miR-29c) are absent in invertebrates but are extremely conserved among vertebrate species. In mammals, they are produced from two intergenic *loci* and are one among the most expressed microRNA families (Landgraf et al., 2007). They are enriched in the CNS (Nolan et al., 2014), are expressed both in neuronal and glial cells and their binding sites are highly overrepresented in brain mRNAs co-immunoprecipitated with argonaute complex (Boudreau et al., 2014). During brain development of rodents and primates, miR-29 is expressed at low levels and its expression dramatically increases during late post-natal development and continues to increase during entire adult life and aging in humans and non-human primates (Somel et al., 2010; Podolska et al., 2011; Fenn et al., 2013). In addition, age-dependent up-regulation of miR-29 was observed also in other organs such us heart, lung, liver, kidney of mice, and aorta of both mice and humans (R. A. Boon et al., 2011; Takahashi, Eda,

Fukushima, & Hohjoh, 2012; Ugalde et al., 2011). Therefore, up-regulation of miR-29 seems to be a conserved hallmark of aging. Although the molecular mechanism that induces mir-29 up-regulation is unknown, the magnitude of the increase in its expression during post-natal development observed in the CNS tissues, along with defects observed in the knock-out mice models, suggest that mir-29 might promote neuron maturation and survival in the CNS. Mice lacking only the miR-29b/a-1 locus (therefore with residual miR-29 activity) reach adulthood, display an ataxic phenotype and a mild loss of Purkinje cells in the cerebellum and die around 9 months of age (Papadopoulou et al., 2015). A similar cerebellar phenotype is induced acutely by injections of miR-29 antagomiR (Roshan et al., 2014). Remarkably, mice with a targeted deletion of both miR-29 loci, although born without evident abnormalities, rapidly accumulate defects during post-natal development and die within the age of 6 weeks (Cushing et al., 2015), suggesting that this microRNA family has a pivotal role during post-natal development and adult life. Interestingly, Siegel and colleagues identified miR-29a as one of the most enriched microRNA in rat forebrain synaptosomes (Siegel et al., 2009). After that, it has been observed that fear conditioning and glutamate receptors activation increase the endogenous level of miR-29a in hippocampus and in primary neurons respectively indicating that neural activity may modulate the expression of miR-29a (Lippi et al., 2011; H. Li et al., 2014). At molecular level, miR-29 reduces the expression of doublecortin (DCX) and actin-related protein 2/3 complex subunit 3 (ARPC3) enhancing the axon branching and reducing mushroom-shaped dendritic spines on hippocampal neurons respectively (Lippi et al., 2011; H. Li et al., 2014). In addition, up-regulation of miR-29 protects neurons against apoptosis during neuronal maturation, forebrain cerebral ischemia and stroke by targeting pro-apoptotic members of the BCL-2 family (Kole AJ et al., 2011; Ouyang YB et al., 2013; Khanna S et al., 2013). Interestingly, this microRNA family was found to target Beta-Site APP-Cleaving Enzyme (BACE1) mRNA and to be downregulated in sporadic Alzheimer's disease (Hébert et al., 2008). Overall, these data strongly suggest a conserved key role for miR-29 family in protecting neurons from different kind of damage and possibly against aging.

1.9 *Nothobranchius furzeri*

Aging process consists in broad changes that occur at molecular, cellular and integrated level and include systemic factors. Due to its complexity, the use of an *in vivo* approach is the only possible approach to shed light on the organismal and systemic mechanisms underlying the aging process. Several species have been used to study ageing and age-related diseases so far, the selection being partially based on practical and economic considerations. *C. elegans* and *D. melanogaster* have been widely used in aging research due to their small size and short lifespan. It is possible to rapidly generate mutant strains and perform high throughput screening. Despite of these advantages, invertebrate models show several morphological, histological and physiological differences to the vertebrates, making difficult the translation of these findings to humans. For instance, at anatomical level, they lack of bone, adaptive immune system and a centralized nervous system. Most importantly, vertebrate-specific pathways cannot be studied in these models. The mouse is the most widely used model system to investigate the biology of aging. However, it shows some practical disadvantages: the lifespan is relatively long (about 2-3 years) making life-long investigations impractical and it is economically much more expensive as compared to the other organism mentioned above. Therefore, it has been suggested that fish may represent a compromise between invertebrates and mammals. If zebrafish or medaka are considered, they are small in size, easy to keep and very prolific, allowing a large number of individuals to be maintained in small rooms with less expediture of time and financial resources. Aging pathways are conserved between fish and mammals (Van Houcke, Groef, Dekeyster, & Moons, 2015). *Nothobranchius furzeri*, the turquoise killifish, is an aquarium fish from Mozambique and in recent years became a promising model organism to study the biology of vertebrate aging. This fish is small in size (about 4-5 cm long), relatively easy to keep and maintain in captivity due to a rapid growth and high fecundity. The lifespan is exceptionally short as compared to other vertebrate species (**figure 1.5A**), although there are different strains with different life expectancy depending on the different permanence and duration of the rainy season in

each habitat (Terzibasi et al., 2008; Polačik, Donner, & Reichard, 2011; Tozzini et al., 2013), all of them exhibit a maximum captive lifespan generally lower than one year (Valdesalici & Cellerino, 2003). Of particular interest is the GRZ strain, that exhibits the shortest recorded lifespan among all the different killifish strains, with a maximum captive lifespan of only 5-6 months (**figure 1.5A**) (Terzibasi et al., 2008; Kirschner et al., 2012). Despite this short lifespan, they show age-dependent cognitive decline and expression of many age-related phenotypes observed in mammals including humans (**figure 1.5B**)(Valenzano et al., 2006; Terzibasi et al., 2009; Valenzano, Terzibasi, Genade, et al., 2006; Hartmann et al., 2009; Di Cicco et al., 2011; Hartmann et al., 2011; Tozzini et al., 2012; Baumgart et al., 2014). Moreover, transgenesis was established (Dario Riccardo Valenzano, Sharp, & Brunet, 2011; Harel et al., 2015), a reference genome sequence is available (Reichwald et al., 2015; Dario Riccardo Valenzano et al., 2015) and extensive data on age-dependent gene regulation are available (Baumgart et al., 2014). Therefore *N. furzeri* represents a novel model organism to investigate the genetic control of aging.

A

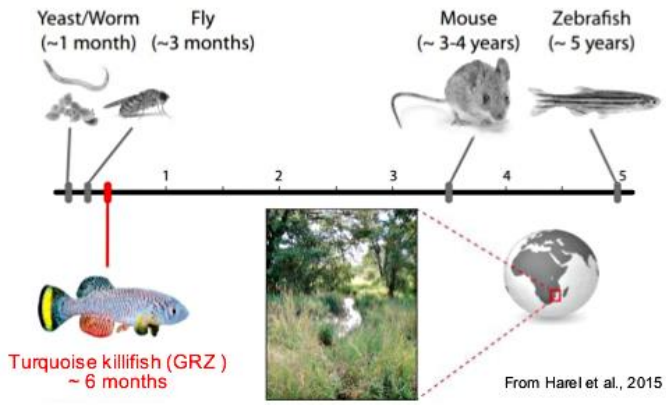

B

Description	Other species
Integrative phenotypes	
Spinal curvature[a, b]	Zebrafish[c], medaka[d]
Emaciation[a, b]	Zebrafish[c], medaka[d]
Disrupted circadian rhythm[b]	*Drosophila*, zebrafish[e], mammals
Reduced spontaneous activity[a, b]	*Drosophila*, mammals
Cognitive impairments[f]	*Drosophila*, zebrafish, mammals
Cellular phenotypes	
Apoptosis (liver)[g]	Medaka[h]
Lipofuscin (liver, brain, gills)[a, i, j]	Nearly universal
Cardiac hypertrophy[g]	Guppy[k], mammals
Kidney tubule dilatation[g]	Guppy[l]
Liver neoplasias[g]	Medaka (low incidence)[m]
Senescence-associated β-Gal[a, i, j]	Zebrafish[n], human[o]
Gliosis[p]	Mammals
Quiescence of neuronal stem cells[p]	Zebrafish[q], mammals
Molecular phenotypes	
Telomere shortening[r]	Medaka[d], human
Lipid peroxidation[s]	Nearly universal
Mitochondrial impairments[t]	Mammals

From Cellerino & Valenzano, 2015

Figure 1.5 Short lived killifish. A) Comparison of different lifespan species commonly used in biomedicine research and representation of killifish habitat in Mozambique. **B)** Table reassuming different aging traits observed in *N.furzeri* and in other species.

2 AIM OF THE PROJECT

Recently, Baumgart et al, has shown a consistent age-dependent mir-29 up-regulation in *Nothobranchius furzeri* brain, liver, skin and heart. Mir-29 resulted one of the few microRNA (along with mir-27) to be coherently up-regulated during aging in all tissues analyzed. These data, obtained in killifish, are in complete agreement with data previously reported in mammals (mouse and humans), indicating that different vertebrates species share an evolutionary conserved mir-29 age-dependent regulation. *In vitro* and *in vivo* evidence suggested a general protective role of mir-29 against different stress or insults (e.g: apoptosis, ischemia, cancer progression). Mir-29 knockout mouse model revealed that the CNS is one of the most affected tissues by mir-29 absence, moreover mir-29 reduction has been described during sporadic form of Alzheimer disease, one of the most relevant age-associated diseases.

Although all these data suggests a relevance for mir-29 in the regulation of aging process, little is known about its function during adult life and aging, especially in the CNS.

Here, I evaluated the biological activity of mir-29 during the adult stages of life in the killifish brain. In particular, I investigated whether neuronal-specific mir-29 loss of function could have a detrimental effect and affect the aging process in killifish brain.

3 RESULTS

3.1 Iron accumulates in *Nothobranchius furzeri* brain.

I investigated age-dependent brain iron accumulation in *N. furzeri* MZM 04/10pl, a strain with a median lifespan of ~ 30 weeks (Terzibasi et al., 2008, 2009; Baumgart et al., 2014). Brain non-heme iron concentration was quantified using a colorimetric assay (Rebouche et al., 2003) in fish of five age groups: 5, 27, 31, 51 weeks. These age steps correspond to sexual maturity (5 weeks), median lifespan (27 weeks), old and very old stages (31 and 51 weeks). I found that iron content increases over time as previously described in mammals (Hallgren et al., 1958; Bartzokis et al., 1997). From 5 to 51 weeks of age, iron amount increases almost 6-fold in animals (**fig. 2.0 A**). This datum was corroborated by histochemical Pearl's staining with DAB intensification on brain sections. Increased labelling was apparent in the brains of older fish, particularly in Purkinje cell layer of the cerebellum (**Fig. 2.0 B**). I also investigated the expression of genes coding for key proteins of iron metabolism by interrogating a public dataset of genome-wide age-dependent transcript regulation in the *N. furzeri* brain at the same five age steps analyzed here (Baumgart et al., 2014). I observed that expression of the transferrin receptor (TFR1A) gene and the solute carrier transporter 11a2 (SLC11A2) gene, directly involved in intracellular iron delivery, significantly declines as a function of age (**Fig. 2.0 C**), with the largest difference observed between 5 weeks and 12 weeks of age. On the other hand, expression of the genes coding for ferritin heavy chain (FTH1A) and Ferroportin (SLC40A1), required for iron storage and discharge, are stable (**Fig. 2.0 C**). Since all of these genes are controlled by the IRE-IRPS system, I investigated whether expression of IREB2 and ACO1 mRNAs is age-dependent and did not detect significant regulation during aging (**Fig. 2.0 D**). IREB2 mRNA is higher-expressed in brain as compared to ACO1 mRNA, while the opposite is observed in the liver (**fig. 2.0 E**). These same differences in the relative expression levels of IREB2 and ACO1 between brain and liver were previously

observed in the mouse (Meyron-Holtz et al., 2004) and suggest that IREB2 is the principal regulator of iron homeostasis in the brain. In mammals, iron regulates IREB2 expression mainly at the post-translational level by iron-dependent proteasomal degradation of IRP2. As expected, Western blot analysis revealed that IRP2 decreases with age (**fig. 2.0 F**). Since IRP2 is negatively regulated by FBXL5, I evaluated also its expression at mRNA and protein level but in both cases no significant modulation over time was detected (**fig. 2.0 G-H**). These data suggest that iron progressively accumulates over time and age-dependent downregulation of IRP2 is not mediated by FBXL5.

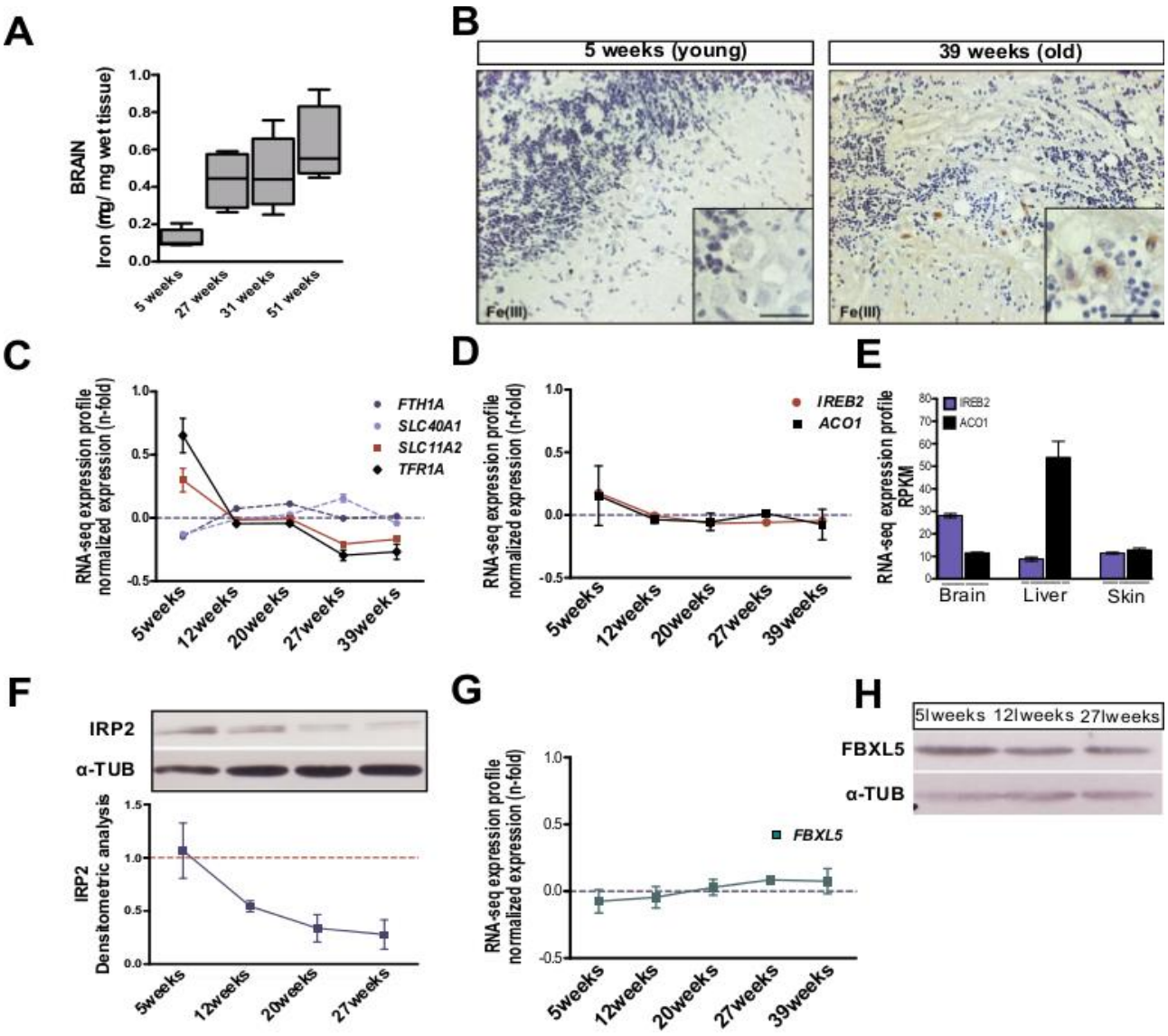

Figure 2.0. <u>Age dependent brain iron accumulation in *Nothobranchius furzeri*</u>. A) Brain non-heme iron content (µg/g wet tissue) in fish of different ages.. Iron increases with age, (P<0.0001, one-way ANOVA),

and no differences were observed between the sexes (data not shown). **B**) DAB-enhanced Perl's staining of the cerebellum of young and old fish. The black arrows point to labelled Purkinje cells. The inset in the bottom right corner of each picture shows a magnification of the Purkinje cells bodies. **C-D**) Age-dependent regulation of the transcripts coding for key genes of iron metabolism, from Baumgart et al., (2014). Expression values (in RPMKs) for each age were centered and scaled to the mean. **E**) Tissue specific expression of *IREB2* and *ACO1* mRNAs in *N. furzeri* brain, liver and skin, data from Baumgart et al., (2014). **F**) Representative Western blot of IRP2 in brain extracts and relative densitometric analysis at different ages. α-TUBULIN was used as loading control and values are normalized to the mean of 5 weeks values, n=3 biological replicates were used for each time point. **G**) Age-dependent expression of FBXL5 mRNA, from Baumgart et al., (2014). ANOVA for linear trend: R=0.1922, P=0.0688. Expression values (in RPMKs) for each age was centered and scaled to the mean, n= 5 animals for age point. **H**) Western blot of FBXL5 in brain lisates at three age point (5, 12 and 27 weeks). α-TUB was used as loading control. For C, D, E, G mean ± standard errors of means is reported and the significance of age-dependent modulation was assessed using 1 way ANOVA with post-test for trend.

3.2 MiR-29 is up-regulated with age in neurons and is negatively-correlated with expression of its targets.

MicroRNA-29 is up-regulated with age in multiple tissues of *N. furzeri* including brain (Baumgart et al., 2012). To assess the effect of miR-29 on global age-dependent gene expression, I took advantage of RNA-seq data from *N. furzeri* brain at five ages (Baumgart et al., 2014) and performed microRNA-seq on the same samples. I confirm a monotonous increase of miR-29 expression with age (**fig. 2.1 A**). Further, I analyzed protein-coding genes with rapid age-dependent decay in expression (for details see Baumgart et al., 2014). This gene set was enriched for genes containing a miR-29 binding site as predicted by MiRanda (FDR <0.05, Fisher's exact test). In addition, miR-29 targets showed an excess of negative correlation with miR-29 expression as opposed to non-targets (**fig. 2.1 B**). These data suggest that miR-29 is a regulator of age-dependent gene expression, as previously reported in primates using similar methods (Somel et al., 2010). I then investigated the transcriptional control of miR-29. The *N. furzeri* genome contains three loci for miR-29 family members but one is expressed at much higher levels. Transcription of the major miR-29 locus is up-regulated more than 15 times with age (**fig. 2.1 C**). I further used in situ hybridization to define miR-29 expression domains in the adult *N.*

furzeri brain. I found this primary transcript intensely expressed in the periventricular gray zone (PGZ) of the optic tectum (**fig. 2.1 D**), and in the granular cell layer (GCL) of cerebellum (**fig. 2.1 E**), where it is co-localized with the neuronal marker HuC/D, thereby confirming neuronal expression of miR-29 originally reported in the mouse (Hébert et al., 2008). In addition, I investigated transcriptional control of miR-29 in the mouse brain since it was already shown that mature miR-29 dramatically increases during the first two months of postnatal life (Hebert S et al., 2008; Li H et al., 2013). Using RT-qPCR, I quantified the expression of both miR-29 primary transcripts in postnatal day 0 (P0) and P60 mouse cerebral cortex. As expected, both increased more than 30 times (**fig. 2.1 F**).

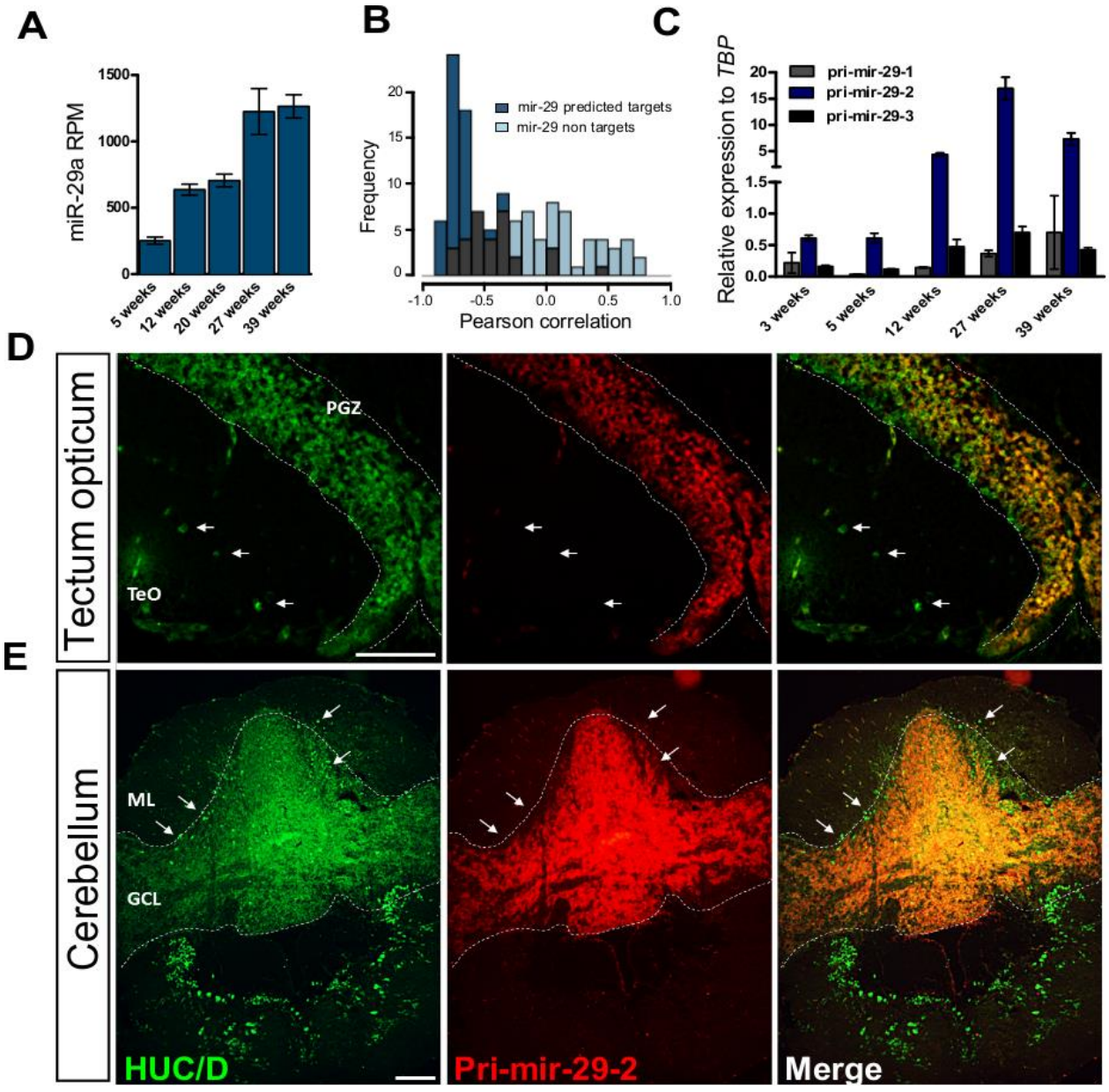

Figure 2.1. Regulation of miR-29 expression A) Expression profile for mir-29a according to NGS data of *Nothobranchius furzeri* brain. Column height corresponds to the mean and error bars to the standard deviation (FDR < 0.05, Spearman's rank correlation ρ=0.86). **B**) Correlation of mir-29 and its targets. Blue bars show the distribution of Pearson's correlation between mir-29a and its predicted target. Light-blue bars show the distribution of values extracted from a bootstrap ($p=10^{-14}$, Kolmogorov-Smirnoff). **C**) Age-dependent expression of miR-29 primary transcripts (Pri-miR-29-1, 2, 3) in the brain of *N. furzeri.* The relative expression was evaluated by RT-qPCR, data were normalized on TATA binding protein (TBP), pri-miR-29-2 results much more expressed than the other clusters and shows a clear age-dependent up-regulation (1 way ANOVA with post-test for trend: R= 0,5285 P<0,0001, n=4 animals for age group). **D-E**) Pri-miR-29-2 expression pattern in N. furzeri brain. (D) shows pri-miR-29-2 signal (red) and HuC/D expression (green) in the optic tectum (TeO). Pri-miR-29-2 shows a nuclear staining and a co-localization with neuronal marker HuC/D in all periventricular gray zone (PGZ), white arrows show neurons in the optic tectum (TeO) negative for pri-miR-29-2. Scale bar 50µm. Cerebellum overview picture (F) shows a clear and strong expression of pri-miR-29-2 just in the granular cell layer (GCL), it is instead is absent in the Purkinje cell (white arrow) and molecular layer (ML). Scale bar 100µm.

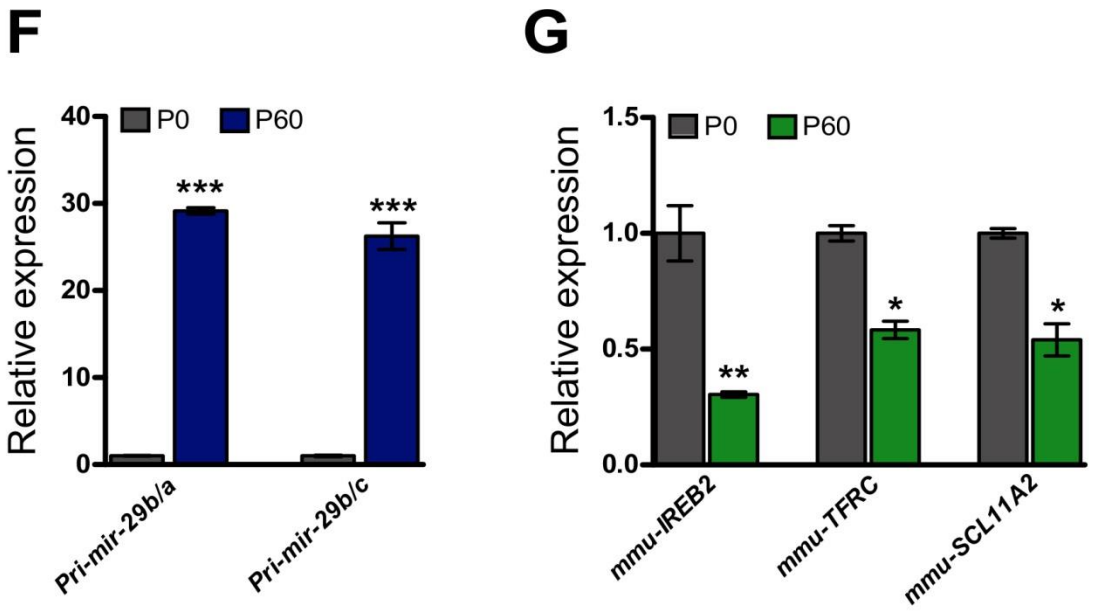

F) Quantification of pri-miR-29 cluster (pri-miR-29b-a; pri-miR-29b-c) in post-natal day 0 and 60 mouse brain. Both primary transcript dramatically increase during post-natal development (P<0,001 and P<0,001 respectively). **G**) Relative expression of iron management genes *IREB2* (P<0,01) *TFRC* (P<0,05), *SLC11A2* (P<0,05) in post-natal day 0 and 60 mouse brain. Both for F and G statistical significance was calculated by Mann-Whitney's U-test, n=6 (P0 brain) and n=7 (P60 brain) biological replicates.

3.3 mir-29 family targets *IREB2* mRNA

I noticed the presence of an 8 nt seed sequence in the 3'UTR of *IREB2* mRNA that is evolutionary conserved in vertebrates (**fig. 2.2 A**) and both miRanda (Betel D et al., 2010) and TargetScan (Agarwal et al., 2015) retrieved *IREB2* mRNA as a target for miR-29 in both fishes and mammals. In addition, StarBase provides support for a physical interaction of miR-29 and *IREB2* 3'-UTR in human and mouse (Li J *et al*., 2014). I assessed the regulation in expression of iron management genes such as *IREB2*, *TFRC*, and *DMT1* in the mouse brain between P0 and P60: all were found to be significantly downregulated (**fig. 2.1 G**). It also relevant to note that mice lacking one locus for miR-29 show up-regulation of *IREB2* (Papadopulous *et al.*, 2015). These data suggest that both in fish and mouse miR-29 is involved in the age-dependent down-regulation of IRP2. To demonstrate a direct interaction between miR-29 family members and *IREB2* mRNA in fish, I isolated the 3'UTRs of *IREB2* from zebrafish and *N. furzeri* cDNA and fused them with the eGFP coding sequence to generate a reporter construct. 100pg of each reporter mRNA were co-injected in fertilized zebrafish embryos with the same amount of control mRNA encoding for the red fluorescence protein (RFP) and 100pg of dre-miR-29a or dre-miR-29b mimic. Control embryos were injected with the same mixture with omission of the miRNA mimics. At 24hpf, 30-40 injected embryos were digested (according to Gallardo & Behra, 2012) and cells fluorescence was analyzed by cytofluorimetry to assess the relative eGFP/RFP fluorescence ratio (**fig. 2.2 B**). For both 3'UTRs, the normalized eGFP fluorescence was significantly reduced in presence of miR-29 mimics (**fig. 2.2 C-D**). For both constructs, a mutation of 3 nucleotides in the putative target sequence of the 3'-UTRs abolished repression (**fig. 2.2 C-D**). In addition, I performed luciferase assay in HEK293T cells to demonstrate direct targeting of *IREB2* 3'UTR by miR-29 in mammals. MiR-29 decreased luciferase activity of a reporter containing mouse *IREB2* 3'UTR and repression was abrogated by mutation of 3 nucleotides in the putative binding site (**fig. 2.2 E**).

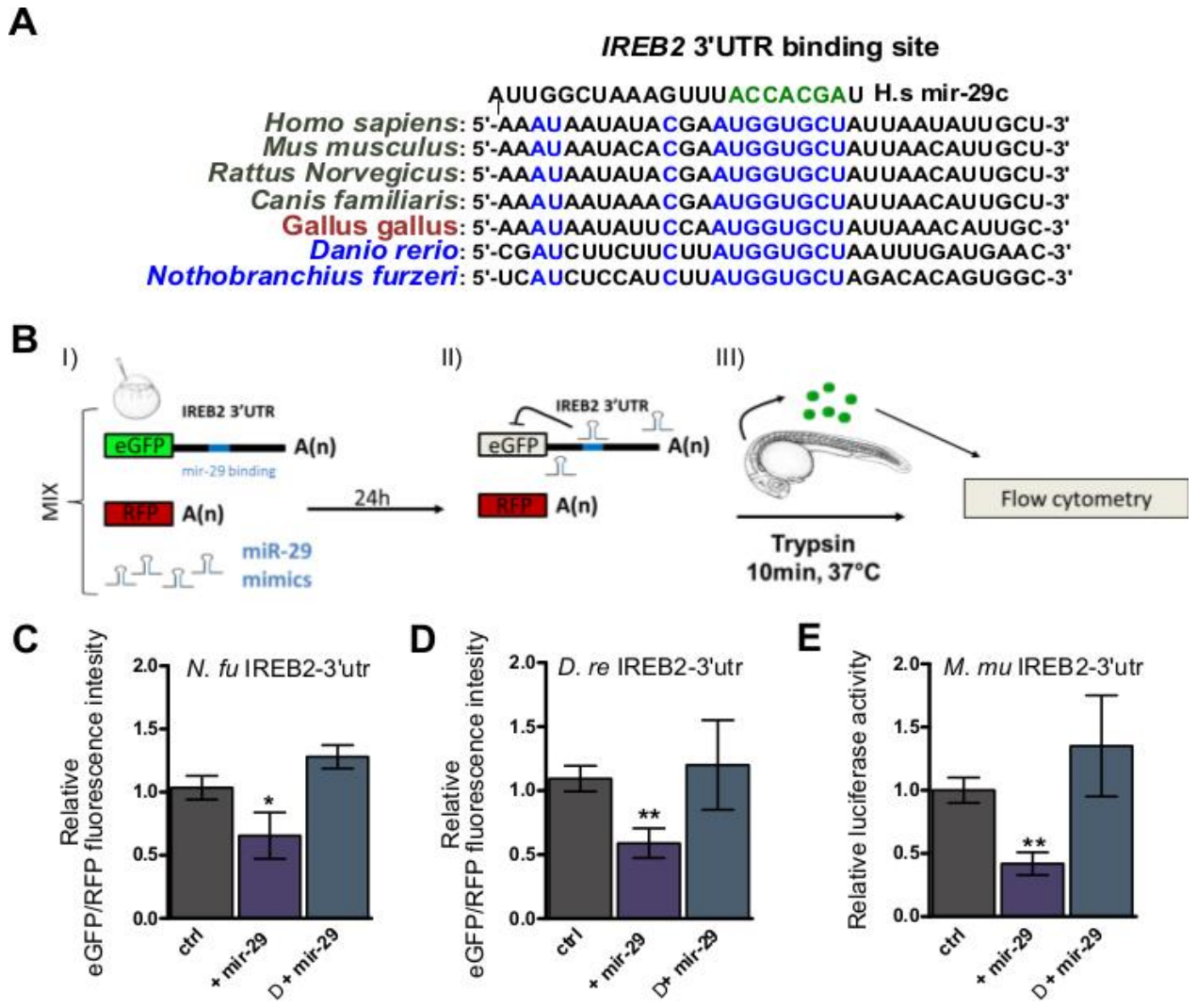

Figure 2.2. MiR-29 family targets IREB2 mRNA. A) Presence of a putative binding site for miR-29 family in the IREB2 mRNA 3'-UTR sequence in several vertebrate species (*H. sapiens*: ENSG00000136381; *M. musculus*: ENSMUSG00000032293; *R. norvegicus*: ENSRNOG00000013271; *C. familiaris*: ENSCAFG00000001766; *G. gallus*: ENSGALG00000003171; *D. rerio*: ENSDARG00000021466; *N. furzeri*: Nofu_GRZ_cDNA_3_0193494), mammalian sequences are in black, birds in purple and teleost fish in blue. Perfect match to the position 2-8 of the miR-29 seed sequence is highlighted in green and is present in all vertebrate sequences shown. **B**) Scheme of the reporter constructs and assay for miR-29 activity. Green fluorescent protein (GFP) mRNA fused with the 3' UTR of IREB2 is injected in one-cell stage zebrafish embryos with or without the miRNA of interest. Red fluorescent protein (RFP) mRNA is injected as a loading control (i). Binding of miR-29 to the reporter mRNA causes repression of GFP signal (ii). Embryos were trypsinized and cells relative fluorescence was read by flow cytofluorimeter (iii). **C-D**) Expression of GFP assessed by cytofluorometric analysis. Fusion with IREB2 3'UTR of *N. furzeri* (C) and D. rerio (D). The gray columns indicate the baseline fluorescence intensity of the construct shown in (B) in the absence of miR-29 mimic. The middle blue columns indicate the fluorescence in the presence of miR-29 mimic and the right light-blue columns the fluorescence of a construct (Δ) where the putative binding site for miR-29 in the IREB2 3'-UTR was mutated to destroy complementarity. Statistical significance of fluorescence difference between baseline and co-injection with miR-29 mimics was evaluated by Student's t-test (*, P<0,05; **, P<0,01 for *N. furzeri* and *D. rerio* respectively). **E**) 293T cells co-transfected with renilla and firefly luciferase construct containing the wild-type or the mutant target sites of mmu-IREB2 3'-UTR along with the miRNA expression plasmid (pcs2+: CMV:RFP-miR-29b/c precursor-polyA-tail) or the empty vector (pcs2+: CMV:RFP-polyA-tail). Histograms show normalized (to renilla) sensor luciferase

activity of empty vector transfected cells (gray column) respect to transfected cells with miRNA expressing vector (blue column) or to mutated sensor with miRNA expressing vector. Bars represent mean± standard deviation (Student's t-test,**, P<0,01) derived from two independent experiment performed in triplicates for each condition.

3.4 Iron overload induces miR-29 in neurons

Given the regulation of *IREB2* by miR-29, a logical question to ask was whether iron regulates miR-29. First, I studied stem-cells derived murine telencephalic neurons *in vitro* (Bertacchi M *et al*., 2014). Incubation of murine neurons with either Fe(II) or Fe(III)-dextran induced a dose-dependent up-regulation of miR-29 (**Fig. 2.3 A-B**). I then induced acute iron overload in adult fish by parental injection of 350µg per gram of weight of Fe-dextran and monitored brain iron concentration and miR-29 expression up to three days post-injection (p.i.). Iron significantly accumulated in the brain 4 hours p.i. (the first time point investigated) reaching a maximum at 8-12 hours p.i. to slowly decrease (**fig. 2.3 C**). I observed a delayed and significant increase of both the prevalent miR-29 primary transcript and miR-29a mature form, following the injection, starting at 24 h p.i. and reaching its maximum at 48h p.i. (**fig. 2.3 C-E**). In addition, iron overload caused up-regulation of miR-29 also in liver and muscle (**fig. 2.3 D**), suggesting that this regulation is not brain specific, but takes place at a systemic level. I then asked whether physiological steady-state levels of iron could influence miR-29 expression. I injected i.p 30µg/g of the iron chelant deferoxamine (DFO). At 24 hours post-injection brain iron amount was reduced by 25% (**fig. 2.3 F**), I did not aim for stronger reduction of iron since this can have serious negative consequences on physiology. I monitored pri-miR-29-2 expression at 24h, 48h and 72h after injection and did not detect any differences (**fig. 2.3 G**), suggesting that lowering iron below physiological levels does not regulate miR-29. Finally I replicated the iron-overload experiment and, after 4 hours, I administered either DFO, and I assessed miR-29 expression at 48h after iron injection. DFO treatment significantly reduced pri-miR-29 up-regulation (**fig. 2.3 H**). My results suggest that intracellular iron increase directly up-regulates miR-29.

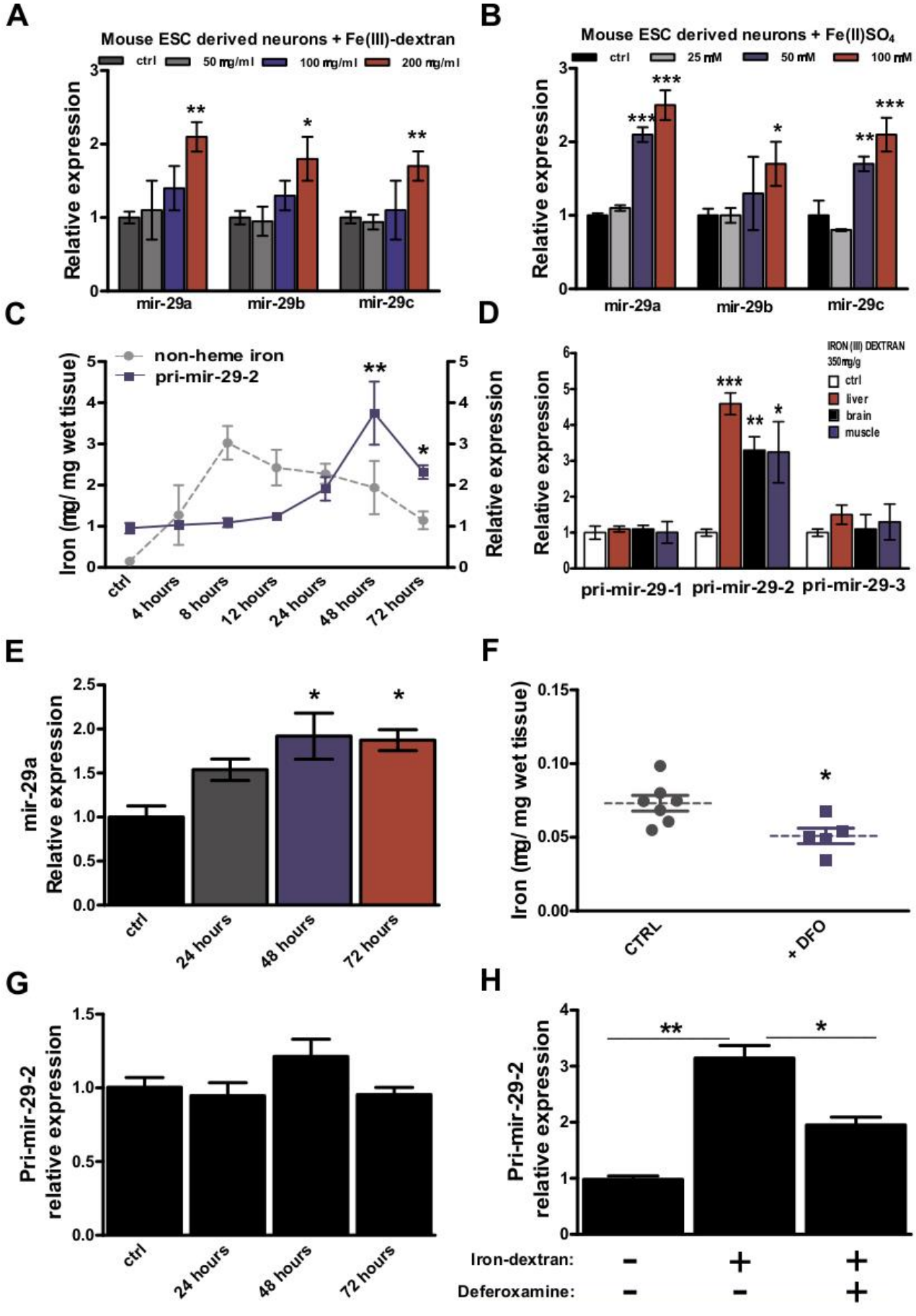
A
Mouse ESC derived neurons + Fe(III)-dextran
ctrl
50 mg/ml
100 mg/ml
200 mg/ml
Relative expression
mir-29a
mir-29b
mir-29c
B
Mouse ESC derived neurons + Fe(II)SO4
ctrl
25 mM
50 mM
100 mM
Relative expression
mir-29a
mir-29b
mir-29c
C
non-heme iron
pri-mir-29-2
Iron (mg/ mg wet tissue)
ctrl
4 hours
8 hours
12 hours
24 hours
48 hours
72 hours
D
IRON (III) DEXTRAN
350mg/g
ctrl
liver
brain
muscle
Relative expression
pri-mir-29-1
pri-mir-29-2
pri-mir-29-3
E
mir-29a
Relative expression
ctrl
24 hours
48 hours
72 hours
F
Iron (mg/ mg wet tissue)
CTRL
+ DFO
G
Pri-mir-29-2
relative expression
ctrl
24 hours
48 hours
72 hours
H
Pri-mir-29-2
relative expression
Iron-dextran:
Deferoxamine:

Figure 2.3. **Iron overload induces miR-29 up-regulation in neurons and brain. A-B**) Modulation of miR-29 family members in murine neurons derived from mESCs incubated respectively with: **A)** 0, 50µg/ml, 100µg/ml, 200µg/ml of Fe(III)-dextran or with **B)** 0, 25µM, 50µM, 100µM of $Fe(II)SO_4$ for 72 hours. Statistical significance between control and iron-treated cells was evaluated by one-way ANOVA with post-hoc Tukey's test (* = P<0,05; ** = P<0,01; *** = P<0,001), n= 3 independent experiments performed in duplicates for each condition. **C**) Time course of non-heme iron amount (quantified by colorimetric analysis) and pri-miR-29-2 expression level in fish brain (quantified by RT-qPCR) following intraperitoneal (i.p.) injection of 350 µg/g of iron dextran, control animals were injected with saline solution. Grey line represents iron amount, blue line represents pri-miR-29-2 relative expression level (setting the baseline to 1). Statistical significance for pri-microRNA expression was calculated by one-way ANOVA with post-hoc Tukey's test (*, P<0,05; **, P<0,01), n=4 biological replicates for each point. **D**) Relative expression of mir-29 primary transcripts (pri-mir-29-1, 2, 3) in liver, brain and muscle 48 hours following intraperitoneal (i.p.) injection of 350 µg/g of iron dextran. Control animals were injected with saline solution. Data were normalized on TBP expression and control animals relative expression was considered as baseline (***, P<0,001; **, P<0,01; *, P<0,05; Mann-Whitney's U-test), n= 5 biological replicates. **E**) Expression of mature *N.fu*-miR-29a at 48 hours after iron injection quantified by RT-qPCR, Mann-Whitney's U-test (*, P<0,05), n=4 biological replicates for each time point, U6 was used as normalization control. **F**) Non-heme iron quantification 24 hours after DFO i.p. injection, control animals were injected with saline solution. Statistical significance was calculated by Mann-Whitney's U-test (*, P<0,05), n= 7 control animals and n=5 DFO injected animals. **G**) Time course of pri-miR-29-2 expression level (quantified by RT-qPCR) following i.p. injection of 30 µg/g of deferoxamine (DFO), one-way ANOVA P=0,1663, n=4 biological replicates for each time point. **H**) Modulation of pri-miR-29-2 expression in fish brain (quantified by RT-qPCR) after iron overload and in combination with administration of 30 µg/g of DFO, control animals were injected with saline solution, Mann-Whitney's U-test (*, P<0,05), n=5 biological replicates. For all the graphs, mean ± standard errors of means are reported.

3.5 Genetic repression of miR-29 function

To investigate the physiological relevance of miR-29 in the regulation of iron homeostasis during adult life, I generated transgenic zebrafish and *N. furzeri* expressing a competitive inhibitor of miR-29 designed by fusing to the eGFP a 3'-UTR with seven repetitions of a miR-29 binding site (miR-29-sponge) (**fig. 2.4 A**, on the top). As a first step, I tested whether miR-29-sponge transcript was directly targeted by miR-29 family members by co-injecting them with the control RFP mRNA (as described above for miR-29 mimics) measuring the eGFP/RFP ratio by fluorocytometry. A strong repression of eGFP signal was

induced by miR-29 mimics (**fig 2.4 B**). Then, I generated a transgenic zebrafish line by placing miR-29-sponge under the control of 5,3 kb of *D. rerio* actin beta 1 promoter (tg:actb2-eGFP-sponge-29) (**fig. 2.4 A**). I then used the F1 generation to assess the functionality of the construct *in vivo*. For this purpose, I took advantage of the extremely low expression of miR-29 during the first two days of embryonic development (Chen PY *et al*., 2005) and injected increasing doses of miR-29a or miR-29b mimics, (~100pg, ~150pg and ~200pg) both in wild-type and in tg:actb2-eGFP-sponge-29. I found that both mimics induced similar effects and 200 pg of mimic induced morphological defects like brachyury, microcephaly and microphthalmia. The percentage of defective embryos was much lower in tg:actb2-eGFP-sponge-29 (**fig. 2.4 C-D**). Recent work showed that at steady-state microRNAs regulate their targets more through mRNA destabilization than by translation repression (Eichhorn SW *et al*., 2014), so I used injected embryos with lower mimic dosages (100pg and 150pg by which did not display overt morphological aberration) in order to evaluate the expression of well-known miR-29 targets. I chose as target *ELNA1* (elastin) and *COL11A1A* (collagen type XI, alpha 1a), because these are genes highly expressed in embryos bearing in their 3'-UTR 4 and 2 predicted target binding sites respectively and quantified their expression through RT-qPCR. I observed a dose-dependent down-regulation of these transcripts in wild-type, but not in tg:actb2-eGFP-sponge-29 injected embryos (**fig. 2.4 E-F**). All these data supported the notion that genetically modified fish with stable sponge overexpression could counteract miR-29 effects. Finally, I measured *IREB2* mRNA but I did not detect down-regulation after miR-29 mimic injection (**fig. 2.4 G**), however I observed a significant downregulation of *TFR1A* mRNA in wild type but not tg:actb2-eGFP-sponge-29 injected embryos (**fig. 2.4 H**). These data suggest that, in fish, miR-29 influences IRP2 translation but not *IREB2* mRNA stability.

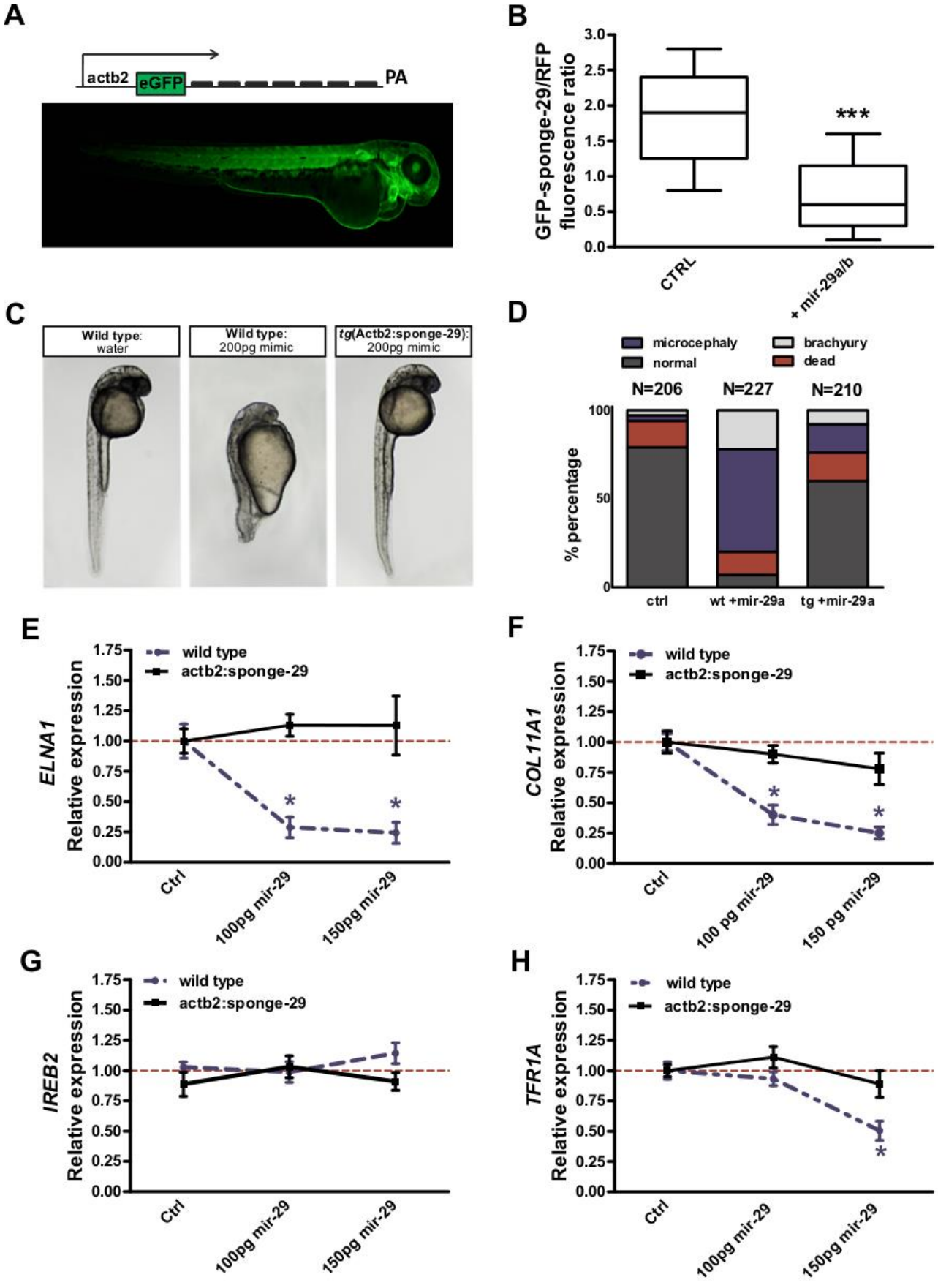
A
actb2
eGFP
PA
B
GFP-sponge-29/RFP fluorescence ratio
3.0
2.5
2.0
1.5
1.0
0.5
0.0
***
CTRL
+ mir-29a/b
C
Wild type: water
Wild type: 200pg mimic
tg(Actb2:sponge-29): 200pg mimic
D
microcephaly
normal
brachyury
dead
N=206
N=227
N=210
% percentage
100
50
0
ctrl
wt +mir-29a
tg +mir-29a
E
ELNA1
Relative expression
wild type
actb2:sponge-29
1.75
1.50
1.25
1.00
0.75
0.50
0.25
0.00
Ctrl
100pg mir-29
150pg mir-29
F
COL11A1
Relative expression
wild type
actb2:sponge-29
Ctrl
100 pg mir-29
150 pg mir-29
G
IREB2
Relative expression
wild type
actb2:sponge-29
Ctrl
100pg mir-29
150pg mir-29
H
TFR1A
Relative expression
wild type
actb2:sponge-29
Ctrl
100pg mir-29
150pg mir-29

Figure 2.4. Genetic repression of miR-29 function by sponge technology. A) Transgenic sponge-29 zebrafish are generated by Tol2-mediated transgenesis, expression cassette consist of 5,3kb of zebrafish actb2 promoter, eGFP fused to a synthetic 3'UTR containing 7 repetition of miR-29 binding site and a SV40 late poly-A tail. The image shows a F1 embryo (72 hours post fertilization) and the ubiquitous expression of eGFP-sponge throughout the body. **B**) Fluorescence cell analysis from 30-40 embryos for each condition. eGFP mRNA fused with sponge-3'UTR was injected in zebrafish embryos along with or without dre-miR-29 mimics. RFP mRNA was injected as loading control. MiR-29 mimics strongly reduced eGFP-sponge signal (***, P<0,001, T-test). Whisker plots indicate the 10%, 25%, median, 75% and 90% ranges. **C-D**) Wild-type and F1 transgenic zebrafish were injected with 200pg of miR-29a or miR-29b mimics at the one cell stage, control embryos were injected just with water and red-phenol. Picture (C) shows representative control embryos, wild-type embryos +200pg mimics, transgenic embryos + 200pg mimics at 24hpf. Stacker bar chart (D) represents the percentages of embryos with different phenotypes (normal, death, microcephaly and brachyury) in the three conditions. **E-H**) Expression level at 24 hours post-fertilization of *COL11A1*, *ELNA, IREB2* and *TFR1A* upon miR-29 mimics injections. One-stage wild-type and sponge-29 line were injected with different doses (100 and 150 pg) of microRNA mimics and the expression level determined by RT-qPCR. Statistical significance was assessed by one-way ANOVA with post-hoc Tukey's test (* = P<0,05), the analysis was performed on total RNA extraction from 30-40 embryos for each condition. Error bars indicate standard errors of means.

3.6 MiR-29 deficiency induces iron imbalance during adult life

Once established that miR-29 sponge counteracts the endogenous miR-29 activity *in vivo* and could perturb regulation of iron-management genes, I investigated the effects miR-29 down-regulation on iron homeostasis in neuronal cells during adult life. To this end, I isolated from zebrafish genomic DNA a 3.1 Kb neuronal specific promoter Dre-kif5a (kinesin 5a), in order to limit miR-29 attenuation to mature neurons. Kif5a promoter fragment was sufficient to maintain the expression of eGFP-sponge-29 throughout life both in zebrafish and *N. furzeri*. Since zebrafish life expectancy is of about five years (Gerhard GS *et al*., 2002), I decided to generate a stable line in *N. furzeri* in order to investigate more rapidly the consequences of miR-29 depletion during adult life. *N. furzeri* F1 fish exhibited a stable expression over time (**fig. 2.5 A-C**) and a double labeling with eGFP and HuC/D proved the neuronal specificity of the expression pattern (**fig. 2.5 D**). I did not observe any macroscopic defects, but a reduced fertility, and a reduced post hatch survival that limited the number of animals that could be analyzed. It should be noted that a full knock-out of miR-29 is postnatally lethal in the mouse, so reduced

viability is expected and the fact that some transgenic fish reached adulthood could be due to the incomplete antagonism of miR-29 by the sponge construct. Following the initial hypothesis that neuronal miR-29 deficiency could lead to a dysregulation of iron homeostasis, I first measured by Western blot the expression of IRP2 and TFR1A in young adult (12 weeks old) wild type and transgenic fish. As expected, both proteins were found up-regulated as compared to control animals (**fig. 2.6 A**). In addition, I assessed IRP2 level also in 5 months old zebrafish kif5a:sponge-29 line brain confirming its up-regulation (**fig. 2.6 B**). I then measured IRP2 levels at 5, 12, 20, 27 weeks of age in sponge-29 line. As compared to wild type fish, I found a similar expression in young age (5 weeks), but when fish grew old, the relative protein level remained largely deregulated in genetically modified fish, indicating that miR-29 significantly influences the down-regulation of IRP2 expression during adult life (**fig. 2.6 C**). Therefore, I measured both iron-management genes expression and iron content in young adult 12 weeks old wild type and kif5a:sponge-29 fish. I quantified by RT q-PCR the expression of *IREB2*, *TFR1A*, *FTH1A*, *SLC401A*, *SLC11A2*, but I found a significant difference (up-regulation) for *TFR1A* only (**fig. 2.6 D**). This is consistent with the notion that iron homeostasis in neurons is regulated mainly by TFRC since neurons intake iron in the form of transferrin-bound iron released by the astrocytes (Rouault, 2013) and variations of TRF1A expression would have the largest consequences on neuronal iron homeostasis. Finally, I quantified non-heme iron content and this was significantly increased as compared to wild type (**fig. 2.6 E**), suggesting that miR-29 deficiency accelerates iron in-take over time.

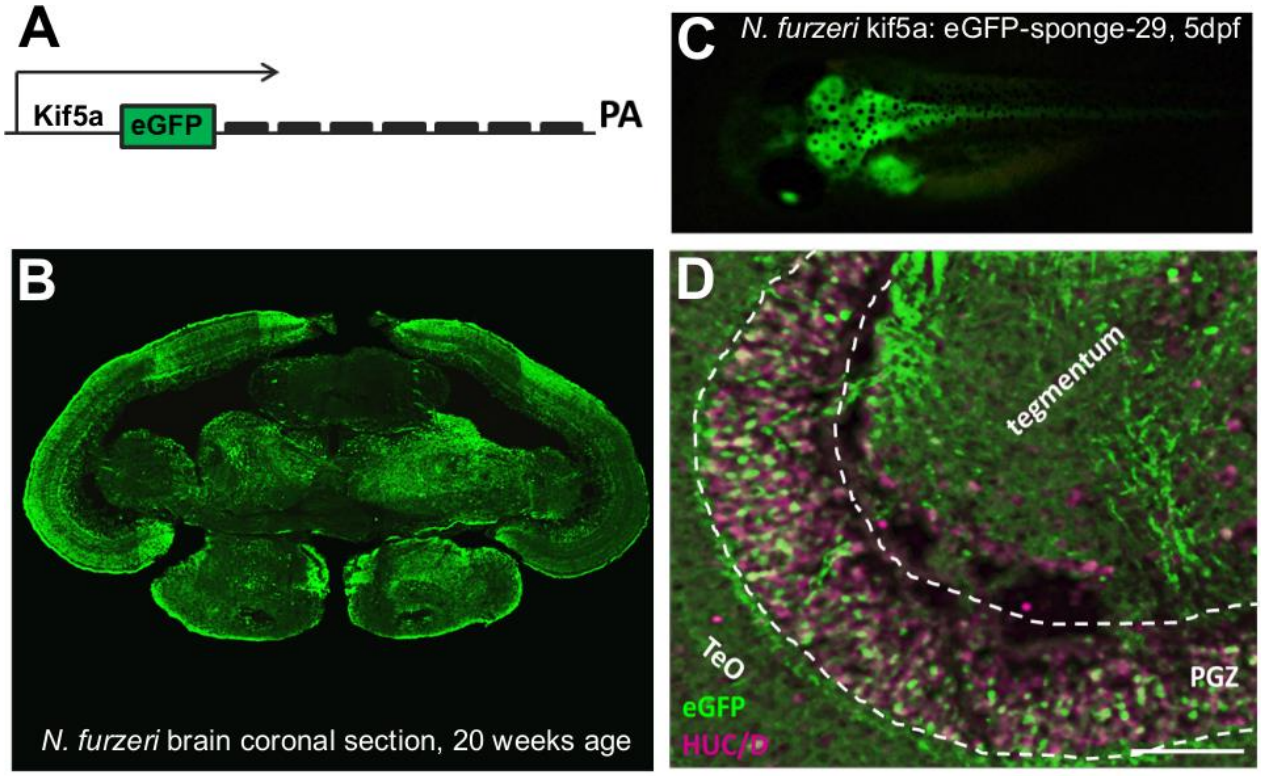

Figure 2.5. Genetic repression of miR-29. **A**) Schematic representation of the kif5a:eGFP-sponge-29 expression cassette. **B**) Brain coronal section with an eGFP immunohistochemistry of kif5a:eGFP-sponge-29 F1 20 weeks-old N. furzeri. **C**) F1 *N. furzeri* line 5 days after hatching. **D**) Representative double-labelling immunohistochemistry for eGFP (green) and neuronal marker HuC/D (pink) in optic tectum of 20 weeks old kif5a:sponge-29 fish. Periventricular gray zone (PGZ), Tectum opticum (TeO). Scale bar: 100µm.

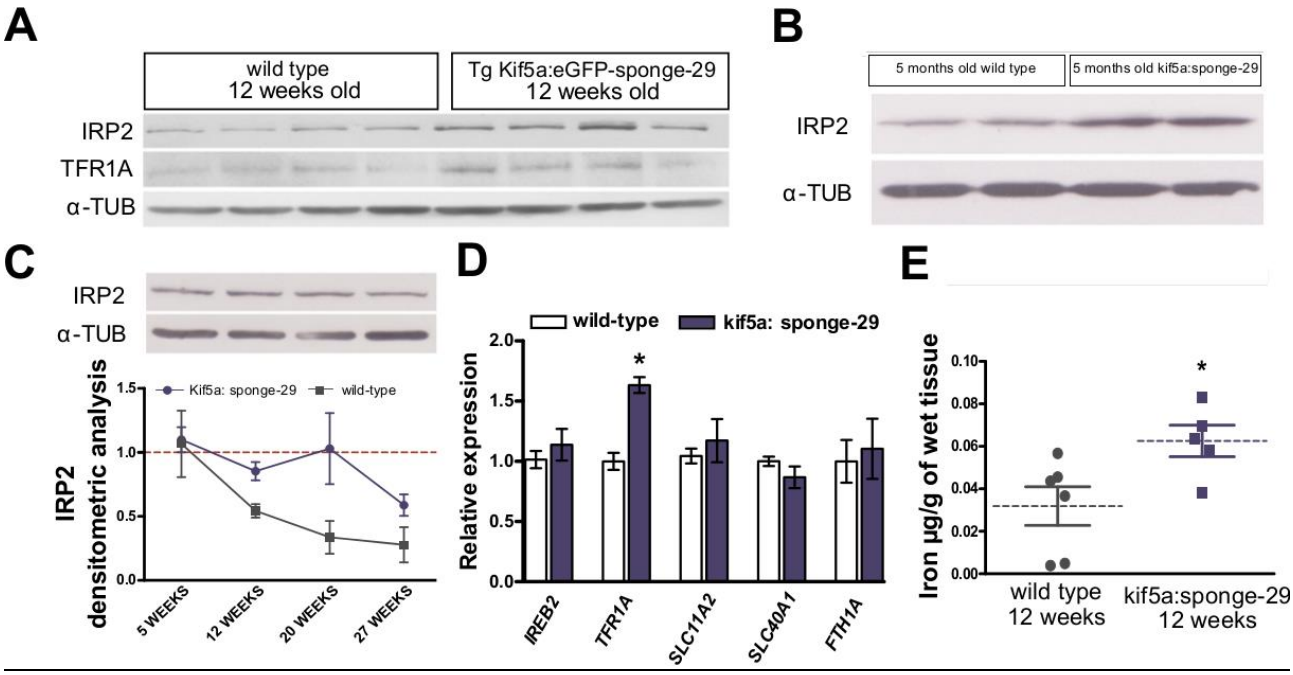

Figure 2.6. Mir-29 loss of funtion affects iron homeostasis during adult life A) Western blot of IRP2 and TFR1A in 12 weeks old kif5a:sponge-29 (n=4) and wild-type (n=4) fish brain extracts. **B**) Representative Western blot of IRP2 in zebrafish brain extracts of 5 months old kif5a:sponge-29 and wild type animals. α-tubulin was used as loading control. **C)** On the top representative Western blot of IRP2 in brain extracts of kif5a:sponge-29 at different ages (5, 12, 20, 27) and relative densitometric analysis on the bottom. The solid blue line represents expression in kif5a:eGFP-sponge-29 animals, values were normalized to the mean of 5 weeks values, n=3 biological replicates for each time point. ANOVA for trend: R= 0,2871, P=0,0691. The gray line represents values reported in fig. 2.1-F. **D**) Expression levels of iron management genes measured through RT-qPCR in kif5a:eGFP-sponge-29 as compared to wild type. *TFR1A* alone was found de-regulated (*, P<0,05, Mann-Whitney' s U-test), n=5 biological replicates. **E**) Brain non-heme iron content (μg/g wet tissue) in kif5a:eGFP-sponge-29 (n=5) compared to wild type (n=6) at age 12 weeks (*, P<0,05, Mann-Whitney' s U-test).

3.7 MiR-29 antagonism exacerbates aging phenotypes in *N. furzeri* brain

To further elucidate the physiological consequences of miR-29 deficiency and, in turn, accelerated iron accumulation in adult brain, I analyzed the global gene expression profile through RNA-seq. I compared the expression profile of 12 weeks old transgenic fish with 12 weeks old wild type fish, using four biological replicates for experimental group. I detected 1305 differentially-expressed genes (DEGs, FDR < 0.05, edgeR). I performed a KEGG pathways analysis on all DEGs. Among up-regulated DEGs I found an over-representation of genes involved in energy production processes such as oxidative phosphorylation and TCA cycle, including genes that encode for proteins known to be influenced by iron. In particular, Oexle et al. (1999) showed that iron affects the activity of citrate synthase (*CS*), aconitase 2 (*ACO*2), isocitrate dehydrogenase 3 (NAD+) beta (*IDH3B*), succinate dehydrogenase complex, subunit A (*SDHA*), three of these genes *(ACO*2, *IDH3B, SDHA*) are up-regulated in transgenic fish (**fig. 2.7 A**). Moreover, among up-regulated DEGs, I found also ribosome biogenesis, lysosome, phagosome and endoplasmic reticulum functions as well as downstream p53 effectors (**fig. 2.7 A**) and an overrepresentation among down-regulated DEGs for genes involved in intracellular and extracellular remodeling, circadian rhythm and the following pathways: JAK-STAT, MAPK, WNT and Notch (**fig. 2.7 B**). Several of these pathways were previously reported to be regulated in the *N. furzeri* brain during aging (see Baumgart M et al., 2014; Reichwald K et

al., 2015). Remarkably, the majority of these showed the same direction of regulation during aging and in response to miR-29 antagonism (red asterisk, **fig. 2.7 A-B**) and only a minority, showed opposite directions of regulation (black asterisk, **fig. 2.7 A-B**). Moreover, in a longitudinal study of *N. furzeri*, Baumgart et al. (2016) reported that higher expression of genes belonging to the oxidative phosphorylation, phagosome, lysosome, ribosome biogenesis and RNA transport pathways is negatively correlated with lifespan. On the other hand, higher expression of ECM-receptor interaction genes is positively correlated with lifespan (Baumgart M et al., 2016). I found that miR-29 antagonism induces an up-regulation of those pathways negatively correlated with lifespan (marked with a grey minus in **fig. 2.7 A-B**), with the exception of RNA transport and spliceosome pathways and a down-regulation of the only pathway positively correlated with lifespan (marked with a plus in **fig. 2.7 A-B**). Among up regulated DEGs, I found 25 genes negatively correlated and 3 positively correlated with lifespan (**fig. 2.7 C**), among down-regulated DEGs, I found 9 genes negatively correlated and 15 positively correlated with lifespan (**fig. 2.7 C**). I interpreted these data as a signature of accelerated aging. To corroborate my hypothesis, I repeated the analysis at the gene level. I intersected the sets of DEGs of sponge-29 transgenic fish and aging (obtained by comparing gene expression of 5 weeks vs. 39 weeks old fish; Baumgart et al., 2014). The intersection contains 525 genes (**fig. 2.7 D**) and 456 (~87%) show the same direction of regulation in aging and miR-29 sponge ($p<10^{-16}$, χ^2 test). Of those, 225 are up-regulated (Type 1 genes, **fig. 2.7 E**) and 231 are down-regulated (type 3 genes, **fig. 2.7 E**) in both cases. Only 68 genes (~13%) showed opposite regulation: 34 down-regulated in sponge-29 and up-regulated during aging (type 2, **fig. 2.7 E**) and 34 with the opposite behavior (type 4, fig. **7E**). Surprisingly, type 4 genes contained, in addition to *TFR1A*, other iron management genes such us the ferroxidase ceruloplasmin (*CP*) and transferrin a (*TFA*), confirming again the relationship between miR-29 and iron. Furthermore, I assessed the expression profile of those genes with a conserved predicted binding site for miR-29. To this end, I retrieved a list of *D. rerio* 548 predicted targets (score ≤ -0,30) from TargetScanFish 6.2 (Ulitsky et al*.,* 2012). Out of those, 38 genes were DEGs in

kif5a:sponge-29 *N. furzeri* fish: 28 up-regulated and 10 down-regulated (fig. S7A). 22/28 *N. furzeri* ortholog up-regulated genes exhibited a conserved binding site (**fig. 2.8**). For 10/28, the miR-29 predicted binding site was conserved also in the mouse and human orthologs and for 5 of these an interaction with miR-29 was observed also by cross-linking immunoprecipitation (CLIP)-seq (**fig. 2.8**). Here, as expected in accordance with the literature, I found genes involved in epigenetic reprogramming: Lysine-Specific Demethylase 6B (*KDM6BB)*, DOT1-like, histone H3 methyltransferase (*DOT1L)*, Enhancer of polycomb homolog 1 (*EPC1*), glutamate metabolism: Glutamate receptor-interacting protein 1 (*GRIP1*), IGF1 signaling: insulin-like growth factor binding protein 2a (*IGFBP2A*). Curiously, among down-regulated DEGs I found well-known mammalian miR-29 targets like: Ten-eleven translocation methylcytosine dioxygenase 3 (*TET3*), DNA (cytosine-5)-methyltransferase 3ab (*DNMT3AB*) and collagen type IV alpha 1 (*COL4A1*). Thus, I examined which was the effect of aging on conserved miR-29 predicted targets. Of 22 up-regulated targets 6/22 were found in type 4 dataset, 12/22 were not regulated by aging, indicating that for those miR-29 could directly influences their expression at transcriptional level. On the other hand 4/22 up-regulated and 9/10 of down-regulated targets were found respectively in type 1 and type 3 dataset (**fig. 2.8**), indicating that probably the global effect of miR-29 depletion on aging is prevalent over the target-specific effect of miR-29. Finally, I analyzed 12 weeks old brains of kif5a:sponge-29 and wild type fish at histological level. Kif5a:sponge-29 fish exhibited an increased accumulation of the aging marker lipofuscin as compared to wild-type (**fig. 2.9 A-B**), a marker of oxidative damage especially against cell or mitochondria membranes (Brunk and Terman, 2002) that is up-regulated in conditions of iron overload (Johnston and Milward, 2010; Johnston et al., 2012). Moreover, I observed an increased immunoreactivity for glial markers GFAP and S100β (**fig. 2.9 C-D**). Overall, these data strongly indicated that miR-29 family regulates brain iron metabolism during adult life and its deficiency induces the exacerbation of some aspects of the aging phenotype.

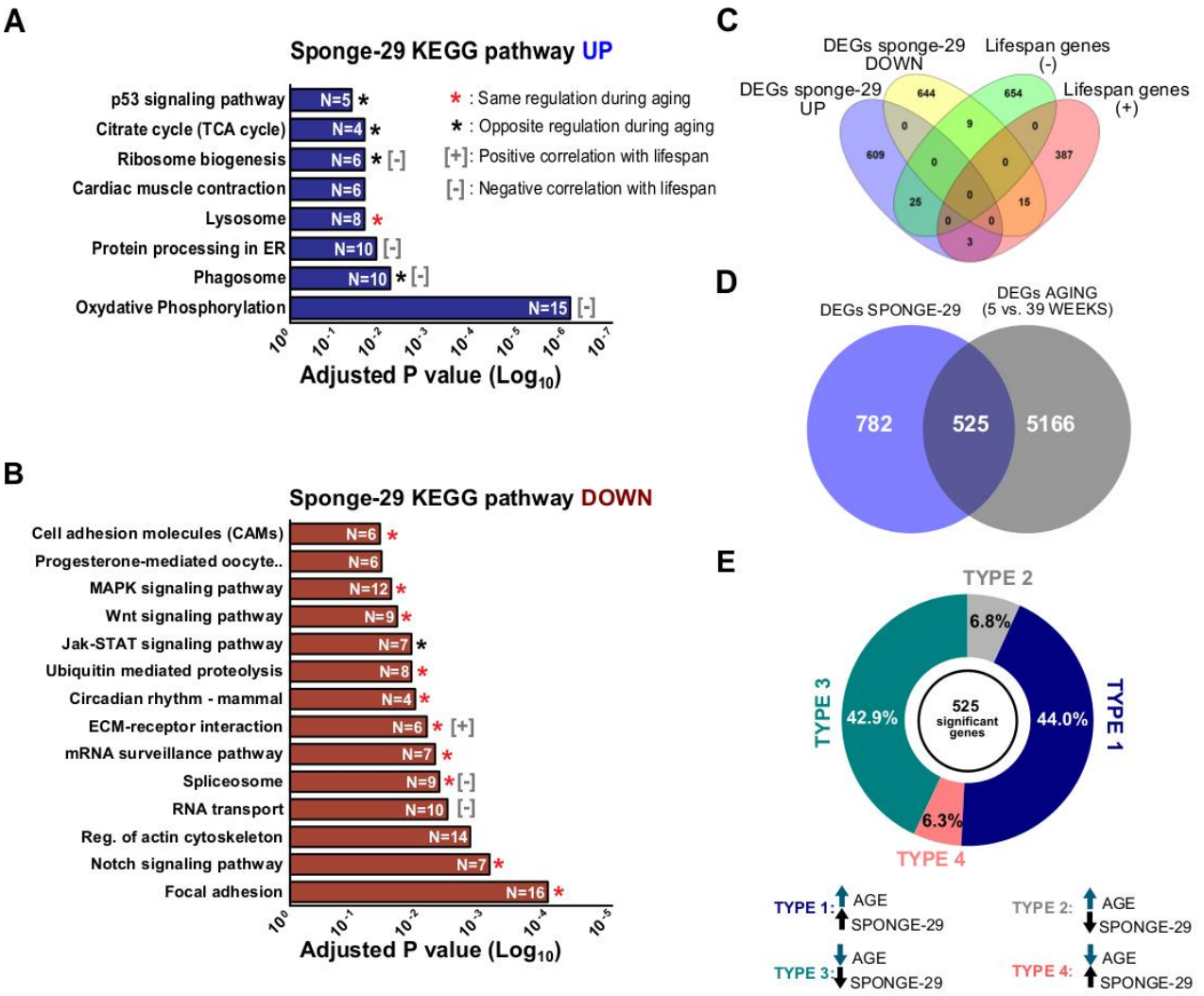

Figure 2.7. **MiR-29 antagonism partially recapitulates aging._A-B**) KEGG pathway overrepresentation analysis on DEGs (FDR≤0,05). The red and black asterisks indicate categories of DEGs regulated with age in the brain (from Reichwald et al., 2015). Red colored asterisk indicates categories that exhibit the same direction of regulation both in aging and sponge-29. Black colored asterisk indicates those with opposite regulation. Gray plus and minus symbols represent categories that positively and negatively correlates with lifespan respectively (from Baumgart *et al*., 2016) **C**) Venn diagram illustrating the intersection between up and downregulated DEGs in sponge-29 and genes positively and negatively correlated with lifespan respectively (P=0,0007 and P=0,0049, Fisher exact test) **D**) Venn diagram illustrating the intersection between DEGs during aging and DEGs in sponge-29. **E**) Correlation analysis of fold-changes of genes in the intersection shown in (D). Pie chart represents the fraction of genes coherently or incoherently regulated by aging and sponge-29.

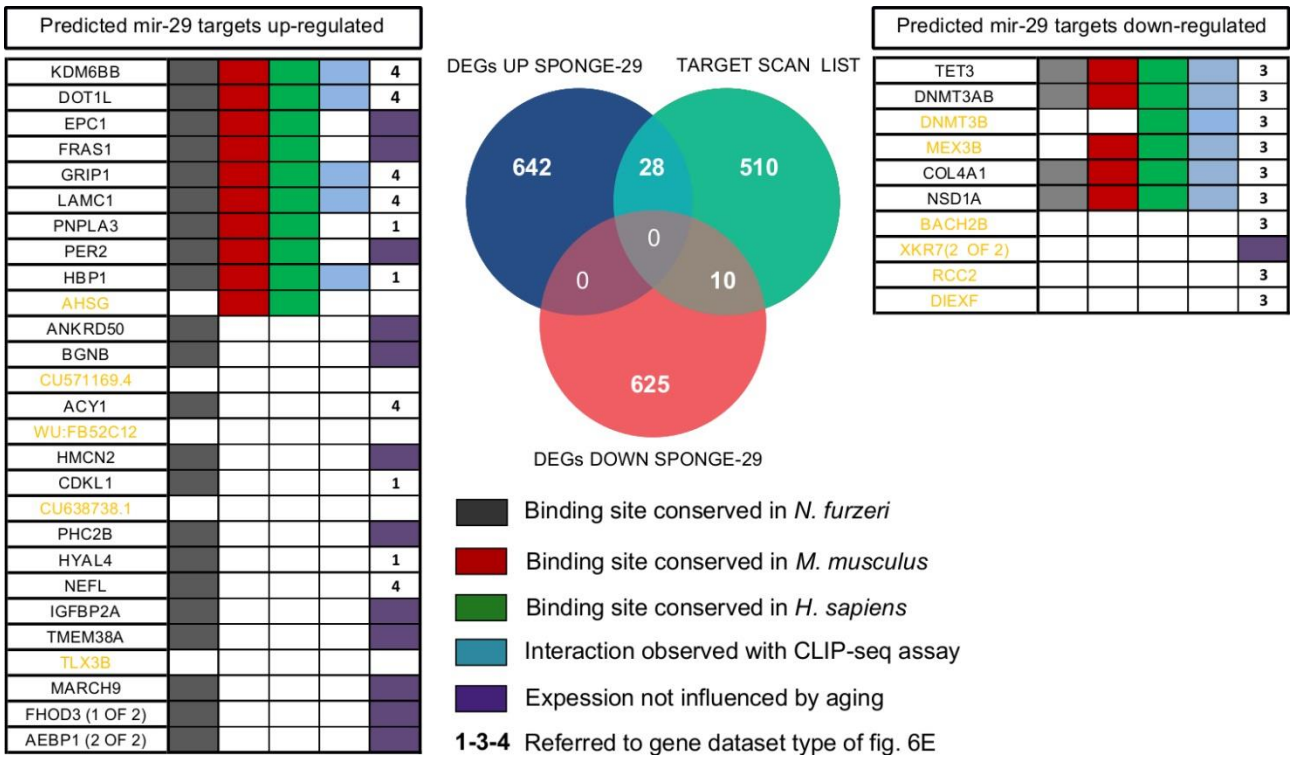

Figure 2.8. Mir-29 predicted target DEGs identification in *N.furzeri* kif5a: sponge-29. In the middle intersection of *D. rerio* mir-29 predicted target genes (from TargetScanFish 6.2, score ≤ -0,30) with *N. furzeri* sponge-29 DEGs. A total of 38 predicted target genes were found deregulated in kif5a:sponge-29 fish, 28/38 upregulated (table on the left) and 10/38 downregulated (table on the right) respectively. Gray, red and green box represent a conserved binding site in the 3'UTR of *N. furzeri*, *M. musculus*, *H. sapiens* respectively. Yellow colored genes lack of a conserved binding site in *N. furzeri*. Light blue box indicate a physically interaction between target gene e and mir-29 observed by cross-linking immunoprecipitation (CLIP-seq). 1-3-4 numbers are relative to gene dataset type in figure 2.7 E.

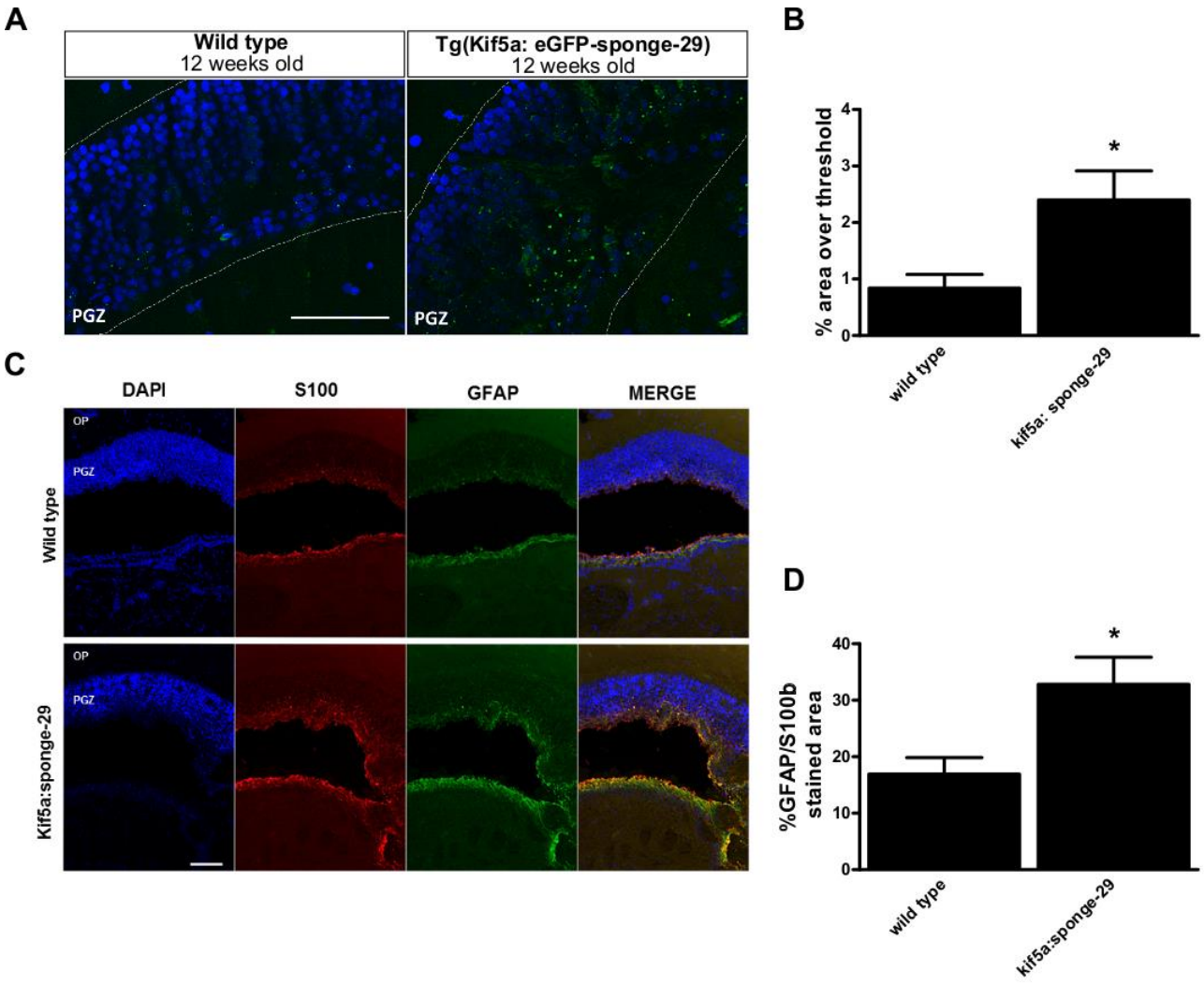

Figure 2.9. **miR-29 deficiency induces lipofuscin accumulation and gliosis A**) Representative images of lipofuscin accumulation in the optic tectum of 12 weeks old kif5a:eGFP-sponge-29 and wild type fish brains. Lipofuscin auto-fluorescent granules (green) were detected with ApoTome microscope, counterstained with DAPI (blue). Scale bar: 50µm. **B**) Quantification of lipofuscin density based on percentage of area over threshold, n=6 (*, P<0,05; Mann-Whitney' s U-test). **C**) Representative images of immunoreactivity for GFAP and S100β markers in the optic tectum of 12 weeks old kif5a:eGFP-sponge-29 and wild type fish brains. **D**) Quantification of GFAP/S100β intensity per area of section. The analysis was performed in n=5 wild type and n=5 kif5a:sponge-29 fish brains (*, P<0,05, Mann-Whitney' s U-test). Scale bar 100µm.

4 DISCUSSION

In this study, I investigated the effects of miR-29 regulation on iron metabolism during adult life in the brain of the short-lived vertebrate that can be cultured in captivity *N. furzeri*. Expression of miR-29 is known to be upregulated during brain aging in vertebrates, here I report that: i) brain iron content increases with age; ii) miR-29 expression is induced by iron overload; iii) miR-29 negatively regulates the expression of *IREB2* gene in neurons during adult life; iv) miR-29 antagonism results in a chronic up-regulation of IRP2 and TFR1A resulting in increased brain iron deposition; v) transcriptome profile revealed an increased expression of TCA cycle and oxidative phosphorylation genes along with enhanced aging-related phenotype upon miR-29 antagonism vi) histological analysis revealed enhanced gliosis and lipofuscin deposition. These data demonstrate that up-regulation of miR-29 during aging is a compensatory response to limit an excessive age-dependent iron accumulation which can actively contribute to cell and tissues decline.

4.1 Iron imbalance during normal aging

Here, I report that iron accumulates during adult life in killifish brain as previously described in mammals and histological analysis revealed deposition both in the gray and white matter. As a consequence, the intracellular iron delivery pathway (IRP2-TFR1A) was reduced through downregulation of IRP2 and *TFR1A* and *SCL11A2* mRNAs. These results suggest that, during adult life, iron deposition increases and in turn influences the expression level of iron-management genes although the mechanisms responsible for this phenomenon are yet unknown. Since iron is a key molecule for a broad number of metabolic activities, it is reasonable to assume that iron accumulation might result as a consequence of the age-dependent decline of metabolic activity in brain cells and in turn, as adaptive response, the intracellular-iron delivery pathway is consistently reduced.

Since iron accumulation was described also during normal aging of humans and other mammals species, like primates and mice, it is debated whether this is just an epiphenomenon or it can contribute to the aging-induced dysfunctions and in particular to cognitive decline. Although we did not investigate this particular aspect in killifish, a wealth of publications strongly suggest that increased iron deposition correlates with cognitive and motor declines. For instance, in human subjects quantitative magnetic resonance imaging (MRI) revealed that iron concentration in specific brain nuclei (mostly in basal ganglia) negatively correlates with performance in different types of cognitive tests during normal aging (Ghadery et al., 2015; Penke et al., 2012). Moreover, administration of iron to mice or rats has consistently resulted in cognitive deficits (Maaroufi et al., 2009; Schröder, Figueiredo, & de Lima, 2013). Finally, it has been observed that iron chelation attenuates cognitive deficits in multiple animal models of aging-related cognitive dysfunction (de Lima et al., 2008). Therefore I can conclude that: i) since age-dependent iron accumulation occurs in different vertebrate species (from fish to mammals) with large differences in lifespan, physiology and anatomy, it can be considered a robust aging hallmark and, ii) since iron amount negatively correlates with neuronal performance, its amount is a marker of neuronal damage.

4.2 mir-29 acts independently to FBXL5 in regulating IRP2 and intracellular iron availability during aging

IRP2 is an RNA-binding protein that acts as master regulator of intracellular iron availability in the brain, therefore influencing both energy production and redox status of cells. IRP2 is rapidly degraded when iron increases via allosteric activation of FBXL5 and this regulation defines a set point for physiological intracellular iron concentrations. Despite this negative feedback regulation, iron accumulates in the brain during aging in *N .furzeri* as previously shown in mammals. Since IRP2 is reduced during aging and iron increases, it was expected to observe an age-dependent increase of FBXL5 protein. FBXL5, however, it is not regulated by age. This observation could suggest that age-

dependent iron accumulation is not observed in the cytosol but rather in other subcellular compartments, most likely mitochondria. This could explain why, even if iron increase with age, FBXL5, a cytosolic iron-sensor, and ferritin (*FTH1*A), do not increase as a consequence. For instance, Seo *et al.* reported that iron accumulates with age in muscle and liver mitochondria of rats (Seo et al., 2008), and recently *Clonan et al*. observed in lung cells that to IRP2 increased level corresponds increased iron deposition specifically in mitochondria without FBXL5 modulation (Cloonan et al., 2016). In view of these considerations, during aging, mir-29 could regulate IREB2 expression independently of FBXL5. The evolutionary conserved mir-29 binding site on *IREB2* 3'-UTR and the experimental validations here reported demonstrate that mir-29 is required for iron homeostasis regulation. In fact, I showed that mir-29 loss of function leads to up-regulation of the IRP2-TFR1 axis and an increased iron accumulation, even in presence of FBXL5. So, I can conclude that, since under physiological conditions iron accumulates escaping the FBXL5-mediated control, mir-29 could be an adaptive response to prevent excessive iron accumulation and damage. The mechanism of action of mir-29 works is different from FBXL5. Indeed, mir-29 chronically reduces *IREB2* translation starting from young-adult age through the all adult life. Moreover, FBXL5 level is influenced both by iron depletion and supplementation. On the contrary, mir-29 expression is affected only by iron load. In fact, reducing iron by 25% with DFO does not change miR-29 expression in the following 72 hours. The same dose of DFO, however, reduced miR-29 up-regulation if provided hours after iron injections when intracellular iron levels are already within the pathological range. Another important difference is that FBXL5 stability is directly and rapidly regulated by iron concentration, instead iron induces mir-29 at the transcriptional level, implicating the requirement of a transcription factor. Therefore on one hand FBXL5 is affected only by intracellular iron level and is activated only during cytosolic iron oscillation, on the other hand mir-29 seems to be activated by a more complex and indirect mechanism that operates on slower temporal scales. Although I did not investigate which are the mediators that induce mir-29 up-regulation upon iron loading or during aging, it was observed recently in mice that mir-29 is positively regulated by the

transcription factor NRF2 (Kurinna et al., 2014). NRF2 emerged as a master regulator of oxidative stress and it is required to protect cell against iron-mediated injury in liver and astrocytes (Cui et al., 2016; Silva-Gomes et al., 2014). Moreover, it has been shown that elevated hepatic iron activates NRF2 (Moon et al., 2012) and NRF2 knockout mice have a deregulated expression of iron-management genes (Tanaka, Ikeda, Yamamoto, Ogawa, & Kamisako, 2012). Finally, since the principal function of NRF2 is to regulate mitochondria ROS production, mir-29 up-regulation might occur as a consequence of a change in mitochondria redox state induced by age-dependent iron accumulation.

4.3 mir-29 loss of function accelerates the aging process

It was previously reported in *Drosophila* that mir-34 is up-regulated with age and regulates age-associated events and long-term brain integrity. Its loss of function induced neurodegeneration and a gene expression profile of accelerated brain aging while overexpression induced life-extension (Liu et al., 2012). This work reveled that a single microRNA can exert a compensatory action during the aging process. Here, for the first time, I report the case of vertebrate system where neuronal specific perturbation of a microRNA induced iron imbalance and accelerated expression of aging phenotypes, both at the level of global gene expression and histological markers. Mir-29 is extremely conserved among vertebrate species, it is one of the most expressed microRNA family, its age-dependent expression is evolutionary conserved from fish to humans and finally, in the brains of both in fish and in mammals, mir-29 expression increases dramatically only after embryonic development. Further, forced expression of miR-29 in immature neurons accelerates their maturation (Kole et al., 2011) and computational analysis in primate cortex showed strong negative correlation between expression of miR-29 and its targets during postnatal development (Somel et al., 2010). All these data strongly suggest that mir-29 could play a pivotal role in regulating age-dependent gene expression. I showed that, in the fish brain, the age-modulated mir-29 cluster is mainly expressed in neuronal cells. This is different to mammals, where miR-29 is expressed both in neurons and glia

(Hebert et al., 2008). However, fish glia retains the characteristic of adult stem cells (radial glia) and this could explain this difference. As neurons are post-mitotic cells with limited regenerative potential, an individual neuron must have the capacity to survive for the organism's entire life, a period that in humans can last a century. Considering that neurons are likely to be exposed to a variety of stresses during this period, one might expect mature neurons to have evolved multiple mechanisms to ensure their long-term survival. Iron imbalance is obviously stressfull for neurons, due to its extreme toxicity, for this reason it is strictly regulated. Astrocytes and microglia are the principal iron storages within ferritin (FTH) in the CNS and release iron into the CSF though the action of ferroportin (FPN). In the CSF, iron is always bound to transferrin and absorbed by neurons through the transferrin receptor (TFR) expressed on their membrane. Since neurons exhibit a strong immunoreactivity for TFR, and low for FTH and FPN (Moos, 1996), is thought that neurons tend to have as less iron as possible and regulates iron availability mainly through the modulation of TFRC (Rouault & Cooperman, 2006). Therefore only the iron amount required for their metabolic activity from surrounding environment is taken-up. In this context, the physiologic function of mir-29 is to reduce the only mechanism of neuronal iron uptake (TFR). When iron starts to accumulate during adult life, likely due to metabolic activity failure, up-regulation of miR-29 shields neurons from probably the most dangerous source of ROS production. Neuronal specific mir-29 loss of function leads therefore to increase iron accumulation, lipofuscin deposition and a gene expression profile of accelerated aging. Although I do not provide a formal proof for a causal relationship between increased iron and accelerated aging, I can consider that the iron imbalance induced by mir-29 loss of function has a predominant role. In fact, TFR, which is the only factor within neurons that regulates their iron availability, resulted chronically up-regulated, in the sponge transgenic line. Consequently, neurons have been exposed to an increased dose of iron compared to normal animals for their entire life and lipofuscin deposition proved an increased oxidative stress in their CNS. Moreover, my hypothesis is strongly supported by experiments in *C. elegans*. Klang and colleagues (Klang IM et al., 2014) indeed reported that in *C. elegans* dietary iron significantly accelerates the onset of

aging-related phenotypes, reduces the lifespan expectancy and increases the age-dependent protein aggregation. Strikingly, they reported that TCA cycle and oxidative phosphorylation proteins as the most representative categories affected by iron-induced aggregation. Sponge-29 lines exhibited up-regulation of the same categories at gene expression level. Overall, these data suggest two important considerations: i) the transcriptional up-regulation of such categories represents a compensatory response to iron induced damages on mitochondria protein, thus up-regulation of these categories also means a worsened mitochondria integrity. This result has a profound implication with aging and lifespan, indeed Baumgart showed that increased expression of oxidative phosphorylation genes (in particular those of complex I) negatively correlates with killifish lifespan (Baumgart et al., 2016). ii) iron principally compromises mitochondria activities, corroborating the idea that the age-dependent iron accumulation occurs in the mitochondria and that mir-29 sustains mitochondria integrity through regulation of iron homeostasis. It is unlikely, however, that the effects of miR-29 antagonism on aging are entirely mediated by iron and do not involve other pathways that are also directly targeted by this pleiotropic miRNA (e.g: epigenetic reprogramming, matrix remodeling). Overall, these data suggest that: i) loss of iron homeostasis gives a significant contribution to the normal aging process in vertebrates. ii) miR-29 is an important hub for preventing aging effects and iii) iron metabolism regulation is part of the protective action exerted by miR-29. My data are in agreement with several independent reports on the protective role of this microRNA: miR-29 promotes neuronal survival in conditions of acute neuronal injury such as ischemia (Khanna S et al., 2013), miR-29 deficiency in mice induces neuronal loss in the cerebellum (Papadopoulou AS et al., 2015), an area where miR-29 is strongly expressed in *N. furzeri* as well, and most importantly, excessive iron accumulation and down-regulation of miR-29 are both associated to Alzheimer's disease (Smith MA et al., 1997; Hebert SS et al., 2008; Smith MA et al., 2010; Wang WX et al., 2011;). My data suggest that these two phenomena are linked and iron accumulation in AD is a consequence of (or at least is exacerbated by) reduced miR-29. All these data, combined with the evolutionary conserved age-dependent regulation of miR-29,

reinforce the general concept that it expression is up-regulated to exert a protective action in the aging brain.

5 CONCLUSIONS

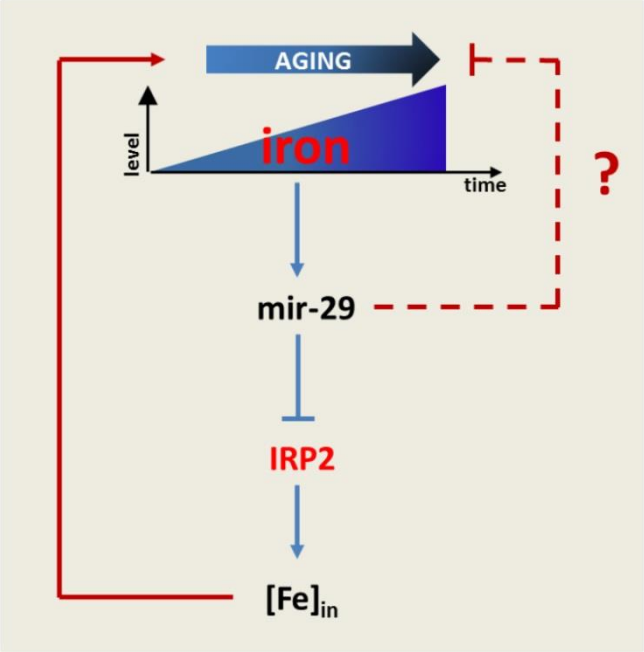

Figure 3.0: **miR-29 counteracts aging process**. A model of miR-29 function in iron metabolism. In response to the age-dependent iron accumulation, miR-29 expression increases and represses IRP2 by limiting excessive intracellular iron accumulation. This represents a compensatory response primed by cells in order to maintain cellular iron homeostasis and slow down the decline progression. Iron homeostasis regulation is likely one of several mechanisms by miR-29 prevents aging-induced physiological decline.

Age-related damage accumulation is an inescapable condition that tends to change cellular homeostasis, on the other hand cells tend to maintain their homeostasis inducing a progressive and adaptive response in order to counteract this inevitable process and preserve their physiological functions. Age-dependent up-regulation of miR-29 is part of this adaptive response, its deficiency leads to exacerbation of aging-induced damage partly due to impaired iron homeostasis (**figure 3.0**).

6 MATERIALS AND METHODS

6.1 Fish maintenance

Nothobranchius furzeri: all experiments were performed on group-house *N. furzeri* of the MZM-04/10 strain. The fish used were raised in 35L tanks at 25°C and were fed two to three times a day with frozen Chironomus larvae or living nauplii of *Artemia salina*, depending on size. Eggs were collected by sieving the sand with a plastic net and kept in wet peat moss during developmental processes and diapauses. Embryos were hatched by flushing the peat with tap water at 16–18°C. Embryos were scooped with a cut plastic pipette and transferred to a clean vessel. Fry were fed with newly hatched Artemia *nauplii* for the first 2 weeks and then weaned with finely chopped Chironomus larvae.

Danio Rerio: all experiments were performed on the Ab strain. Fish were maintained at 28°C under continuous flow in zebrafish facility with automatic control for a 14-hour light and 10-hour dark cycle (Zebtech system). To generate embryos for injection, male and female fish were placed the night before injection in a one liter fish tank with the inner mesh and divider. Zebrafish embryos were obtained from natural spawning by removing the divider and light stimulation.

6.2 Vectors design and generation of transgenic lines

For the generation of all transgenesis vectors, I used multisite gateway technology (Kwan MK et al., 2007). Design of vector (kif5aa: EGFPCAAX-SPONGE-29-SV40pa): mir-29 sponge consisted of 7 repetition of mir-29 complementary sequences with a mismatch of 4 nucleotides immediately after the seed sequence. The sponge sequence was previously chemically synthetized by Eurofin (Milan) then cloned in the 3' entry p3E-polyA using the restriction site BamHI. 3,094 kb of zebrafish kif5aa promoter region (Source: ZFIN;

Acc:ZDB-GENE-070912-141) was amplified by PCR from genomic DNA, (from -2969 to +125 bp including a small portion of the first exon, before the ATG), using primers Kif5a-SalI f: (5'-gtcgac –GTTGTCCAGCACGGATGTATAGGTA-3') and Kif5a-XmaI r:(5'-cccggg-ATAGCGGGGCAGAGGACGGCAG-3') and cloned into gateway 5'-entry p5E-MCS. Then, the multisite gateway recombination reaction was performed as described in the Invitrogen Multi-Site Gateway Manual, an equimolar amount of entry vectors, 20 fg of each, (p5E-kif5aa, pEM-EGFPCAAX, and p3E-sponge-20-SV40pa) and destination vector (pDESTol2CG2) were combined with LR Clonase II Plus enzyme mix. For the generation of (actb2: EGFPCAAX-SPONGE-29-SV40pa) was used as 5'entry p5-bactin2 (from Tol2kit v1.2) together with the other plasmids following the protocol mentioned above. All these vectors also contain the eGFP reporter gene driven by the zebrafish cardiac myosin light chain (cmlc2) promoter. All vectors generated were extracted and purified using Qiagen plasmid midi kit (toxin free). Eggs were harvested and injected at zygote stage as described in the following protocols (Valenzano DR *et al*., 2011 and Xu Q, 1999 for *N. furzeri* and *D. rerio* microinjections respectively). For microinjection borosilicate microcapillaries were used. Capillaries were pulled with a micropipette puller (P97, Sutter Instrument). The needles were filled with 2µl of water solution containing 20-30 ng/ µl of plasmid DNA, 20-30 ng/µl of Tol2 transposase mRNA, 0,4M KCl and 1% phenol red as visual control of successful injections. The embryos were injected with ~2nL of mix solution and the drop volume was estimated under a microscope using a calibrated slide. Injections were performed under the Nikon C-PS stereoscope. F0 fishes were screened under fluorescence microscope at 3-4th day after hatching (*N. furzeri*) and at 24hpf for zebrafish larvae. Three different founders were selected for line establishment.

6.3 *IREB2* 3'UTR vectors assembly and mir-29 targeting validation

In order to experimentally validate *IREB2* as direct mir-29 target in fishes, 671bp and 633 bp from *IREB2* 3'UTR of *N. furzeri* and *D. rerio,* respectively, were amplified by PCR from

cDNA of both species (*N. furzeri* reference: Nofu_GRZ_cDNA_3_0193494, *D. rerio* reference: ZFIN; Acc:ZDB-GENE-051205-1) using the primers nf*IREB2*-3'UTR-BamH-F: (5'-ttcgggggatccCATGTTTGACTCTGAGAAGGAC-3') and nf*IREB2*-3'UTR-BamH-R:(5'-ttcgggggatccGTTCTGTGCCCAGTTTGCCC-3') for *N. furzeri* and Dr*IREB2*-3'UTR-BamH-F: (5'-gtcacgC-GGATCCTCACATGGACCTCTGAACACC-3') and Dr*IREB2*-3'UTR-BamH-R: (5'-gatcggc-GGATCCCACAGCGAAAGTATCACAGCC-3') for *D. rerio* and cloned in the 3' entry p3E-polyA, then p5E-CMV/SP6, pME-EGFPCAAX, p3E-*IREB2*-3'UTR-polyA and pDESTol2CG2 were combined using multisite gateway (see above). Finally, the plasmid producing fluorescence standard control was assembled combining p5E-CMV/SP6, pME-RFP, p3E-polyA and pDESTol2CG2. I renamed these plasmids as N.f CMV/SP6: eGFP-*IREB2*-pA, D.r CMV/SP6: eGFP-*IREB2*-pA and CMV/SP6: RFP-pA. For all of these reporters, *in vitro* transcription was carried out as described below. About 2nl of solution containing 100pg of egfp-*IREB2* sensor mRNA, 100pg of RFP standard, 100pg of Dre-mir-29a mimic (Qiagen) and 100pg of Dre-mir-29b mimic (exiqon) was microinjected in the zygote stage embryos (for the control embryos was assembled the same mix without microRNA mimic). At 24hpf, 30-40 embryos were collected from each experimental condition, dechorionated and dissociated according to Gallardo & Behra, 2012. Dissociated cell were diluted in PBS 1x, loaded in the flow cytometer machine (FacsCalibur, Becton-Dickinson) and the eGFP/RFP fluorescence ratio was analyzed and quantified. For mmu-*IREB2* 3'UTR validation we used dual luciferase reporter assay system (Promega). Mmu-*IREB2* 3'utr (transcript ID: ENSMUST00000034843) containing the putative mir-29 binding site was cloned in pMIR-REPORT™ luciferase reporter system (Termo Fisher) using the restriction enzymes SpeI and MluI. Mmu-mir-29b1/a precursor was cloned in CMV/SP6: RFP-Pa vector, downstream of RFP using the restriction enzyme MluI. Transfection on Hek293 was performed using lipofectamine 2000 (Invitrogen). CMV:RFP-mir-29b/c precursor-polyA-tail was co-transfected with pMIR-report and Renilla control vector following the manufacturer's instructions. In the control experiment was co-trasfected the same vector without mir-29a/b1 precursor sequence. 24 hours after transfection both Renilla and Firefly luciferase activity were measured using the luminometer (GloMax 96 microplate

Luminometer w/dual injectors). Mutant vectors were generated using the QuikChange II XL Site-Directed Mutagenesis kit (Stratagene) according to the manifacturer's protocol.

6.4 In vitro RNA and DIG-labeled probes synthesis

The Tol2 mRNA was transcribed from the pCS-TP plasmid whereas eGFP-*IREB2*-3'utr and standard fluorescence control mRNAs were transcribed from plasmids: N.f CMV/SP6: eGFP-*IREB2*-pA, D.r CMV/SP6: eGFP-*IREB2*-pA and CMV/SP6: RFP-pA respectively. All were previously linearized using NotI and purified with Wizard® SV Gel and PCR Clean-Up System (Promega). Then 1µg of each linearized plasmid was transcribed using the mMESSAGE mMACHINE SP6 kit (Ambion) according to the manifacturer's protocol. For DIG-labeled probe synthesis, initially sequences were amplified by PCR from cDNA using a reverse primer carrying a T7 promoter sequence on its 5'end. 200ng of PCR product, previously purified with Wizard® SV Gel and PCR Clean-Up System (Promega), were directly transcribed using T7 enzyme (Fermentas) and digoxygenated RNTP mix (Roche) 2 hours at 37ºC. In vitro transcription mix were precipitated with 1/10 of volume of LiCl (5M) and 2,5 volumes of isopropanol, than washed with 70% ethanol and finally resuspended in nuclease-free water and stored at -80°.

6.5 Total RNA extraction and RT-qPCR

Dissected tissues were immediately put in 500 µl of Qiazol lysis reagent and manually homogenized with pounder. Total RNA was extracted using miRneasy mini kit (Qiagen) according to the manufacture's protocol. 200ng of each RNA extraction was retrotranscribed for cDNA synthesis using mirscript II RT kit (Qiagen). qPCR was performed using Rotorgene 6000 (Corbet). PCR mix solutions were prepared using SsoAdvanced™ Universal SYBR® Green Supermix (Biorad) and 4ng of cDNA for each sample as template. The relative gene quantification was calculated using the ΔΔCt method, as reference genes were used *TBP*, *ACTB2* and *GAPDH* for *N.furzeri*, *D. rerio* and mouse respectively.

6.6 Histology and histochemistry

All the immunohistochemical procedures were performed on frozen tissue sections. Animals were killed with overdose of MS-222, brains were dissected and fixed in PFA 4%, washed in PBS 1X twice then equilibrated in sucrose 30% and embedded in Tissue-Tek OCT (Leica). Frozen tissues were cut with cryostat (Leica), 12-14 µm thick sections were immediately put on superfrost plus slides (Thermo Scientific), dried in the oven at 55ºC for 1 hour. Sections were rehydrated in PBS 1x permeabilized with tritonX 0,3% and blocked in BSA 5%, goat serum 1%. Primary antibodies were all incubated over night at 4ºC according to the following dilutions: Anti-HuC/D (1:50, Invitrogen, A-21271), Anti-eGFP (1:1000, Abcam,), Anti-GFAP (1:400, Millipore, mab5324), Anti-S100 (1:400, Dako, zo311). Secondary antibodies coupled to Alexa Fluor dye (488, 546, 635, Invitrogen) were incubated 2 hours RT (1:500).

In situ hybridizations were performed according to Thisse, C. and Thisse, B. (2008) with minor modifications. Slides were incubated with proteinase K for 10 minutes at room temperature (RT)(1:80000; Fermentas, 20mg/ml), post-fixed with PFA 4% 20 minutes RT, then were incubated with a digoxigenin (DIG)-labeled probes (60ºC, ON). Immediately before incubation probes were put in hybridization solution denaturated at 98ºC for 3 min. Sections were washed with SSC2x twice at 60ºC for 15min. each, then with SSC 0,5x three times 10 min each at room temperature and incubated with anti-Dig AP Fab (Roche; 1/2000 4ºC ON) in blocking solution (Roche). The day after, slides were placed 20 min RT in TMN solution (Tris-MgCl2-NaCl buffer) with the addition of levamisole 1 mM (Sigma) in order to inhibit endogenous alkaline phosphatase and transferred in Fast red solution (Roche tablets). The staining was constantly monitored under epiflourescence microscope and blocked by washing in PBS 1X. Images were acquired using epifluorescence microscope (Nikon, Eclipse600) or confocal microscope (Leica DMIRE2).

For lipofuscin detection, unstained sections were deparaffinized and mounted using a water-based medium within DAPI (Invitrogen). An important property of lipofuscin is its

broad autofluorescence. So it was acquired using Zeiss apotome(2) at an excitation wavelength of 488 and 550nm as well and under UV excitation was acquired DAPI staining. Images were analyzed using Image-j, threshold were determined by operator and applied to images to discriminate lipofuscin granules from background signal. The area occupied by granules was expressed as a percentage of total image area analyzed.

6.7 Iron staining (Perls staining)

For iron staining, according to (Meguro R et al., 2007) with minor modifications, brains were dissected and fixed in PFA 4% and embedded in paraffin. 5-7 µm thick sections were deparaffinized and immersed in 4% ferrocyanide and 2% HCl for 1 hour at 37ºC, then immersed in methanol containing 0,5 % H_2O_2, 0,01 NaN_3 for 30 min RT, finally immersed in 0.1 M phosphate buffer containing DAB 0,05% , 0,005% H_2O_2 for 30 min. Sections were counterstained with hematoxylin, dehydrated and mounted.

6.8 Non heme iron quantification

For iron quantification was followed the protocol published by (Rebouche JC. *et al*. 2003). Extracted tissues were put in empty 1.5ml tubes, previously weighed, and were weighed again in order to precisely determine wet tissue weight. Homogenates were prepared in high-purity water. 100 µl of homogenate tissues were combined in a new 1.5ml tube with an equal volume of protein precipitation solution (1N HCl, 10% trichloroacetic acid) and placed in thermoblock at 95ºC for 1 hour. Tubes were cooled RT for 10 min then were centrifuged for 15 min at 4ºC. 70 µl of supernatant was collected from each tube sample and combined with an equal volume of chromogenic solution (Ferrozine 0,5 mM, ammonium acetate 1,5 M and Tioglicolic acid 0,1%). After 30 min absorbance was measured at 562 nm using spectrophotometer. Standard curve were prepared using 0, 0,5, 1, 2, 4, 8, 10, 20 µg/ml of iron standard solution (Sigma).

6.9 Iron and drugs delivery

Fish were previously anesthetized with Trichaine methanesulfonate and weighed. A single dose respectively of 350 μg/g body weight iron dextran (Sigma, 100mg/ml), 30 μg/g body weight deferoxamine (DFO, Novartis) and 50 μ/g body weight 4-OH-Tempol (Sigma) was injected intraperitonealy. Injections were performed under a stereo microscope (Leica) using Amilton syringes 10μl, control animals were sham-injected with saline solution. At 4, 8, 12, 24, 48 and 72 hours after injection brains were removed from anesthetized animals and put in a previously weighed tube for iron measurement or immediately frozen in liquid nitrogen for the following RNA extraction.

6.10 Western blot

Samples were lysed in RIPA-buffer (50 mM Tris-HCl, pH 7.5, 150 mM NaCl, 1% Triton X-100, 0.1% SDS, 0,5% deoxycolic acid) containing protease inhibitor (Complete Protease Inhibitor Cocktail Tablets, Roche Diagnostics) and centrifuged at 12300 rpm for 10 min at 4°C and supernatants were collected. Total protein concentration was determined by BCA protein assay (Pierce). Aliquots of homogenate with equal protein concentrations were separated in 10% acrylamide gel and transferred to nitrocellulose membranes by mini trans-blot (Bio-Rad). The membranes were blocked with milk (5% w/v) and probed with appropriate primary and secondary IgG-HRP conjugated antibodies (Millipore). Enhanced chemiluminiscence detection system (GE Healthcare) was used for developing on autoradiography-films (GE Healthcare). Densitometric quantification was performed using image-j and normalized to the relative amount of α-Tubulin and expressed as n-fold of control samples. In this study were used the following antibodies: Anti-IRP2 (1:1000, Abcam, ab181153), Anti-TFRC (1:500, Abcam, ab84036), α-TUB (1:20000, Sigma, t5168); secondary HRP antibodies: goat-anti rabbit (1:2000, Santa Cruz, sc2004), goat-anti mouse (1:2000, Santa Cruz, sc2005).

6.11 Cell culture and iron exposure

Following a previously published protocol (Bertacchi et al., Cell Mol Life Sci, 2013), murine ES cell line E14Tg2A was differentiated into cortical neurons. In brief, mouse embryonic stem cells (mESC) were cultured in a chemically defined medium on laminin-coated culture dishes for 20 days. mESC-derived neurons were then treated with iron dextran (50 ug/mL, 100 ug/mL and 200 ug/mL) and Iron(II) sulfate (25 uM, 50 uM and 100 uM) in Neurobasal Medium (Thermo Fisher Scientific) supplemented with B27 (Thermo Fisher Scientific) for 72 hrs, medium was changed daily. Subsequently, two wells of six-well plate were pooled for each thesis; RNA extraction and PCR analysis were carried out from three biological replicates.

6.12 RNA-sequencing and analysis

RNA was extracted using Quaziol (Qiagen). Library preparation using Illumina's TruSeq RNA sample prep kit v2 and sequenced on Illumina HiSeq2500, 50bp single-read mode in multiplexing obtaining around 50-40 mio reads per sample. Read mapping was performed using Tophat 2.0.6 (Kim D et al., 2013) and featureCounts v1.4.3- p1 (Liao Y et al., 2014) using as refences the *N. furzeri* genome (Reichwald K et al., 2015) or Zv9.73. Differential gene expression analysis was performed using R software, for DEGs identification was used the statistical test of edgeR package (Robinson et al., 2010). For multiple testing correction a false discovery rate <0.05 was chosen. KEGG pathway analysis was performed using the software Web-based gene set analysis tool kit (WebGestalt) (Zhang et al., 2005) using an FDR<0,05.

6.13 Annotation of small RNAs

The processing and annotation of small RNA-Seq raw data was performed using an R 3.0.2 and ShortRead Bioconductor package (Morgan et al., 2009).

First, raw data were preprocessed with the following parameters:

- Quality filtering: eliminated all the reads containing an “N”;
- Adapter trimming: used function trimLRPatterns(), allowing up to 2 mismatches and using as adapter sequence "TGGAATTCTCGGGTGCCAAGGAACTCCAGTCAC";
- Size filtering: removed all the reads with length < 18 and > 33 nucleotides.

Second, reads were aligned, resulting in a direct annotation and quantification. The alignment was divided in two steps, to allow the recognition and the annotation of the reads exceeding reference length. In fact, the algorithm of Bowtie 1.0.0 does not allow aligning longer reads to shorter references. Specifically:

- Alignment against the reference (miRBase 20; Kozomara et al., 2014) with up to 2 mismatches. In this step the reference used was the mature sequence of microRNAs for the analysed organism (except for Nothobranchius furzeri, for which Danio rerio reference was used). Each read was aligned using these criteria with Bowtie 1.0.0 (settings:-q --best –norc);
- The remaining reads, which could not align in the previous step, were used as reference for a second alignment step. In this case, the annotated mature microRNAs were aligned against the reads;
- The information obtained in the two alignment phases was conveyed in one single table, containing a list of all the retrieved sequences and their relative counts.

6.14 Enrichment analysis of miR-29 binding sites

Target predictions were obtained using MiRanda (version: august 2010) with default parameters (Enright et al., 2003).

Enrichment analysis was performed to test the overrepresentation of specific microRNAs' targets in the identified transcript clusters of genes with different expression profiles with age (Baumgart et al.,2014).

To this purpose, three different tests have been used: Binomial test, Fisher's test and Hypergeometric test. Only microRNAs having a Hochberg's corrected p-value < 0.05 in the three tests were considered as having their targets overrepresented in one cluster.

7 REFERENCES

Acosta-Cabronero, J., Betts, M. J., Cardenas-Blanco, A., Yang, S., & Nestor, P. J. (2016). In Vivo MRI Mapping of Brain Iron Deposition across the Adult Lifespan. The Journal of Neuroscience : The Official Journal of the Society for Neuroscience, 36(2), 364–74. http://doi.org/10.1523/JNEUROSCI.1907-15.2016

Anderton, B. H. (2002). Ageing of the brain. Mechanisms of Ageing and Development. http://doi.org/10.1016/S0047-6374(01)00426-2

Andolfo, I., De Falco, L., Asci, R., Russo, R., Colucci, S., Gorrese, M., … Iolascon, A. (2010). Regulation of divalent metal transporter 1 (DMT1) non-IRE isoform by the microRNA Let-7d in erythroid cells. Haematologica, 95(8), 1244–1252. http://doi.org/10.3324/haematol.2009.020685

Arriagada, P. V, Marzloff, K., & Hyman, B. T. (1992). Distribution of Alzheimer-Type Pathological-Changes in Nondemented Elderly Individuals Matches the Pattern in Alzheimers-Disease. Neurology, 42(9), 1681–1688. Retrieved from <Go to ISI>://A1992JM88400007

Baker, D. J., Wijshake, T., Tchkonia, T., LeBrasseur, N. K., Childs, B. G., van de Sluis, B., … van Deursen, J. M. (2011). Clearance of p16Ink4a-positive senescent cells delays ageing-associated disorders. Nature, 479(7372), 232–6. http://doi.org/10.1038/nature10600

Baumgart, M., Groth, M., Priebe, S., Savino, A., Testa, G., Dix, A., … Cellerino, A. (2014). RNA-seq of the aging brain in the short-lived fish N. furzeri - conserved pathways and novel genes associated with neurogenesis. Aging Cell, 13(6), 965–974. http://doi.org/10.1111/acel.12257

Berridge, M. J., Lipp, P., & Bootman, M. D. (2000). The versatility and universality of calcium signalling. Nature Reviews. Molecular Cell Biology, 1(1), 11–21. http://doi.org/10.1038/35036035

Bertacchi, M., Pandolfini, L., Murenu, E., Viegi, A., Capsoni, S., Cellerino, A., … Cremisi, F. (2013). The positional identity of mouse ES cell-generated neurons is affected by BMP signaling. Cellular and Molecular Life Sciences, 70(6), 1095–1111. http://doi.org/10.1007/s00018-012-1182-3

Bian, S., Hong, J., Li, Q., Schebelle, L., Pollock, A., Knauss, J. L., … Sun, T. (2013). MicroRNA Cluster miR-17-92 Regulates Neural Stem Cell Expansion and Transition to Intermediate Progenitors in the Developing Mouse Neocortex. Cell Reports, 3(5), 1398–1406. http://doi.org/10.1016/j.celrep.2013.03.037

Boehm, M., & Slack, F. (2005). A developmental timing microRNA and its target regulate life span in C. elegans. Science (New York, N.Y.), 310(5756), 1954–1957. http://doi.org/10.1126/science.1115596

Bonilla, E., Medina-Leendertz, S., & Díaz, S. (2002). Extension of life span and stress resistance of Drosophila melanogaster by long-term supplementation with melatonin. Experimental Gerontology, 37(5), 629–638. http://doi.org/10.1016/S0531-5565(01)00229-7

Bonkovsky, H. L., Hou, W., Steuerwald, N., Tian, Q., Li, T., Parsons, J., … Schrum, L. (2013). Heme status affects human hepatic messenger RNA and microRNA expression. World Journal of Gastroenterology, 19(10), 1593–1601. http://doi.org/10.3748/wjg.v19.i10.1593

Boon, R. a, Iekushi, K., Lechner, S., Seeger, T., Fischer, A., Heydt, S., … Dimmeler, S. (2013). MicroRNA-34a regulates cardiac ageing and function. Nature, 495(7439), 107–10. http://doi.org/10.1038/nature11919

Boon, R. a, Iekushi, K., Lechner, S., Seeger, T., Fischer, A., Heydt, S., … Dimmeler, S. (2013). MicroRNA-34a regulates cardiac ageing and function. Nature, 495(7439), 107–10. http://doi.org/10.1038/nature11919

Boon, R. A., Seeger, T., Heydt, S., Fischer, A., Hergenreider, E., Horrevoets, A. J. G., … Dimmeler, S. (2011). MicroRNA-29 in aortic dilation: Implications for aneurysm formation. Circulation Research, 109(10), 1115–1119. http://doi.org/10.1161/CIRCRESAHA.111.255737

Boudreau, R. L., Jiang, P., Gilmore, B. L., Spengler, R. M., Tirabassi, R., Nelson, J. A., … Davidson, B. L. (2014). Transcriptome-wide discovery of microRNA binding sites in Human Brain. Neuron, 81(2), 294–305. http://doi.org/10.1016/j.neuron.2013.10.062

Boulias, K., & Horvitz, H. R. (2012). The C. elegans MicroRNA mir-71 acts in neurons to promote germline-mediated longevity through regulation of DAF-16/FOXO. Cell Metabolism, 15(4), 439–450. http://doi.org/10.1016/j.cmet.2012.02.014

Boulias, K., & Horvitz, H. R. (2012). The C. elegans MicroRNA mir-71 acts in neurons to promote germline-mediated longevity through regulation of DAF-16/FOXO. Cell Metabolism, 15(4), 439–450. http://doi.org/10.1016/j.cmet.2012.02.014

Breuer, W., Greenberg, E., & Cabantchik, Z. I. (1997). Newly delivered transferrin iron and oxidative cell injury. FEBS Letters, 403(2), 213–219. http://doi.org/10.1016/S0014-5793(97)00056-2

Buchholz, J. N., Behringer, E. J., Pottorf, W. J., Pearce, W. J., & Vanterpool, C. K. (2007). Age-dependent changes in Ca2+ homeostasis in peripheral neurones: Implications for changes in function. Aging Cell. http://doi.org/10.1111/j.1474-9726.2007.00298.x

Burke, S. N., & Barnes, C. A. (2006). Neural plasticity in the ageing brain. Nat Rev Neurosci, 7(1), 30–40. http://doi.org/10.1038/nrn1809

Cable, E. E., Connor, J. R., & Isom, H. C. (1998). Accumulation of iron by primary rat hepatocytes in long-term culture: changes in nuclear shape mediated by non-transferrin-bound forms of iron. The American Journal of Pathology, 152(3), 781–92. Retrieved from http://www.pubmedcentral.nih.gov/articlerender.fcgi?artid=1858381&tool=pmcentrez&rendertype=abstract

Castoldi, M., Spasic, M. V., Altamura, S., Elm??n, J., Lindow, M., Kiss, J., … Muckenthaler, M. U. (2011). The liver-specific microRNA miR-122 controls systemic iron homeostasis in mice. Journal of Clinical Investigation, 121(4), 1386–1396. http://doi.org/10.1172/JCI44883

Chu, Y., & Kordower, J. H. (2007). Age-associated increases of alpha-synuclein in monkeys and humans are associated with nigrostriatal dopamine depletion: Is this the target for Parkinson's disease? Neurobiology of Disease, 25(1), 134–49. http://doi.org/10.1016/j.nbd.2006.08.021

Connor, J. R., Menzies, S. L., Martin, S. M. S., & Mufson, E. J. (1990). Cellular distribution of transferrin, ferritin, and iron in normal and aged human brains. Journal of Neuroscience Research, 27(4), 595–611. http://doi.org/10.1002/jnr.490270421

Copeland, J. M., Cho, J., Lo, T., Hur, J. H., Bahadorani, S., Arabyan, T., … Walker, D. W. (2009). Extension of Drosophila Life Span by RNAi of the Mitochondrial Respiratory Chain. Current Biology, 19(19), 1591–1598. http://doi.org/10.1016/j.cub.2009.08.016

Cui, Z., Zhong, Z., Yang, Y., Wang, B., Sun, Y., Sun, Q., … Bian, L. (2016). Ferrous Iron Induces Nrf2 Expression in Mouse Brain Astrocytes to Prevent Neurotoxicity. Journal of Biochemical and Molecular Toxicology, 28(6), 246–255. http://doi.org/10.1002/jbt.21803

Cushing, L., Costinean, S., Xu, W., Jiang, Z., Madden, L., Kuang, P., … L??, J. (2015). Disruption of miR-29 Leads to Aberrant Differentiation of Smooth Muscle Cells Selectively Associated with Distal Lung Vasculature. PLoS Genetics, 11(5). http://doi.org/10.1371/journal.pgen.1005238

de Chaves, E. P., & Narayanaswami, V. (2008). Apolipoprotein E and cholesterol in aging and disease in the brain. Future Lipidol, 3(5), 505–530. Retrieved from http://www.ncbi.nlm.nih.gov/pubmed/19649144

De Lencastre, A., Pincus, Z., Zhou, K., Kato, M., Lee, S. S., & Slack, F. J. (2010). MicroRNAs both promote and antagonize longevity in C. elegans. Current Biology, 20(24), 2159–2168. http://doi.org/10.1016/j.cub.2010.11.015

de Lima, M. N. M., Dias, C. P., Torres, J. P., Dornelles, A., Garcia, V. A., Scalco, F. S., … Schröder, N. (2008). Reversion of age-related recognition memory impairment by iron chelation in rats. Neurobiology of Aging, 29(7), 1052–1059. http://doi.org/10.1016/j.neurobiolaging.2007.02.006

Dexter, D. T., Wells, F. R., Lees, A. J., Agid, F., Agid, Y., Jenner, P., & Marsden, C. D. (1989). Increased nigral iron content and alterations in other metal ions occurring in brain in Parkinson's disease. Journal of Neurochemistry, 52(6), 1830–1836. http://doi.org/10.1111/j.1471-4159.1989.tb07264.x

Di Cicco, E., Tozzini, E. T., Rossi, G., & Cellerino, A. (2011). The short-lived annual fish Nothobranchius furzeri shows a typical teleost aging process reinforced by high incidence of age-dependent neoplasias. Experimental Gerontology, 46(4), 249–256. http://doi.org/10.1016/j.exger.2010.10.011

Di Monte, D. A., Schipper, H. M., Hetts, S., & Langston, J. W. (1995). Iron-mediated bioactivation of 1-methyl-4-phenyl-1,2,3,6-tetrahydropyridine (MPTP) in glial cultures. Glia, 15(2), 203–206. Retrieved from http://www.ncbi.nlm.nih.gov/entrez/query.fcgi?cmd=Retrieve&db=PubMed&dopt=Citation&list_uids=8567072

Dickstein, D. L., Kabaso, D., Rocher, A. B., Luebke, J. I., Wearne, S. L., & Hof, P. R. (2007). Changes in the structural complexity of the aged brain. Aging Cell. http://doi.org/10.1111/j.1474-9726.2007.00289.x

Dillin, A., Hsu, A.-L., Arantes-Oliveira, N., Lehrer-Graiwer, J., Hsin, H., Fraser, A. G., … Kenyon, C. (2002). Rates of behavior and aging specified by mitochondrial function during development. Science (New York, N.Y.), 298(5602), 2398–2401. http://doi.org/10.1126/science.1077780

Dixon, S. J., & Stockwell, B. R. (2014). The role of iron and reactive oxygen species in cell death. Nature Chemical Biology, 10(1), 9–17. http://doi.org/10.1038/nchembio.1416

Duce, J. A., Tsatsanis, A., Cater, M. A., James, S. A., Robb, E., Wikhe, K., … Bush, A. I. (2010). Iron-Export Ferroxidase Activity of ??-Amyloid Precursor Protein is Inhibited by Zinc in Alzheimer's Disease. Cell, 142(6), 857–867. http://doi.org/10.1016/j.cell.2010.08.014

Esiri, M. M., Nagy, Z., Smith, M. Z., Barnetson, L., Smith, A. D., & Joachim, C. (1999). Cerebrovascular disease and threshold for dementia in the early stages of Alzheimer's disease. Lancet, 354(9182), 919–920. http://doi.org/10.1016/S0140-6736(99)02355-7

Faller, M., Matsunaga, M., Yin, S., Loo, J. a, & Guo, F. (2007). Heme is involved in microRNA processing. Nature Structural & Molecular Biology, 14(1), 23–9. http://doi.org/10.1038/nsmb1182

Fenn, A. M., Smith, K. M., Lovett-Racke, A. E., Guerau-de-Arellano, M., Whitacre, C. C., & Godbout, J. P. (2013). Increased miR-29b in the aged brain correlates with the reduction of IGF-1 and CX3 CL1. Neurobiol Aging, 34(12), 2748–2758. http://doi.org/10.1016/j.neurobiolaging.2013.06.007

Gakh, O., Park, S., Liu, G., Macomber, L., Imlay, J. A., Ferreira, G. C., & Isaya, G. (2006). Mitochondrial iron detoxification is a primary function of frataxin that limits oxidative

damage and preserves cell longevity. Human Molecular Genetics, 15(3), 467–479. http://doi.org/10.1093/hmg/ddi461

Gardenghi, S., Ramos, P., Marongiu, M. F., Melchiori, L., Breda, L., Guy, E., … Rivella, S. (2010). Hepcidin as a therapeutic tool to limit iron overload and improve anemia in β-thalassemic mice. Journal of Clinical Investigation, 120(12), 4466–4477. http://doi.org/10.1172/JCI41717

Gerhard, G. S., Kauffman, E. J., Wang, X., Stewart, R., Moore, J. L., Kasales, C. J., … Cheng, K. C. (2002). Life spans and senescent phenotypes in two strains of Zebrafish (Danio rerio). Experimental Gerontology, 37(8-9), 1055–1068. http://doi.org/10.1016/S0531-5565(02)00088-8

Ghadery, C., Pirpamer, L., Hofer, E., Langkammer, C., Petrovic, K., Loitfelder, M., … Schmidt, R. (2015). R2* mapping for brain iron: Associations with cognition in normal aging. Neurobiology of Aging, 36(2), 925–932. http://doi.org/10.1016/j.neurobiolaging.2014.09.013

Gray, D. a, & Woulfe, J. (2005). Lipofuscin and aging: a matter of toxic waste. Science of Aging Knowledge Environment, 2005(5), re1. http://doi.org/10.1126/sageke.2005.5.re1

Grillari, J., Hackl, M., & Grillari-Voglauer, R. (2010). miR-17-92 cluster: Ups and downs in cancer and aging. Biogerontology. http://doi.org/10.1007/s10522-010-9272-9

Hackl, M., Brunner, S., Fortschegger, K., Schreiner, C., Micutkova, L., M??ck, C., … Grillari, J. (2010). miR-17, miR-19b, miR-20a, and miR-106a are down-regulated in human aging. Aging Cell. http://doi.org/10.1111/j.1474-9726.2010.00549.x

Harel, I., Benayoun, B. A., Machado, B., Singh, P. P., Hu, C. K., Pech, M. F., … Brunet, A. (2015). A platform for rapid exploration of aging and diseases in a naturally short-lived vertebrate. Cell, 160(5), 1013–1026. http://doi.org/10.1016/j.cell.2015.01.038

Harman, D. (1992). Free radical theory of aging. Mutation Research/DNAging, 275(3-6), 257–266. http://doi.org/10.1016/0921-8734(92)90030-S

Hartmann, N., Reichwald, K., Lechel, A., Graf, M., Kirschner, J., Dorn, A., … Englert, C. (2009). Telomeres shorten while Tert expression increases during ageing of the short-lived fish Nothobranchius furzeri. Mechanisms of Ageing and Development, 130(5), 290–296. http://doi.org/10.1016/j.mad.2009.01.003

Hartmann, N., Reichwald, K., Wittig, I., Dröse, S., Schmeisser, S., Lück, C., … Englert, C. (2011). Mitochondrial DNA copy number and function decrease with age in the short-lived fish Nothobranchius furzeri. Aging Cell, 10(5), 824–831. http://doi.org/10.1111/j.1474-9726.2011.00723.x

Höck, J., Weinmann, L., Ender, C., Rüdel, S., Kremmer, E., Raabe, M., … Meister, G. (2007). Proteomic and functional analysis of Argonaute-containing mRNA-protein complexes in human cells. EMBO Reports, 8(11), 1052–60. http://doi.org/10.1038/sj.embor.7401088

Hof, P. R., & Morrison, J. H. (2004). The aging brain: Morphomolecular senescence of cortical circuits. Trends in Neurosciences. http://doi.org/10.1016/j.tins.2004.07.013

Ibáñez-Ventoso, C., Yang, M., Guo, S., Robins, H., Padgett, R. W., & Driscoll, M. (2006). Modulated microRNA expression during adult lifespan in Caenorhabditis elegans. Aging Cell, 5(3), 235–246. http://doi.org/10.1111/j.1474-9726.2006.00210.x

Jorm, a F., & Jolley, D. (1998). The incidence of dementia: a meta-analysis. Neurology, 51(3), 728–733. http://doi.org/10.1212/WNL.51.3.728

Kastman, E. K., Willette, A. a, Coe, C. L., Bendlin, B. B., Kosmatka, K. J., McLaren, D. G., … Johnson, S. C. (2010). A calorie-restricted diet decreases brain iron accumulation and preserves motor performance in old rhesus monkeys. The Journal of Neuroscience : The Official Journal of the Society for Neuroscience, 30(23), 7940–7947. http://doi.org/10.1523/JNEUROSCI.2553-12.2012

Kato, M., Chen, X., Inukai, S., Zhao, H., & Slack, F. J. (2011). Age-associated changes in expression of small, noncoding RNAs, including microRNAs, in C. elegans. RNA (New York, N.Y.), 17(10), 1804–20. http://doi.org/10.1261/rna.2714411

Keller, J. N., Dimayuga, E., Chen, Q., Thorpe, J., Gee, J., & Ding, Q. (2004). Autophagy, proteasomes, lipofuscin, and oxidative stress in the aging brain. International Journal of Biochemistry and Cell Biology. http://doi.org/10.1016/j.biocel.2004.05.003

Kennedy, B. K., Steffen, K. K., & Kaeberlein, M. (2007). Ruminations on dietary restriction and aging. Cellular and Molecular Life Sciences. http://doi.org/10.1007/s00018-007-6470-y

Kirschner, J., Weber, D., Neuschl, C., Franke, A., B??ttger, M., Zielke, L., … Reichwald, K. (2012). Mapping of quantitative trait loci controlling lifespan in the short-lived fish

Nothobranchius furzeri- a new vertebrate model for age research. Aging Cell, 11(2), 252–261. http://doi.org/10.1111/j.1474-9726.2011.00780.x

Klang, I. M., Schilling, B., Sorensen, D. J., Sahu, A. K., Kapahi, P., Andersen, J. K., … Lithgow, G. J. (2014). Iron promotes protein insolubility and aging in C. elegans. Aging, 6(11), 975–991.

Kurinna, S., Schäfer, M., Ostano, P., Karouzakis, E., Chiorino, G., Bloch, W., … Werner, S. (2014). A novel Nrf2-miR-29-desmocollin-2 axis regulates desmosome function in keratinocytes. Nature Communications, 5, 5099. http://doi.org/10.1038/ncomms6099

Kwok, J. B. (2010). Role of epigenetics in Alzheimer's and Parkinson's disease. Epigenomics, 2(5), 671–682. http://doi.org/10.2217/epi.10.43

Landgraf, P., Rusu, M., Sheridan, R., Sewer, A., Iovino, N., Aravin, A., … Tuschl, T. (2007). A Mammalian microRNA Expression Atlas Based on Small RNA Library Sequencing. Cell, 129(7), 1401–1414. http://doi.org/10.1016/j.cell.2007.04.040

Lee, C. K., Klopp, R. G., Weindruch, R., & Prolla, T. a. (1999). Gene expression profile of aging and its retardation by caloric restriction. Science (New York, N.Y.), 285(5432), 1390–1393. http://doi.org/10.1126/science.285.5432.1390

Lei, P., Ayton, S., Finkelstein, D. I., Spoerri, L., Ciccotosto, G. D., Wright, D. K., … Bush, A. I. (2012). Tau deficiency induces parkinsonism with dementia by impairing APP-mediated iron export. Nature Medicine, 18(2), 291–295. http://doi.org/10.1038/nm.2613

Li, N., Bates, D. J., An, J., Terry, D. A., & Wang, E. (2011). Up-regulation of key microRNAs, and inverse down-regulation of their predicted oxidative phosphorylation target genes, during aging in mouse brain. Neurobiology of Aging, 32(5), 944–955. http://doi.org/10.1016/j.neurobiolaging.2009.04.020

Li, N., Bates, D. J., An, J., Terry, D. A., & Wang, E. (2011). Up-regulation of key microRNAs, and inverse down-regulation of their predicted oxidative phosphorylation target genes, during aging in mouse brain. Neurobiology of Aging, 32(5), 944–955. http://doi.org/10.1016/j.neurobiolaging.2009.04.020

Li, W. J., Jiang, H., Song, N., & Xie, J. X. (2010). Dose- and time-dependent α-synuclein aggregation induced by ferric iron in SK-N-SH cells. Neuroscience Bulletin, 26(3), 205–210. http://doi.org/10.1007/s12264-010-1117-7

Lin, E., Graziano, J. H., & Freyer, G. A. (2001). Regulation of the 75-kDa Subunit of Mitochondrial Complex I by Iron. Journal of Biological Chemistry, 276(29), 27685–27692. http://doi.org/10.1074/jbc.M100941200

Lippi, G., Steinert, J. R., Marczylo, E. L., D'Oro, S., Fiore, R., Forsythe, I. D., … Young, K. W. (2011). Targeting of the Arpc3 actin nucleation factor by miR-29a/b regulates dendritic spine morphology. Journal of Cell Biology, 194(6), 889–904. http://doi.org/10.1083/jcb.201103006

Liu, N., Landreh, M., Cao, K., Abe, M., Hendriks, G.-J., Kennerdell, J. R., … Bonini, N. M. (2012). The microRNA miR-34 modulates ageing and neurodegeneration in Drosophila. Nature, 482(7386), 519–523. http://doi.org/10.1038/nature10810

Maaroufi, K., Ammari, M., Jeljeli, M., Roy, V., Sakly, M., & Abdelmelek, H. (2009). Impairment of emotional behavior and spatial learning in adult Wistar rats by ferrous sulfate. Physiology & Behavior, 96(2), 343–349. http://doi.org/10.1016/j.physbeh.2008.10.019

Maes, O. C., An, J., Sarojini, H., & Wang, E. (2008). Murine microRNAs implicated in liver functions and aging process. Mechanisms of Ageing and Development, 129(9), 534–541. http://doi.org/10.1016/j.mad.2008.05.004

Maes, O. C., An, J., Sarojini, H., & Wang, E. (2008). Murine microRNAs implicated in liver functions and aging process. Mechanisms of Ageing and Development, 129(9), 534–541. http://doi.org/10.1016/j.mad.2008.05.004

Mair, W., & Dillin, A. (2008). Aging and survival: the genetics of life span extension by dietary restriction. Annual Review of Biochemistry, 77, 727–754. http://doi.org/10.1146/annurev.biochem.77.061206.171059

Mantyh, P. W., Ghilardi, J. R., Rogers, S., DeMaster, E., Allen, C. J., Stimson, E. R., & Maggio, J. E. (1993). Aluminum, iron, and zinc ions promote aggregation of physiological concentrations of beta-amyloid peptide. Journal of Neurochemistry, 61, 1171–1174.

Martinez-Ramirez, S., Greenberg, S. M., & Viswanathan, A. (2014). Cerebral microbleeds: overview and implications in cognitive impairment. Alzheimer's Research & Therapy, 6(3), 33. http://doi.org/10.1186/alzrt263

Masoro, E. J. (2000). Caloric restriction and aging: An update. Experimental Gerontology. http://doi.org/10.1016/S0531-5565(00)00084-X

Massie, H. R., Aiello, V. R., & Banziger, V. (1983). Iron accumulation and lipid peroxidation in aging C57BL/6J mice. Experimental Gerontology, 18(4), 277–285. http://doi.org/10.1016/0531-5565(83)90038-4

Massie, H. R., Aiello, V. R., & Williams, T. R. (1993). Inhibition of iron absorption prolongs the life span of Drosophila. Mechanisms of Ageing and Development, 67(3), 227–237. http://doi.org/10.1016/0047-6374(93)90001-8

Mattson, M. P. (1997). Cellular actions of beta-amyloid precursor protein and its soluble and fibrillogenic derivatives. Physiological Reviews, 77(4), 1081–1132.

Mattson, M. P. (2000). Apoptosis in neurodegenerative disorders. Nature Reviews. Molecular Cell Biology, 1(2), 120–9. http://doi.org/10.1038/35040009

Mattson, M. P., Chan, S. L., & Duan, W. (2002). Modification of brain aging and neurodegenerative disorders by genes, diet, and behavior. Physiological Reviews, 82(3), 637–672. http://doi.org/10.1152/physrev.00004.2002

Melis, J. P. M., van Steeg, H., & Luijten, M. (2013). Oxidative DNA damage and nucleotide excision repair. Antioxidants & Redox Signaling, 18(18), 2409–19. http://doi.org/10.1089/ars.2012.5036

Melov, S. (2000). Extension of Life-Span with Superoxide Dismutase/Catalase Mimetics. Science, 289(September), 1567–1569. http://doi.org/10.1126/science.289.5484.1567

Meyron-Holtz, E. G., Ghosh, M. C., Iwai, K., LaVaute, T., Brazzolotto, X., Berger, U. V, … Rouault, T. A. (2004). Genetic ablations of iron regulatory proteins 1 and 2 reveal why iron regulatory protein 2 dominates iron homeostasis. The EMBO Journal, 23(2), 386–95. http://doi.org/10.1038/sj.emboj.7600041

Moody, D. M., Brown, W. R., Challa, V. R., & Anderson, R. L. (1995). Periventricular venous collagenosis: association with leukoaraiosis. Radiology, 194(2), 469–476 (Abstract only). http://doi.org/10.1148/radiology.194.2.7824728

Moon, M. S., Mcdevitt, E. I., Zhu, J., Stanley, B., Krzeminski, J., Amin, S., … Isom, H. C. (2012). Elevated hepatic iron activates NF-E2-related factor 2-regulated pathway in a

dietary iron overload mouse model. Toxicological Sciences, 129(1), 74–85. http://doi.org/10.1093/toxsci/kfs193

Moos, T. (1996). Immunohistochemical localization of intraneuronal transferrin receptor immunoreactivity in the adult mouse central nervous system. The Journal of Comparative Neurology, 375(4), 675–692. http://doi.org/10.1002/(SICI)1096-9861(19961125)375:4<675::AID-CNE8>3.0.CO;2-Z

Murchison, D., & Griffith, W. H. (2007). Calcium buffering systems and calcium signaling in aged rat basal forebrain neurons. Aging Cell. http://doi.org/10.1111/j.1474-9726.2007.00293.x

Nishino, J., Kim, I., Chada, K., & Morrison, S. J. (2008). Hmga2 Promotes Neural Stem Cell Self-Renewal in Young but Not Old Mice by Reducing p16Ink4a and p19Arf Expression. Cell, 135(2), 227–239. http://doi.org/10.1016/j.cell.2008.09.017

Nolan, K., Mitchem, M. R., Jimenez-Mateos, E. M., Henshall, D. C., Concannon, C. G., & Prehn, J. H. M. (2014). Increased expression of MicroRNA-29a in ALS mice: Functional analysis of its inhibition. Journal of Molecular Neuroscience, 53(2), 231–241. http://doi.org/10.1007/s12031-014-0290-y

Olive, V., Bennett, M. J., Walker, J. C., Ma, C., Jiang, I., Cordon-Cardo, C., … He, L. (2009). miR-19 is a key oncogenic component of mir-17-92. Genes and Development, 23(24), 2839–2849. http://doi.org/10.1101/gad.1861409

Olivieri, S., Conti, a., Iannaccone, S., Cannistraci, C. V., Campanella, a., Barbariga, M., … Alessio, M. (2011). Ceruloplasmin Oxidation, a Feature of Parkinson's Disease CSF, Inhibits Ferroxidase Activity and Promotes Cellular Iron Retention. Journal of Neuroscience, 31(50), 18568–18577. http://doi.org/10.1523/JNEUROSCI.3768-11.2011

Papadopoulou, A. S., Serneels, L., Achsel, T., Mandemakers, W., Callaerts-Vegh, Z., Dooley, J., … De Strooper, B. (2015). Deficiency of the miR-29a/b-1 cluster leads to ataxic features and cerebellar alterations in mice. Neurobiology of Disease, 73, 275–288. http://doi.org/10.1016/j.nbd.2014.10.006

Paris, I., Martinez-Alvarado, P., Cárdenas, S., Perez-Pastene, C., Graumann, R., Fuentes, P., … Segura-Aguilar, J. (2005). Dopamine-dependent iron toxicity in cells derived from rat hypothalamus. Chemical Research in Toxicology, 18(3), 415–419. http://doi.org/10.1021/tx0497144

Penke, L., Vald??s Hernand??z, M. C., Maniega, S. M., Gow, A. J., Murray, C., Starr, J. M., … Wardlaw, J. M. (2012). Brain iron deposits are associated with general cognitive ability and cognitive aging. Neurobiology of Aging, 33(3). http://doi.org/10.1016/j.neurobiolaging.2010.04.032

Piper, M. D. W., Partridge, L., Raubenheimer, D., & Simpson, S. J. (2011). Dietary restriction and aging: A unifying perspective. Cell Metabolism. http://doi.org/10.1016/j.cmet.2011.06.013

Podolska, A., Kaczkowski, B., Kamp Busk, P., Søkilde, R., Litman, T., Fredholm, M., & Cirera, S. (2011). MicroRNA expression profiling of the porcine developing brain. PloS One, 6(1), e14494. http://doi.org/10.1371/journal.pone.0014494

Polačik, M., Donner, M. T., & Reichard, M. (2011). Age structure of annual Nothobranchius fishes in Mozambique: Is there a hatching synchrony? Journal of Fish Biology, 78(3), 796–809. http://doi.org/10.1111/j.1095-8649.2010.02893.x

Preston, J. E. (2001). Ageing choroid plexus-cerebrospinal fluid system. Microscopy Research and Technique, 52(1), 31–37. http://doi.org/10.1002/1097-0029(20010101)52:1<31::AID-JEMT5>3.0.CO;2-T

Rauhala, P., & Chiueh, C. C. (2000). Effects of atypical antioxidative agents, S-nitrosoglutathione and manganese, on brain lipid peroxidation induced by iron leaking from tissue disruption. Ann.N.Y.Acad.Sci., 899, 238–254.

Recalcati, S., Tacchini, L., Alberghini, A., Conte, D., & Cairo, G. (2003). Oxidative Stress-Mediated Down-Regulation of Rat Hydroxyacid Oxidase 1, a Liver-Specific Peroxisomal Enzyme. Hepatology, 38(5), 1159–1166. http://doi.org/10.1053/jhep.2003.50417

Redzic, Z. B., Preston, J. E., Duncan, J. A., Chodobski, A., & Szmydynger-Chodobska, J. (2005). The Choroid Plexus-Cerebrospinal Fluid System: From Development to Aging. Current Topics in Developmental Biology.

Reichwald, K., Petzold, A., Koch, P., Downie, B. R., Hartmann, N., Pietsch, S., … Platzer, M. (2015). Insights into Sex Chromosome Evolution and Aging from the Genome of a Short-Lived Fish. Cell, 163(6), 1527–1538. http://doi.org/10.1016/j.cell.2015.10.071

Rogers, J. T., Randall, J. D., Cahill, C. M., Eder, P. S., Huang, X., Gunshin, H., … Gullans, S. R. (2002). An iron-responsive element type II in the 5???-untranslated region of the

Alzheimer's amyloid precursor protein transcript. Journal of Biological Chemistry, 277(47), 45518–45528. http://doi.org/10.1074/jbc.M207435200

Roshan, R., Shridhar, S., Sarangdhar, M. A., Banik, A., Chawla, M., Garg, M., … Pillai, B. (2014). Brain-specific knockdown of miR-29 results in neuronal cell death and ataxia in mice. RNA, 20(8), 1287–1297. http://doi.org/10.1261/rna.044008.113

Rouault, T. A. (2013). Iron metabolism in the CNS: implications for neurodegenerative diseases. Nature Reviews Neuroscience, 14(8), 551–564. http://doi.org/10.1038/nrn3453

Rouault, T. A., & Cooperman, S. (2006). Brain Iron Metabolism. Seminars in Pediatric Neurology. http://doi.org/10.1016/j.spen.2006.08.002

Russell, D. (2002). Cerebral microemboli and cognitive impairment. In Journal of the Neurological Sciences (Vol. 203–204, pp. 211–214). http://doi.org/10.1016/S0022-510X(02)00293-9

Salahudeen, A. a, Thompson, J. W., Ruiz, J. C., Ma, H.-W., Kinch, L. N., Li, Q., … Bruick, R. K. (2009). An E3 ligase possessing an iron-responsive hemerythrin domain is a regulator of iron homeostasis. Science, 326(5953), 722–726. http://doi.org/10.1126/science.1176326

Salazar, J., Mena, N., Hunot, S., Prigent, A., Alvarez-Fischer, D., Arredondo, M., … Hirsch, E. C. (2008). Divalent metal transporter 1 (DMT1) contributes to neurodegeneration in animal models of Parkinson's disease. Proceedings of the National Academy of Sciences of the United States of America, 105(47), 18578–18583. http://doi.org/10.1073/pnas.0804373105

Sanchez, M., Galy, B., Dandekar, T., Bengert, P., Vainshtein, Y., Stolte, J., … Hentze, M. W. (2006). Iron regulation and the cell cycle: Identification of an iron-responsive element in the 3???-untranslated region of human cell division cycle 14A mRNA by a refined microarray-based screening strategy. Journal of Biological Chemistry, 281(32), 22865–22874. http://doi.org/10.1074/jbc.M603876200

Sangokoya, C., Doss, J. F., & Chi, J. T. (2013). Iron-Responsive miR-485-3p Regulates Cellular Iron Homeostasis by Targeting Ferroportin. PLoS Genetics, 9(4). http://doi.org/10.1371/journal.pgen.1003408

Schiavi, A., Maglioni, S., Palikaras, K., Shaik, A., Strappazzon, F., Brinkmann, V., … Ventura, N. (2015). Iron-Starvation-Induced Mitophagy Mediates Lifespan Extension upon

Mitochondrial Stress in C. elegans. Current Biology, 25(14), 1810–1822. http://doi.org/10.1016/j.cub.2015.05.059

Schröder, N., Figueiredo, L. S., & de Lima, M. N. M. (2013). Role of brain iron accumulation in cognitive dysfunction: evidence from animal models and human studies. Journal of Alzheimer's Disease : JAD, 34(4), 797–812. http://doi.org/10.3233/JAD-121996

Schultz, C., Ghebremedhin, E., Del Tredici, K., Rub, U., & Braak, H. (2004). High prevalence of thorn-shaped astrocytes in the aged human medial temporal lobe. Neurobiol Aging, 25(3), 397–405. http://doi.org/10.1016/S0197-4580(03)00113-1

Seo, A. Y., Xu, J., Servais, S., Hofer, T., Marzetti, E., Wohlgemuth, S. E., … Leeuwenburgh, C. (2008). Mitochondrial iron accumulation with age and functional consequences. Aging Cell, 7(5), 706–716. http://doi.org/10.1111/j.1474-9726.2008.00418.x

Sheffield, L. G., & Berman, N. E. (1998). Microglial expression of MHC class II increases in normal aging of nonhuman primates. Neurobiology of Aging, 19(1), 47–55. Retrieved from http://www.ncbi.nlm.nih.gov/pubmed/9562503

Siegel, G., Obernosterer, G., Fiore, R., Oehmen, M., Bicker, S., Christensen, M., … Schratt, G. M. (2009). A functional screen implicates microRNA-138-dependent regulation of the depalmitoylation enzyme APT1 in dendritic spine morphogenesis. Nature Cell Biology, 11(6), 705–U36. http://doi.org/Doi 10.1038/Ncb1876

Siesjö, B. K., Agardh, C. D., & Bengtsson, F. (1989). Free radicals and brain damage. Cerebrovascular and Brain Metabolism Reviews, 1(3), 165–211. Retrieved from http://www.ncbi.nlm.nih.gov/pubmed/2701375

Silva-Gomes, S., Santos, A. G., Caldas, C., Silva, C. M., Neves, J. V., Lopes, J., … Duarte, T. L. (2014). Transcription factor NRF2 protects mice against dietary iron-induced liver injury by preventing hepatocytic cell death. Journal of Hepatology, 60(2), 354–361. http://doi.org/10.1016/j.jhep.2013.09.004

Silvestri, L., & Camaschella, C. (2008). A potential pathogenetic role of iron in Alzheimer's disease. Journal of Cellular and Molecular Medicine. http://doi.org/10.1111/j.1582-4934.2008.00356.x

Simpkins, J. W., Perez, E., Wang, X., Yang, S., Wen, Y., & Singh, M. (2009). The potential for estrogens in preventing Alzheimer's disease and vascular dementia. Therapeutic

Advances in Neurological Disorders, 2(1), 31–49. http://doi.org/10.1177/1756285608100427

Smith-Vikos, T., & Slack, F. J. (2012). MicroRNAs and their roles in aging. Journal of Cell Science, 125(Pt 1), 7–17. http://doi.org/10.1242/jcs.099200

Somel, M., Guo, S., Fu, N., Yan, Z., Hu, H. Y., Xu, Y., … Khaitovich, P. (2010). MicroRNA, mRNA, and protein expression link development and aging in human and macaque brain. Genome Research, 20(9), 1207–1218. http://doi.org/10.1101/gr.106849.110

Sparks, D. L., Liu, H., Scheff, S. W., Coyne, C. M., & Hunsaker 3rd, J. C. (1993). Temporal sequence of plaque formation in the cerebral cortex of non-demented individuals. J Neuropathol Exp Neurol, 52(2), 135–142. Retrieved from http://www.ncbi.nlm.nih.gov/entrez/query.fcgi?cmd=Retrieve&db=PubMed&dopt=Citation&list_uids=8440995

Takahashi, M., Eda, A., Fukushima, T., & Hohjoh, H. (2012). Reduction of type IV collagen by upregulated miR-29 in normal elderly mouse and klotho-deficient, senescence-model mouse. PloS One. http://doi.org/10.1371/journal.pone.0048974

Tanaka, Y., Ikeda, T., Yamamoto, K., Ogawa, H., & Kamisako, T. (2012). Dysregulated expression of fatty acid oxidation enzymes and iron-regulatory genes in livers of Nrf2-null mice. Journal of Gastroenterology and Hepatology (Australia), 27(11), 1711–1717. http://doi.org/10.1111/j.1440-1746.2012.07180.x

Terman, A., & Brunk, U. T. (2004). Aging as a catabolic malfunction. International Journal of Biochemistry and Cell Biology. http://doi.org/10.1016/j.biocel.2004.03.009

Terman, A., & Brunk, U. T. (2004). Lipofuscin. The International Journal of Biochemistry & Cell Biology, 36(8), 1400–1404. http://doi.org/10.1016/j.biocel.2003.08.009

Terzibasi, E., Lefrançois, C., Domenici, P., Hartmann, N., Graf, M., & Cellerino, A. (2009). Effects of dietary restriction on mortality and age-related phenotypes in the short-lived fish Nothobranchius furzeri. Aging Cell, 8(2), 88–99. http://doi.org/10.1111/j.1474-9726.2009.00455.x

Terzibasi, E., Valenzano, D. R., Benedetti, M., Roncaglia, P., Cattaneo, A., Domenici, L., & Cellerino, A. (2008). Large differences in aging phenotype between strains of the short-

lived annual fish Nothobranchius furzeri. PLoS ONE, 3(12). http://doi.org/10.1371/journal.pone.0003866

Tozzini, E. T., Baumgart, M., Battistoni, G., & Cellerino, A. (2012). Adult neurogenesis in the short-lived teleost Nothobranchius furzeri: Localization of neurogenic niches, molecular characterization and effects of aging. Aging Cell, 11(2), 241–251. http://doi.org/10.1111/j.1474-9726.2011.00781.x

Tozzini, E. T., Dorn, A., Ng'oma, E., Polačik, M., Blažek, R., Reichwald, K., … Cellerino, A. (2013). Parallel evolution of senescence in annual fishes in response to extrinsic mortality. BMC Evolutionary Biology, 13, 77. http://doi.org/10.1186/1471-2148-13-77

Ugalde, A. P., Ramsay, A. J., de la Rosa, J., Varela, I., Mariño, G., Cadiñanos, J., … López-Otín, C. (2011). Aging and chronic DNA damage response activate a regulatory pathway involving miR-29 and p53. The EMBO Journal, 30(11), 2219–2232. http://doi.org/10.1038/emboj.2011.124

Uversky, V. N., Li, J., & Fink, A. L. (2001). Metal-triggered structural transformations, aggregation, and fibrillation of human ??-synuclein: A possible molecular link between parkinson's disease and heavy metal exposure. Journal of Biological Chemistry, 276(47), 44284–44296. http://doi.org/10.1074/jbc.M105343200

Uylings, H. B. M. (1998). Layer-specific dendritic regression of pyramidal cells with ageing in the human prefrontal cortex. European Journal of Neuroscience, 10(4), 1261–1269. http://doi.org/10.1046/j.1460-9568.1998.00137.x

Valdesalici, S., & Cellerino, A. (2003). Extremely short lifespan in the annual fish Nothobranchius furzeri. Proceedings of the Royal Society B: Biological Sciences, 270 Suppl, 189–191. http://doi.org/10.1098/rsbl.2003.0048

Valenzano, D. R., Benayoun, B. A., Singh, P. P., Zhang, E., Etter, P. D., Hu, C. K., … Brunet, A. (2015). The African Turquoise Killifish Genome Provides Insights into Evolution and Genetic Architecture of Lifespan. Cell, 163(6), 1539–1554. http://doi.org/10.1016/j.cell.2015.11.008

Valenzano, D. R., Sharp, S., & Brunet, A. (2011). Transposon-Mediated Transgenesis in the Short-Lived African Killifish Nothobranchius furzeri, a Vertebrate Model for Aging. G3 (Bethesda, Md.), 1(7), 531–8. http://doi.org/10.1534/g3.111.001271

Valenzano, D. R., Terzibasi, E., Cattaneo, A., Domenici, L., & Cellerino, A. (2006). Temperature affects longevity and age-related locomotor and cognitive decay in the short-lived fish: Nothobranchius furzeri. Aging Cell, 5(3), 275–278. http://doi.org/10.1111/j.1474-9726.2006.00212.x

Valenzano, D. R., Terzibasi, E., Genade, T., Cattaneo, A., Domenici, L., & Cellerino, A. (2006). Resveratrol prolongs lifespan and retards the onset of age-related markers in a short-lived vertebrate. Current Biology, 16(3), 296–300. http://doi.org/10.1016/j.cub.2005.12.038

Van Houcke, J., Groef, L. De, Dekeyster, E., & Moons, L. (2015). The zebrafish as a gerontology model in nervous system aging, disease, and repair. Ageing Research Reviews, 24, 358–368. http://doi.org/10.1016/j.arr.2015.10.004

Vashisht, A. A., Zumbrennen, K. B., Huang, X., Powers, D. N., Durazo, A., Sun, D., … Wohlschlegel, J. A. (2009). Control of iron homeostasis by an iron-regulated ubiquitin ligase. Science, 326(5953), 718–721. http://doi.org/10.2307/40328537

Wei, S., Shi, W., Li, M., & Gao, Q. (2014). Calorie restriction down-regulates expression of the iron regulatory hormone hepcidin in normal and D-galactose-induced aging mouse brain. Rejuvenation Research, 17(1), 19–26. http://doi.org/10.1089/rej.2013.1450

Cloonan, S. M., Glass, K., Laucho-Contreras, M. E., Bhashyam, A. R., Cervo, M., Pabón, M. A., … Choi, A. M. K. (2016). Mitochondrial iron chelation ameliorates cigarette smoke-induced bronchitis and emphysema in mice. *Nature Medicine*, *22*(2), 163–74. http://doi.org/10.1038/nm.4021

Weinstein, G., Beiser, A. S., Choi, S. H., Preis, S. R., Chen, T. C., Vorgas, D., … Seshadri, S. (2014). Serum brain-derived neurotrophic factor and the risk for dementia: the Framingham Heart Study. JAMA Neurology, 71(1), 55–61. http://doi.org/10.1001/jamaneurol.2013.4781

Weller, R. O., Yow, H. Y., Preston, S. D., Mazanti, I., & Nicoll, J. A. (2002). Cerebrovascular disease is a major factor in the failure of elimination of Abeta from the aging human brain: implications for therapy of Alzheimer's disease. Ann N Y Acad Sci, 977, 162–168.

Wichaiyo, S., Yatmark, P., Morales Vargas, R. E., Sanvarinda, P., Svasti, S., Fucharoen, S., & Morales, N. P. (2015). Effect of iron overload on furin expression in wild-type and ??-

thalassemic mice. Toxicology Reports, 2, 415–422. http://doi.org/10.1016/j.toxrep.2015.01.004

Yamamoto, A., Shin, R. W., Hasegawa, K., Naiki, H., Sato, H., Yoshimasu, F., & Kitamoto, T. (2002). Iron (III) induces aggregation of hyperphosphorylated τ and its reduction to iron (II) reverses the aggregation: Implications in the formation of neurofibrillary tangles of Alzheimer's disease. Journal of Neurochemistry, 82(5), 1137–1147. http://doi.org/10.1046/j.1471-4159.2002.01061.x

Yang, J., Chen, D., He, Y., Mel??ndez, A., Feng, Z., Hong, Q., … Chen, X. (2013). MiR-34 modulates Caenorhabditis elegans lifespan via repressing the autophagy gene atg9. Age, 35(1), 11–22. http://doi.org/10.1007/s11357-011-9324-3

Ying, W., Han, S. K., Miller, J. W., & Swanson, R. A. (1999). Acidosis potentiates oxidative neuronal death by multiple mechanisms. Journal of Neurochemistry, 73(4), 1549–1556. http://doi.org/10.1046/j.1471-4159.1999.0731549.x

Zecca, L., Youdim, M. B. H., Riederer, P., Connor, J. R., & Crichton, R. R. (2004). Iron, brain ageing and neurodegenerative disorders. Nature Reviews. Neuroscience, 5(11), 863–73. http://doi.org/10.1038/nrn1537

Zhang, D. L., Hughes, R. M., Ollivierre-Wilson, H., Ghosh, M. C., & Rouault, T. A. (2009). A Ferroportin Transcript that Lacks an Iron-Responsive Element Enables Duodenal and Erythroid Precursor Cells to Evade Translational Repression. Cell Metabolism, 9(5), 461–473. http://doi.org/10.1016/j.cmet.2009.03.006

Zhang, Y., Ueno, Y., Liu, X. S., Buller, B., Wang, X., Chopp, M., & Zhang, Z. G. (2013). The MicroRNA-17-92 cluster enhances axonal outgrowth in embryonic cortical neurons. The Journal of Neuroscience : The Official Journal of the Society for Neuroscience, 33(16), 6885–94. http://doi.org/10.1523/JNEUROSCI.5180-12.2013

Zucca, F. A., Segura-Aguilar, J., Ferrari, E., Muñoz, P., Paris, I., Sulzer, D., … Zecca, L. (2015). Interactions of iron, dopamine and neuromelanin pathways in brain aging and Parkinson's disease. Progress in Neurobiology. http://doi.org/10.1016/j.pneurobio.2015.09.012